

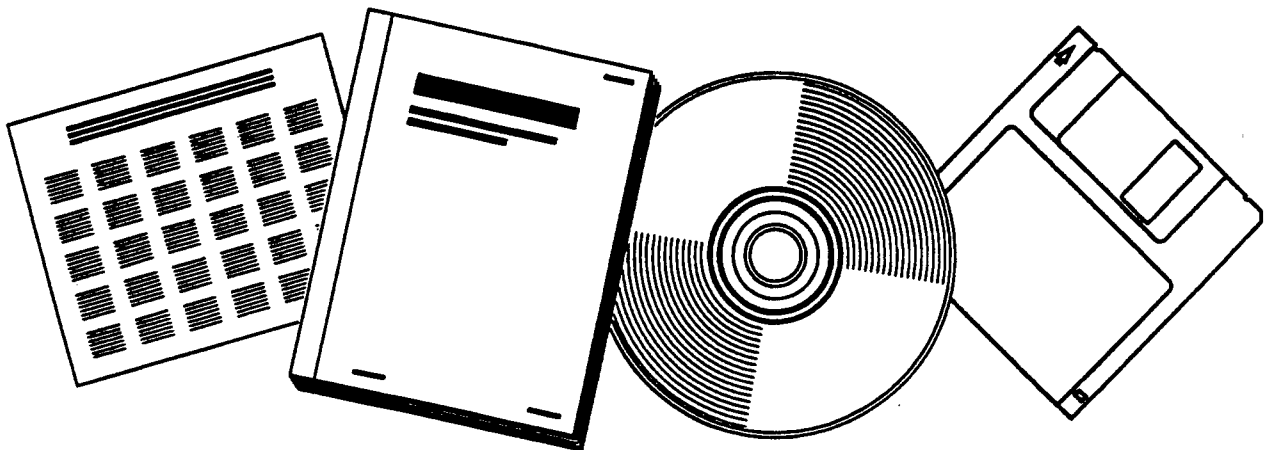


PB98-106727

NTIS[®]
Information is our business.

FIELD MEASUREMENT AND EVALUATION OF TIME-DEPENDENT LOSSES IN PRESTRESSED CONCRETE BRIDGES

AUG 97



U.S. DEPARTMENT OF COMMERCE
National Technical Information Service

Field Measurement and Evaluation of Time-Dependent Losses in Prestressed Concrete Bridges

Project Number: WPI-0510735



PB98-106727

Final Report

Submitted to
Florida Department of Transportation
Dr. Moussa Issa PE., (Project Manager)

by
Dr. Okey Onyemelukwe PE., (Principal Investigator)
Dr. Sashi Kunnath PE., (Co-Principal Investigator)

University of Central Florida
Orlando, Florida 32816

August, 1997

Technical Report Documentation Page

1. Report No WPI 0510735		2. Government Accession No.  PB98-106727		3. Recipient's Catalog No.	
4. Title and Subtitle Field measurement and Evaluation of Time-Dependent Losses in Prestressed Concrete Bridges 8 / 97			5. Report Date 08 / 1997		
7. Author(s) Okey U. Onyemelukwe, Ph.D., PE. & Sashi K. Kunnath, Ph.D., PE.			6. Performing Organization Code		
			8. Performing Organization Report		
9. Performing Organization name and address University of Central Florida Civil & Environmental Engineering Dept. 4000 Central Florida Blvd. Orlando, Fl. 32816			10. Work Unit No.		
			11. Contact or Grant No. B. 9908 99700-3318-119		
12. Sponsoring Agency name and address Florida Department of transportation 605 Suwannee Street Tallahassee, Fl 32399-0450			13. Type of Report and Period Covered Research 08/95 - 02/97		
			14. Sponsoring Agency Code		
15. Supplementary Notes					
16. Abstract: <p>This report presents the bridge instrumentation technique used in this research project, along with the bridge monitoring procedure, and methodologies employed for the data collection and reduction. It also discusses comparison between the time-dependent pre-stressed losses and concrete stresses, deduced from the strain measured in the field, and their empirically determined counterparts often used in various codes of practice, particularly ACI-PCI and AASHTO.</p>					
17. Key Words Prestressed Concrete Bridges Pretensioned Girders Prestressed Losses Time-Dependent Behavior Creep, Shrinkage, Steel Relaxation			18. Distribution Statement		
19. Security Classif. (of this report) unclassified	20. Security classes (of this page) Unclassified	21. No of pages 178	22. Price		

Disclaimer Sheet

The opinions, finding and conclusions expressed in this publication are those of the authors and not necessarily those of the Florida Department of Tracsportation or the US Department of Transpportation.

This publication was prepared in cooperation with the state of the Florida Department of Transportation & the US Department of Transportation.

SI* (MODERN METRIC) CONVERSION FACTORS

APPROXIMATE CONVERSIONS TO SI UNITS

APPROXIMATE CONVERSIONS FROM SI UNITS

Symbol	When You Know	Multiply By	To Find	Symbol	When You Know	Multiply By	To Find	Symbol
LENGTH								
in	inches	25.4	millimeters	mm	millimeters	0.039	inches	in
ft	feet	0.305	meters	m	meters	3.28	feet	ft
yd	yards	0.914	meters	m	meters	1.09	yards	yd
mi	miles	1.61	kilometers	km	kilometers	0.621	miles	mi
AREA								
in ²	square inches	645.2	square millimeters	mm ²	square millimeters	0.0016	square inches	in ²
ft ²	square feet	0.093	square meters	m ²	square meters	10.764	square feet	ft ²
yd ²	square yards	0.836	square meters	m ²	square meters	1.195	square yards	ac
ac	acres	0.405	hectares	ha	hectares	2.47	acres	mi ²
mi ²	square miles	2.59	square kilometers	km ²	square kilometers	0.386	square miles	
VOLUME								
fl oz	fluid ounces	29.57	milliliters	ml	milliliters	0.034	fluid ounces	fl oz
gal	gallons	3.785	liters	l	liters	0.264	gallons	gal
ft ³	cubic feet	0.028	cubic meters	m ³	cubic meters	35.71	cubic feet	ft ³
yd ³	cubic yards	0.765	cubic meters	m ³	cubic meters	1.307	cubic yards	yd ³
NOTE: Volumes greater than 1000 l shall be shown in m ³ .								
MASS								
oz	ounces	28.35	grams	g	grams	0.035	ounces	oz
lb	pounds	0.454	kilograms	kg	kilograms	2.202	pounds	lb
T	short tons (2000 lb)	0.907	megagrams	Mg	megagrams	1.103	short tons (2000 lb)	T
TEMPERATURE (exact)								
°F	Fahrenheit temperature	5(F-32)/9 or (F-32)/1.8	Celcius temperature	°C	Celcius temperature	1.8C + 32	Fahrenheit temperature	°F
ILLUMINATION								
fc	foot-candles	10.76	lux	lx	lux	0.0929	foot-candles	fc
fl	foot-Lamberts	3.426	candela/m ²	cd/m ²	candela/m ²	0.2919	foot-Lamberts	fl
FORCE and PRESSURE or STRESS								
lbf	poundforce	4.45	newtons	N	newtons	0.225	poundforce	lbf
psi	poundforce per square inch	6.89	kilopascals	kPa	kilopascals	0.145	poundforce per square inch	psi

* SI is the symbol for the International System of Units. Appropriate rounding should be made to comply with Section 4 of ASTM E380.

EXECUTIVE SUMMARY

Problem Statement

The Florida Department of Transportation (FDOT) is frequently confronted with contractor suggested redesigns of some of its pre-stressed concrete bridge projects. In which case most of them call for changing the bridge girder design from its original post-tensioned continuous members to longer simple supported spans. Often, these result in deeper simple span girders with larger cross-sectional areas, moment of inertia and consequently, greater ultimate capacity. Thus, enabling the designer to eliminate the post-tensioning and change the statical scheme from continuous to simply supported.

However, although the girders are designed as simple spans, the attached deck slabs remain as continuous members. The final configuration of both the deck slab and the girder acting as a unit, is in essence a hybrid between a strictly statically indeterminate structure and a determinate structure. Further investigation of this sort of design is necessary, since the time-dependent behavior of these members with respect to creep, shrinkage and steel relaxation is drastically different for indeterminate structures as compared to simple ones.

Project Objectives

It is the objective in this research to instrument an actual bridge having this hybrid configuration, and to monitor the time-dependent losses in the bridge for an extended period of time. The bridge instrumented for this purpose is the Westbound Gandy Bridge, located between Pinellas and Hillsborough counties on State Road No. 600. To accomplish the primary objective, the following studies will be conducted:

- Instrument sections of the bridge girders and deck slab for strain and temperature measurements, which will be used in determining the pre-stress losses in the members.
- Utilize the field measured data to determine the effects of the relative shrinkage between the continuous slab and the simply supported beam
- Reduction and processing of the measured data to form a useful database for future use by FDOT in related projects
- Use analytical and code procedures for pre-stressed concrete bridge design to establish the adequacy or ramifications of the modified and hybrid design. Especially, since most of these redesigns claim the simply supported system has the same structural capabilities as the continuous post-tensioned design, and that both designs should be considered equivalent.

Project Findings

This report presents the bridge instrumentation technique used in this research project, along with the bridge monitoring procedure, and methodologies employed for data collection and reduction. It also discusses comparisons between the time-dependent pre-stress losses and concrete stresses, deduced from the strain measured in the field, and their empirically determined counterparts often used in various codes of practice, particularly ACI-PCI and AASHTO. The strain data utilized in this first phase of the project covered 150 days, starting from the date the bridge girders were cast at the pre-stressed concrete yard in Tampa, Florida. During this period the bridge deck slab was not in place yet, hence, the girders were loaded by the pre-stressing force and self-weight only. Therefore, composite action and effect of deck continuity which are also pertinent to this project, will be covered in the second phase report. The second phase of the study is currently underway.

Project Conclusions

Utilizing the early time-dependent data, up to 150 days, the conclusions listed below were drawn from this phase of the study.

First, the pre-stress loss variation with depth of cross-section is non-uniform, and varies in a segmental linear distribution at the mid-span and linearly towards the support. This observation is contrary to the uniform distribution implied by most codes, when a single value is used at the steel centroid level.

Secondly, using this non-uniform stress distribution for the computation of the concrete stresses resulted in a non-linear concrete stress distribution. However, none of the allowable stress limits provided by the codes (ACI-PCI & AASHTO) were exceeded in any case.

Thirdly, the field measured immediate losses attributed mainly to elastic shortening were consistently greater than those specified by the codes. The elastic shortening values are expressed as percentages of the jacking stress, and ranged from about 10.2% to 14.1%, compared to 8.4% to 8.8% suggested by the Codes.

TABLE OF CONTENTS

FDOT TECHNICAL REPORT DOCUMENTATION PAGE	i
DISCLAIMER PAGE	ii
CONVERSION TABLE	iii
EXECUTIVE SUMMARY	iv
LIST OF TABLES	x
LIST OF FIGURES	xi
1 INTRODUCTION	
1.1 Background	1
1.2 Methods for Prestressing Concrete.....	4
1.3 Westbound Gandy Bridge Project.....	6
2 GIRDER AND BRIDGE INSTRUMENTATION	
2.1 Introduction	9
2.1.1 Bridge Configuration.....	9
2.1.2 Modified AASHTO Type VI.....	12
2.2 Equipment Used for Instrumentation	15
2.2.1 Strain Gauges	15
2.2.2 Other Equipment Used	16
2.3 Girder Instrumentation	17
2.3.1 Gauge Placement Along Girder Span	17
2.3.2 Gauge Placement Across Girder Cross-section.....	18
2.3.3 Gauge Placement Along Strand	23
2.4 Composite Slab Instrumentation	23
2.4.1 Introduction	23
2.4.2 Gauge Placement Along the Slab Longitudinal Axis...	26

	2.4.3 Gauge Placement Across Depth of Slab.....	26
2.5	Installation of Strain Gauges	27
	2.5.1 Girder Strain Gauges	27
	2.5.2 Slab Strain Gauges	32
2.6	Equipment Attachment to Bridge.....	33
2.7	Shrinkage Cylinders	34
2.8	Modulus of Elasticity	40
	2.8.1 Introduction	40
	2.8.2 ACI 318-95 Definition of E_c	40
	2.8.3 Experimental Determination of E_c	41
	2.8.4 CEB-FIP MC 1990 Method for Determining $E_c(t)$	42
	2.8.5 Calculating $E_c(t)$ and Comparing to Design	44
3	CODE TREATMENT OF PRESTRESS LOSS	
	3.1 Introduction	47
	3.2 AASHTO-LRFD Method for Determining Prestress Loss	48
	3.2.1 Introduction	48
	3.2.2 Total Prestress Loss.....	48
	3.2.3 Instantaneous Losses	49
	3.2.3.1. Anchorage Set Loss	49
	3.2.3.2. Frictional Losses	50
	3.2.3.3. Elastic Shortening	50
	3.2.4 Lump Sum Approximation for	50
	3.2.5 Detailed Estimates of the Time-Dependent Losses.....	53
	3.2.5.1 Shrinkage	53
	3.2.5.2 Creep	53
	3.2.5.3 Steek Relaxation	54
	3.3 ACI-PCI Method	55
	3.3.1 Introduction	55
	3.3.2 Sources of Loss from ACI Code	56
	3.3.3 Typical Range of Total Loss according to PCI	56
	3.3.4 Frictional Loss according to ACI	56
	3.3.5 Equations for Determining Prestress Loss	57
	According to PCI.....	58
	3.4 Spreadsheet Prestress Loss Results	60
4	DATA ANALYSIS AND EXPERIMENTAL RESULTS	
	4.1 Introduction	63
	4.2 Determination of Prestressed Loss from Measured Data	66
	4.3 Ambient Temperature and Relative Humidity	70
	4.4 Immediate Prestress Loss	73
	4.4.1 Introduction	73

4.4.2	At Midspan.....	73
4.4.3	At Quarter-span and 1.52 m from Support.....	76
4.4.4	Variation Along the Length of the Beam.....	79
4.5	Time-Dependent Prestress Loss.....	81
4.5.1	Introduction.....	81
4.5.2	At Midspan.....	81
4.5.3	At Quarter-span and 1.52 m from Support.....	84
4.5.4	Variation Along the Length of the Beam.....	87
4.6	Lump Sum Prestress Loss.....	88
4.6.1	Introduction.....	88
4.6.2	At Midspan.....	88
4.6.3	At Quarter-span and 1.52 m from Support.....	91
4.6.4	Variation Along the Length of the Beam.....	91
5	EFFECTS OF PRESTRESS LOSS ON BRIDGE DESIGN	
5.1	Introduction.....	95
5.2	Cross-sectional Prestress Loss Variation.....	96
5.2.1	Midspan of Beam 1.....	97
5.2.2	Quarter-span of Beam 3.....	97
5.2.3	From the End Support (1.52 m) Beam 4.....	102
5.2.4	Discussion.....	105
5.3	Percentage Comparisons of Prestress Loss.....	105
5.3.1	Introduction.....	105
5.3.2	Initial Prestress to Jacking Stress Ratio.....	105
5.3.3	The Effectiveness Ratio, R.....	109
5.3.4	Lump Sum Loss to Jacking Stress Ratio.....	111
5.3.5	Elastic Shortening to Jacking Stress Ratio.....	116
5.3.6	Effective Stress to Jacking Stress Ratio.....	119
5.3.7	Actual T.D. to Code T.D. Ratio.....	122
5.3.8	Actual L.S. to Code L.S. Ratio.....	122
5.3.9	T.D. to E.S. Ratio.....	122
5.4	Tendon and Concrete Stresses.....	128
5.4.1	Introduction.....	128
5.4.2	Prestressing Tendon Stresses.....	128
5.4.3	Concrete Stresses.....	131
5.4.3.1	ACI Code Limits on Concrete Stresses	131
5.4.3.2	Determination of Actual Concrete Stresses	133
5.5	Relative Humidity and Temperature	
	Effects on Prestress Loss.....	140
5.5.1	Introduction.....	140
5.5.2	Selection of Points.....	141
5.5.3	Relative Humidity.....	141
5.5.4	Ambient Temperature.....	142

	5.6 Effects of Prestress Loss on Camber and Deflection	143
	5.6.1 Introduction	143
	5.6.2 Field Measurement of Camber and Deflection	144
	5.6.3 Comparing Camber and Deflection Results.....	145
6	Conclusions	147
APPENDIX A		
	PLOTS OF EXPERIMENTAL	
	STRESS-STRAIN CURVES	150
APPENDIX B		
	ACI COMMITTEE 209 FOR DETERMINING $E_c(t)$	153
APPENDIX C		
	Plots of Relative Humidity Vs. Lumpsum Losses.....	155
	Plots of Temperature Vs. Lumpsum Losses.....	155
	REFERENCES	163

LIST OF TABLES

2-1	Properties for Standard and Modified Type VI Girders	13
2-2	Detailed information about composite slab gauges.....	25
2-3	Experimental results of E_c and f_c'	42
2-4	28 day strength for girders.....	44
2-5	Design $E_c(t)$ versus CEB-FIP $E_c(t)$	46
3-1	AASHTO lump sum time-dependent equations.....	52
3-2	Values of K_{re} and J	59
3-3	Values of C	60
3-4	Spreadsheet results for midspan	61
3-5	Spreadsheet results for other locations.....	62
4-1	Example of the raw collected data	64
5-1	Limitations on strand stress.....	129
5-2	Resulting tendon stresses	130
5-3	Allowable concrete stresses.....	132
5-4	Camber and deflection readings	144
B-1	ACI Committee 209 $E_c(t)$ versus Design $E_c(t)$	154

LIST OF FIGURES

2-1	Bridge configuration.....	10
2-2	Bridge cross-section	11
2-3	Standard and Modified AASHTO Type VI.....	13
2-4	Ends and Midspan cross-section with tendons.....	14
2-5	Instrumented locations	20
2-6	Midspan gauge distribution.....	21
2-7	Quarter-span gauge distribution	22
2-8	1.52 m gauge distribution.....	22
2-9	Slab gauge distribution.....	24
2-11	Bridge cross-section with equipment	33
4-1	Unfiltered strain and internal temperature data.....	65
4-2	Unfiltered ambient temperature and relative humidity	66
4-3	Relative humidity and ambient temperature for Beams 1 and 4	72
4-4	Relative humidity and ambient temperature for Beams 2 and 3	72
4-5	Elastic shortening Beam 1 Midspan.....	74
4-6	Elastic shortening Beam 4 Midspan.....	74

4-7	Elastic shortening Beam 3 Midspan.....	75
4-8	Average elastic shortening for midspans.....	76
4-9	Elastic shortening Beam 3 Quarter-span.....	77
4-10	Elastic shortening 1.52 m Beam 1.....	78
4-11	Elastic shortening 1.52 m Beam 4.....	78
4-12	Average elastic shortening for 1.52 m.....	79
4-13	Elastic shortening variation with length.....	80
4-14	Time-dependent prestress loss Beam 1 Midspan	82
4-15	Time-dependent prestress loss Beam 4 Midspan	82
4-16	Time-dependent prestress loss Beam 3 Midspan	83
4-17	Average time-dependent prestress loss for midspans.....	83
4-18	Time-dependent prestress loss Beam 3 Quarter-span	85
4-19	Time-dependent prestress loss 1.52 m Beam 1	85
4-20	Time-dependent prestress loss 1.52 m Beam 4	86
4-21	Average time-dependent prestress loss for 1.52 m.....	86
4-22	Time-dependent prestress loss with length	87
4-23	Lump sum prestress loss Beam 1 Midspan	89
4-24	Lump sum prestress loss Beam 4 Midspan	89
4-25	Lump sum prestress loss Beam 3 Midspan	90
4-26	Average lump sum prestress loss for midspans.....	90
4-27	Lump sum prestress loss Beam 3 Quarter-span	92
4-28	Lump sum prestress loss 1.52 m Beam 1	92

4-29	Lump sum prestress loss 1.52 m Beam 4	93
4-30	Average lump sum prestress loss for 1.52 m.....	93
4-31	Lump sum prestress loss with length	94
5-1a-b	Cross-sectional loss variation Beam 1 Midspan	98
5-1c-d	Cross-sectional loss variation Beam 1 Midspan	99
5-2a-b	Cross-sectional loss variation Beam 3 Quarter-span.....	100
5-2c-d	Cross-sectional loss variation Beam 3 Quarter-span.....	101
5-3a-b	Cross-sectional loss variation 1.52 m Beam 4	103
5-3c-d	Cross-sectional loss variation 1.52 m Beam 4	104
5-4	f_{pi} / f_{pj} for Midspan Beam 1	108
5-5	f_{pi} / f_{pj} for Quarter-span Beam 3.....	108
5-6	f_{pi} / f_{pj} for 1.52 m Beam 4.....	109
5-7	1-R for Midspan Beam 1.....	112
5-8	1-R for Quarter-span Beam 3.....	113
5-9	1-R for 1.52 m Beam 4	113
5-10	Lump sum loss to jacking stress ratio for Midspan Beam 1	114
5-11	Lump sum loss to jacking stress ratio for Quarter-span Beam 3.....	115
5-12	Lump sum loss to jacking stress ratio for 1.52 m Beam 4	115
5-13	Elastic shortening to jacking stress ratio Beam 1 Midspan.....	117
5-14	Elastic shortening to jacking stress ratio Beam 3 Quarter-span.....	117
5-15	Elastic shortening to jacking stress ratio 1.52 m Beam 4.....	118
5-16	Effective stress to jacking stress ratio Beam 1 Midspan	118

5-17	Effective stress to jacking stress ratio Beam 3 Quarter-span	120
5-18	Effective stress to jacking stress ratio 1.52 m Beam 4.....	120
5-19	Actual T.D. over Code T.D. Ratio Beam 1 Midspan	121
5-20	Actual T.D. over Code T.D. Ratio Beam 3 Quarter-span	121
5-21	Actual T.D. over Code T.D. Ratio 1.52 m Beam 4	123
5-22	Actual L.S. over Code L.S. Ratio Beam 1 Midspan.....	123
5-23	Actual L.S. over Code L.S. Ratio Beam 3 Quarter-span.....	124
5-24	Actual L.S. over Code L.S. Ratio 1.52 m Beam 4	124
5-25	T.D. to E.S. Ratio Beam 1 Midspan.....	126
5-26	T.D. to E.S. Ratio Beam 3 Quarter-span.....	126
5-27	T.D. to E.S. Ratio 1.52 m Beam 4.....	127
5-28	Midspan Beam 1 at transfer.....	136
5-29	Midspan Beam 1 at transfer.....	137
5-30	Quarter-span Beam 3 at transfer.....	137
5-31	Quarter-span Beam 3 at transfer.....	138
5-32	1.52 m Beam 4 at transfer	138
5-33	1.52 m Beam 4 at transfer	139
5-34	Camber for Midspan of Beams 1, 4, and 3.....	146
A-1	Experimental Stress-Strain Curve - Day 1	150
A-2	Experimental Stress-Strain Curve - Day 2	151
A-3	Experimental Stress-Strain Curve - Day 3	151
A-4	Experimental Stress-Strain Curve - Day 5	152

A-5	Experimental Stress-Strain Curve - Day 7	152
C-1	Relative Humidity versus Loss Midspan Beam 1	155
C-2	Relative Humidity versus Loss Midspan Beam 3	156
C-3	Relative Humidity versus Loss Quarter-span Beam 3.....	157
C-4	Relative Humidity versus Loss 1.52 m Beam 4	158
C-5	Ambient Temperature versus Loss Midspan Beam 1.....	159
C-6	Ambient Temperature versus Loss Midspan Beam 3.....	160
C-7	Ambient Temperature versus Loss Quarter-span Beam 3.....	161
C-8	Ambient Temperature versus Loss 1.52 m Beam 4	162

CHAPTER 1

INTRODUCTION

1.1 Background

The Florida Department of Transportation (FDOT) is frequently confronted with contractor suggested redesigns of some prestressed concrete bridge projects. In which case, most of the contractors call for changing the bridge girder design from its original post-tensioned continuous members to longer simple supported spans. Often, these result in deeper simple span girders with larger cross-sectional areas, moment of inertia and consequently, greater ultimate capacity. Thus, enabling the designer to eliminate the post-tensioning and change the statical scheme from continuous to simply supported.

Therefore, although the girders are designed as simple spans, the attached deck slabs remain as continuous members. The final configuration of both the deck slab and the girder acting as a unit, is in essence a hybrid between a strictly statically indeterminate structure and a determinate structure. Further investigation of this sort of design is necessary, since the time-dependent behavior of these members with respect to creep, shrinkage and steel relaxation is drastically different for indeterminate structures when compared to simple ones.

Therefore, it is the objective in this project to conduct the following studies:

- Instrument sections of the bridge girder and deck slab for strain and temperature measurements, which will be used in determining the prestress losses in the members
- Utilize the field measured data to determine the effects of the relative shrinkage between the continuous slab and the simply supported beam.
- Reduce and process the measured data to form a useful database for future use by FDOT in related projects
- Use analytical and code procedures for prestressed concrete bridge design to establish the adequacy or ramifications of the modified design. Especially, since most of these redesigns claim that the simply supported system has the same structural capabilities as the continuous post-tensioned design, and that both designs should be considered equivalent.

In this report the effects of time-dependent prestress losses in prestressed concrete bridges are studied. Time-dependent behavior of concrete is an important consideration in the design and analysis of structures, especially with respect to prestressed concrete bridges. Both prestressed concrete and conventional reinforced concrete tend to deform

with time. The reasons for these continuous deformations include creep and shrinkage. These deformations directly affect the strains in the concrete, which also change with time. Therefore, creep and shrinkage must be compensated, before a member can perform at its best. Without accounting for creep and shrinkage effects, serviceability problems may arise with excessive camber, deflection, and/or flexural stresses. The change in stress due to the above mentioned phenomena are classified as part of the prestress losses, and must be accounted for in the design of prestressed concrete members.

There are two categories of prestress loss: instantaneous losses and time-dependent losses. The instantaneous prestress losses are made up primarily of anchorage slip, friction, and elastic shortening. These losses occur only once and do not necessarily vary with time. The time-dependent losses consist of creep and shrinkage of concrete and relaxation of the prestressing steel. These losses vary throughout the lifetime of a member and increase rapidly at the early age of the concrete, while increase over the remaining life occurs at a decreasing rate.

Prestress losses are often accounted for by two different approaches. One method takes a known lump sum value established from similar members as the prestress loss for the member being examined. In this approach, the prestressed loss is often expressed as a percentage of the initial stress applied to the steel strands. The other method involves calculating each contribution of the loss separately, summing these components and taking that sum as the total prestress loss. In the sections that follow, a general overview

of prestressing of concrete structures will be presented. After which, more specific details as they apply to the Westbound Gandy Bridge project will be covered.

1.2 Methods for Prestressing Concrete

Prestressed concrete involves the pre-application of compressive force, transferred from the steel tendons, to the surrounding concrete. This compressive load, which is typically eccentric, is designed to counteract the service load that will be applied on the member during its lifetime. Upon application of this prestress force, the beam will concave downward from the casting bed and rest on its ends. This bowing action caused by the preloading is referred to as camber or “negative deflection.” The stress distribution resulting from the prestress force would consist of tensile stresses toward the top of the member and compressive stresses toward its bottom. As the service loads are applied the member tends to deform downward or deflect, overcoming the initial camber. This results in the member being mainly kept in compression toward its top, and with little or no tensile stresses near the bottom. Since concrete is much stronger in compression than it is in tension, it would be beneficial to keep the member in as much compression as possible. This is precisely what prestressing does, allowing more of the member to be in compression and controlling tensile stresses under service conditions

Prestressed concrete offers many advantages over conventional reinforced concrete. For example, prestressed concrete allows for the use of stronger materials, such

as high-strength steel (with yield strengths of 1862 MPa (270 ksi)) and high-strength concrete (with compressive strengths of 48.3 MPa (7 ksi) and above). These materials cannot be used with conventional reinforced concrete because their properties are not consistent with that type of design. The higher strength concrete and steel allow for smaller and lighter sections, than those used for conventional reinforced concrete members with the same load carrying capacity. Cracking, deflections, and service load stresses can be controlled easily using these high-strength materials with prestressed concrete.

It is theoretically possible to design a member with zero tensile stress and such a case is known as full prestressing. This case is very limiting and often leads to troublesome excessive camber after loads are applied. This excessive camber in flexural prestressed members can create uneven driving surfaces in bridges, or promote cracking in walls of buildings as well as other problems. These problems have lead to a viable alternative to full prestressing known as partial prestressing. Lying somewhere between both conventional reinforced concrete and full prestressing is partial prestressing. This midway alternative requires the use of conventional steel reinforcement in addition to prestressing steel, depending on the design, to provide additional load carrying capacity. Quite often the non-prestressed steel is also used to control the crack width that develops in the member.

Prestressed concrete is used in many different types of structures such as bridges, parking garages, and floor beams in buildings to name a few. The advantages of

prestressed concrete are vast, which explains why the use of this form of construction has continued to increase throughout the years.

1.3 Westbound Gandy Bridge Project

This report studies the effects of time-dependent prestress losses in prestressed concrete girders by instrumenting an actual bridge. Strain measurements, taken from these girders, are used to deduce the actual prestress loss. The strain readings were obtained by using embedded vibrating wire strain gauges.

The Westbound Gandy Bridge in Pinellas and Hillsborough Counties of Florida, is the actual bridge used in this case study. The original design for the Approach span consisted of 25 typical units made up primarily of 4-span continuous post-tensioned girders of 43.9 m (144 ft). The re-design consists of 31 typical units made up primarily of 3-simply supported spans of 43.9 m (144 ft). The new bridge configuration is primarily composed of 43.9 m (144 ft) pretensioned modified AASHTO Type VI concrete girders. According to the Value Engineering Report [1], this girder is 15.25 cm (6 in) deeper than the Florida Bulb-T, and has 18% additional area, but a 44% greater moment of inertia and 64% greater ultimate capacity. Composite action is then achieved with a continuous slab over the 3-simply supported spans. This hybrid structural configuration is lacking in performance data, especially with respect to prestress losses, camber, and deflection. To investigate these conditions four strategically located girders were chosen for

instrumentation in this project. Three locations along the span were picked for the placement of a series of gauges. These points are at the midspan, quarter-span and 1.52 m (5 ft) from the end support.

Therefore, all instrumented girders have gauges at their midspans as well as gauges at either the quarter-span or 1.52 meters (5 feet) from the end support.

At each of the location selected along the span, series of gauges were placed throughout the cross-section. Some of the cross-sectional points chosen had physical significance, such as the steel, concrete, and composite section centroids. Additional points between those already mentioned were picked to account for the variation between them.

Data collection began in December 1995 at the Hardaway Prestress Plant in Tampa, Florida, where the beams were casted. The beams were placed at the bridge site in April 1996 by Misener Marine Construction Company, where data collection is still on going, and is currently scheduled to continue for another two years.

This report will deal with the data collected from the studied beams just after they were cast and stressed, through their placement upon the bridge, and before the composite slab was poured. The data from this period in all covers 150 days.

The format and content of the rest of the body of this report is presented next. Chapter 2, Girder and Bridge Instrumentation, entails all instrumentation aspects of the girder and bridge studied, what equipment was used and how it was installed, what gauge locations were chosen and why, and other important experimental details. Chapter 3, Code Treatment of Prestress Losses, illustrates how various Codes treat prestress losses.

Chapter 4, Data Analysis and Experimental Results, explains how results were obtained, separates the immediate losses from the time-dependent losses, contains various plots of prestress loss, and compares Code results with those obtained. Chapter 5, Effects of Prestress Loss on Bridge Design, examines the effects of prestress losses within the girder cross-sections, utilizes percent comparison with Codes, calculates tendon and concrete stresses, investigates the relationship of relative humidity and ambient temperature with prestress losses, and compares actual camber readings to those calculated using the prestress loss of Chapter 4. Chapter 6, Conclusions and Recommendations contains observations and future work.

CHAPTER 2

GIRDER AND BRIDGE INSTRUMENTATION

2.1 Introduction

The Westbound Gandy Bridge is made up of many different span lengths, with the most frequent occurring span length being 43.9 m (144 ft). Since this span length is most prevalent, girders of this length were selected for this study. Each of these 43.9 m (144 ft) girders have the shape of the AASHTO Type VI girder with some modifications. Four of these Modified AASHTO Type VI girders were selected for instrumentation in this project.

2.1.1 Bridge Configuration

The design of the bridge calls for three simply-supported pretensioned girders with a continuous reinforced concrete deck, to form composite action over the three spans. A typical cross-section of the bridge consists of four girders, two of which are interior, and two of which are exterior. This bridge configuration and typical cross-section can be seen in Figures 2-1 and 2-2, respectively. In order to see the variation of the loading effects for the interior spans versus the exterior spans after the slab was cast, two of each type were

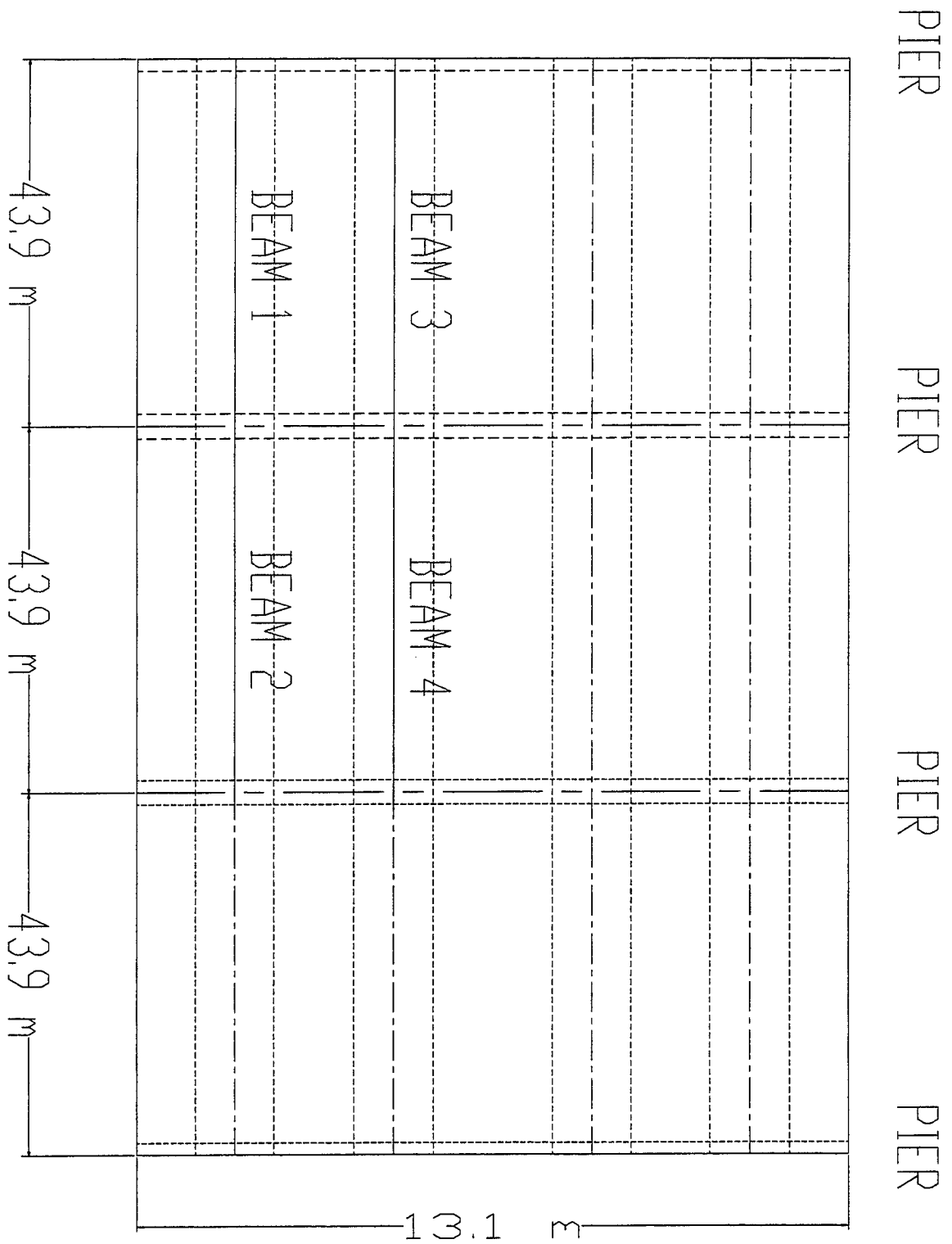


Figure 2-1 Bridge Configuration of the Westbound Gandy Bridge in Tampa, Florida.

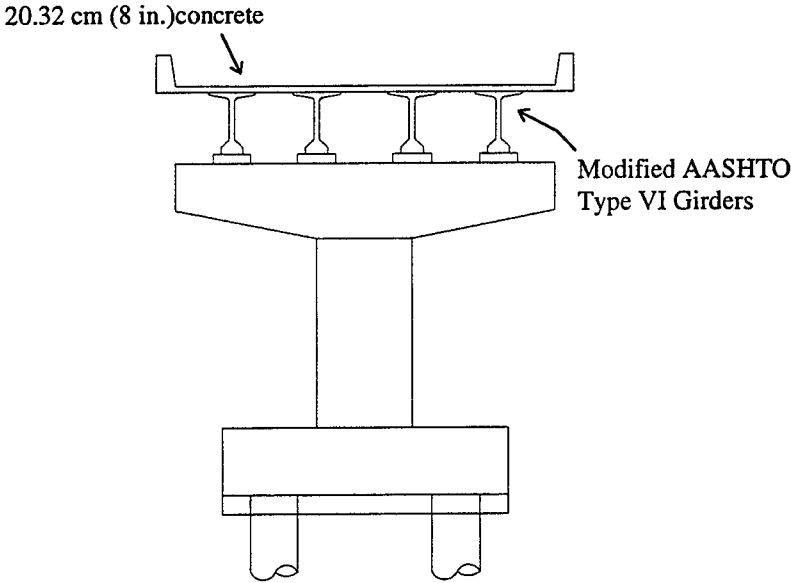


Figure 2-2 Cross-section of the Westbound Gandy Bridge.

chosen for instrumentation. These four girders are representative of the entire three-span system, and are labeled in Figure 2-1 as Beams 1 through 4.

2.1.2 Modified AASHTO Type VI

As mentioned earlier, the girder type investigated in this project is the Modified AASHTO Type VI. This girder is derived from the Standard Type VI Bridge Girders suggested by AASHTO. In Figure 2-3, both the Standard AASHTO and the Modified AASHTO Type VI girders are presented with their properties in Table 2-1. The Modified Type VI is 15.2 cm (6 in) taller, and has a maximum top flange width 47.5 cm (18 in) wider, when compared to that of the Standard Type VI as well as other dimensional changes. These changes allow for an increase in the gross moment of inertia of the section, I_g , of 21 % while only increasing the self weight of the member by less than 2 %.

The design of the Modified AASHTO Type VI girder used on the Westbound Gandy Bridge consists of, 64 - 1.27 cm ($1/2$ inch) oversized or special 1862 MPa (270 ksi) -seven-wire low relaxation prestressing strands pulled at 150.3 kN (33.8 kips) each. These 1.27 cm ($1/2$ inch) oversized or special strands have an area per strand of 1.08 cm² (0.167 in²), which is larger than the area of standard strands this size at, 0.987 cm² (0.153 in²). Of the 64 strands used, 50 are straight and 14 are draped using a two point depressed configuration. In addition to these strands, there are 2 - 0.95 cm ($3/8$ inch 270) ksi strands in the top flange stressed at 44.5 kN (10 kips) each. These two strands are used as hanger bars for the shear reinforcement, and should not be considered part of the initial prestressing force applied. Since there is no conventional steel reinforcement used

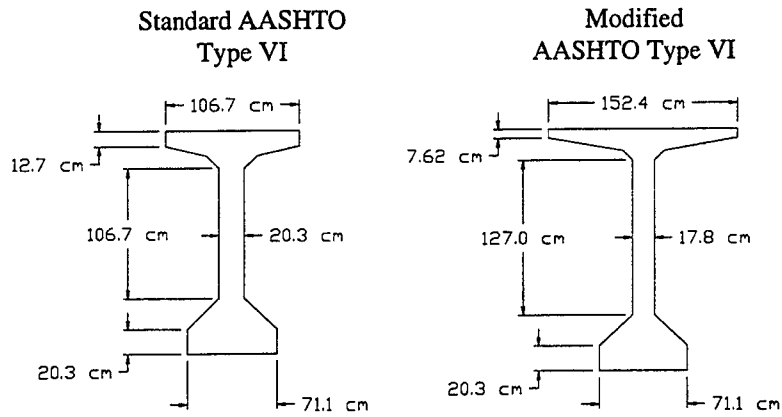


Figure 2-3 Standard and Modified AASHTO Type VI Girder Cross-sections.

Table 2-1 Properties for the Standard and Modified Type VI Girders

AASHTO Type VI	Height		Area		I_c		Girder Weight ($w_0 = 0.145\text{kpf}$)	
	cm	in	cm^2	in^2	cm^4	in^4	kN/m	kpf
Standard	182.9	72	7,000	1,085	$3.05 \cdot 10^7$	733,320	191.2	1.092
Modified	198.1	78	7,129	1,105	$3.89 \cdot 10^7$	935,544	194.9	1.113

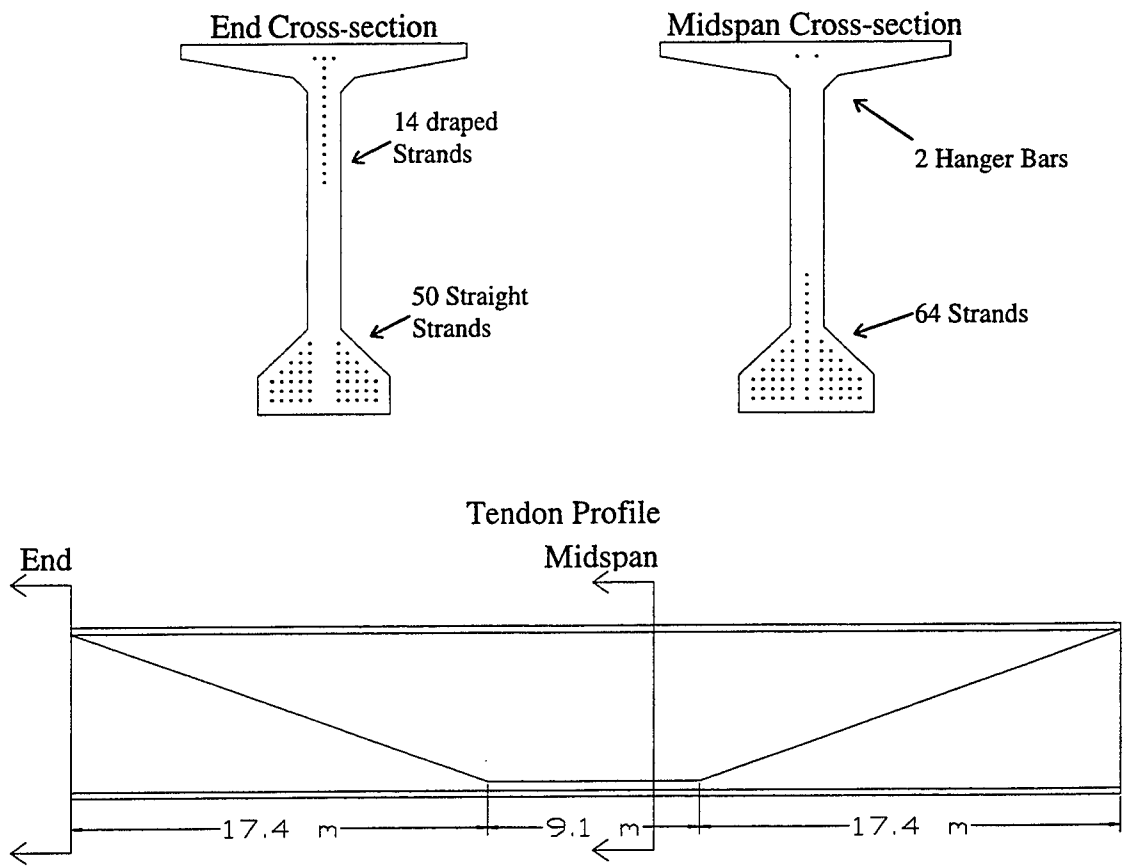


Figure 2-4 Cross-sections and tendon profile for Modified Type VI girder for Westbound Gandy Bridge.

in the girders, they may be considered as fully prestressed. Figure 2-4. shows the end and midspan cross- sections of the girder with tendons, along with the tendon profile of the Modified AASHTO Type VI girder used on the bridge.

2.2 Equipment Used for Instrumentation

2.2.1 Strain Gauges

In order to monitor the strain readings in the four girders investigated, a strain measuring device had to be selected. In addition to strains created by the applied loads, temperature variations also induce strains in concrete members. Therefore, the gauge selected needed the capacity to measure temperature readings as well as strain. This was to allow for the extraction of the temperature effects from the overall strain. Also, the gauge needed to be embedded in the concrete, in order to achieve the strain readings from deep within the girder.

The strain measuring device selected was Model VCE-4200 Vibrating Wire Embedded Strain Gauge, manufactured by Geokon Inc [2]. This vibrating wire strain gauge has the capacity to measure both temperature and strain within the concrete.

2.2.2 Other Equipment Used

In addition to the strain gauges, there are many other pieces of equipment necessary to collect and store strain and temperature readings. The strain gauges work in conjunction with multiplexers to convey strain and temperature readings to a data acquisition system.

Data was collected in two ways for this project. One way of collecting data was by directly connecting a computer to the data acquisition system and collecting. Another alternative was by accessing a cellular phone module, is located within the data acquisition system, and then collecting. This access could be achieved from a remote location by using computer equipped with a modem.

Environmental conditions are also important when considering prestress losses in concrete structures. Of particular importance are the readings of the ambient temperature and the relative humidity because they directly influence the prestress losses

The use of all the aforementioned equipment mentioned required a constant power source. Therefore, a 12-volt rechargeable battery was connected to the data acquisition system. This power source allowed for data to be collected and stored in the storage module. It also allowed the cellular phone module to be turned on for a preset time intervals for data collection via a modem. Since these activities tend to drain the battery, a recharging device had to be used. The battery was recharged in this project via a 20 watt solar panel which was connected to it.

2.3 Girder Instrumentation

2.3.1 Gauge Placement Along Girder Span

Choosing the locations along the span in which to place the vibrating wire strain gauges was important, especially since it was necessary to determine the prestress loss variation with length. Three points of importance were selected along the span of the girders. These points consisted of the midspan, quarter-span, and 1.52 m (5 ft) from the end support. The midspan and the quarter-span are located at 21.95 m (72 ft) and 10.97 m (36 ft) from the end support, respectively. Two of these three points were chosen for each of the beams instrumented.

There are many reasons for these points to be selected along the span. The midspan was chosen because the maximum camber occurs there after the prestress is applied. The maximum deflection also occurs at the midspan after all loads are applied. The choice of the location at 1.52 m (5 ft) from the end support was made because a very small moment is felt at this location. It is also significant because it is beyond the transfer length of the girders. Beyond the transfer length, the concrete will have absorbed the full application of the prestressing force. The final location at the quarter-span was chosen to better define the prestress loss variation along the span because it provides an intermediate point between the losses in the area of the large moment at the midspan, and that of the small moment at 1.52 m (5 ft) from the support.

Of these points, only two locations were selected for each of the four girders instrumented. The distribution is as follows: the midspan of all four girders, 1.52 m (5

ft) from one end support of both Beam 1 and Beam 4, and quarter-span point of Beam 2 and Beam 3. Beams 1 and 2 are exterior girders and Beams 3 and 4 are interior girders when placed on the bridge. Figure 2-5 depicts this distribution.

2.3.2 Gauge Placement Across Girder Cross-section

Since there were three independent locations instrumented along the span, there were three cross-sections to be considered. Each of these cross-sections has its own local properties, as well as global properties which are uniform throughout. It was then necessary to determine which points within each cross-section were significant when considering prestress losses. Once these points were found, vibrating wire strain gauges were placed at these locations. The midspan is considered the most important cross-section for obvious reasons. Therefore, this cross-section logically contained the most strain gauges. Each midspan cross-section contains eight vibrating wire strain gauges within it. (Beam 1 has an additional three gauges. See Section 2.3.3.) A typical instrumented midspan cross-section can be seen in Figure 2-6. The locations 7.62 cm (3 in) and 190.5 cm (75 in) from the bottom of the girder were selected, because this was the closest you can get to the outermost fibers according to the ACI code 318R-95 [3]. The location of 23.57 cm (9.28 in) represents the steel centroid of all the prestressing strands within the cross-section. The choice of 99.06 cm (39 in) was made because this

point is very close to the girder concrete centroid. Since the composite section concrete centroid would occur at about 154.9 cm (61 in) after the deck was placed, this point was also chosen. The points 53.34 cm (21 in), 65.58 cm (27 in), and 175.3 cm (69 in) were picked to show the loss variation between the selected points of significance.

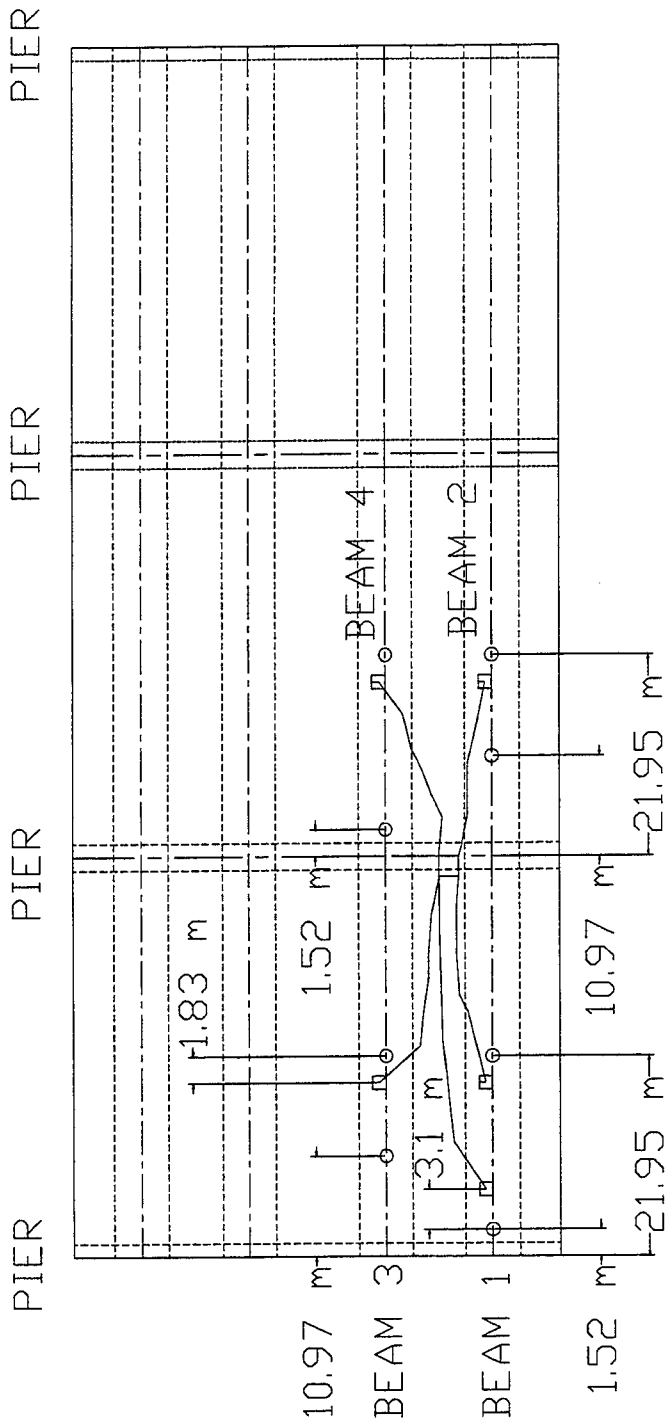


Figure 2-5 Instrumented locations along studied girders

**Midspan Gauge Distribution
8 Total Gauges**

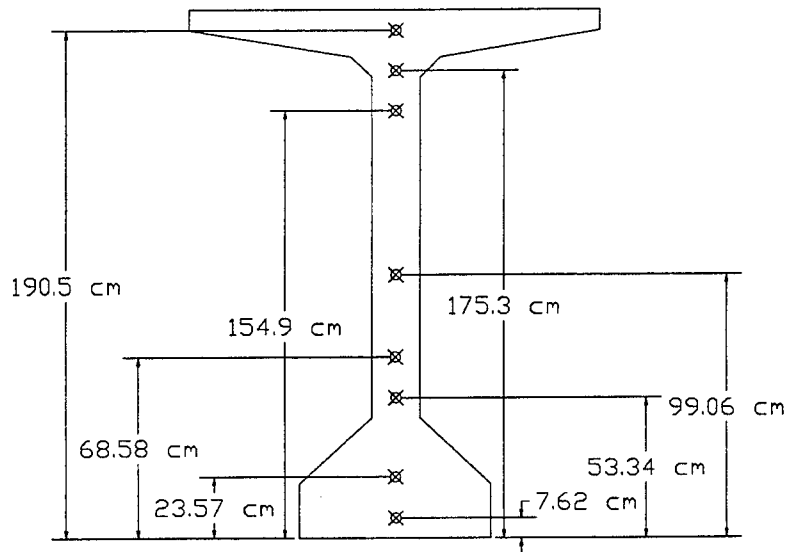


Figure 2-6 Midspan gauge distribution for all Beams studied.

The quarter-span and 1.52 m (5 ft) from the support, each location has six vibrating wire strain gauges located throughout their respective cross-sections. (Beam 1 has an additional three gauges at the 1.52 m (5 ft) from the support. See Section 2.3.3.)

Each of these cross-sections contain the gauges placed at 7.62 cm (3 in), 175.3 cm (69 in), and 190.5 cm (75 in), which are similar to the midspan cross-section. The centroid of the steel in the bottom flange or the straight tendons is 18.80 cm (7.4 in) for both cross-sections, and a gauge was placed at this point also. An additional gauge was placed at the steel centroid of the draped strands for both cross-sections. This location is

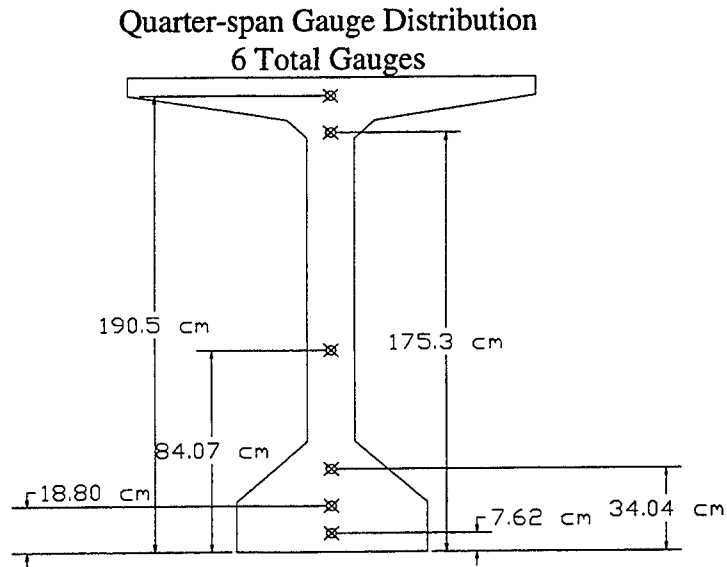


Figure 2-7 Quarter-span gauge distribution for Beams 2 and 3.

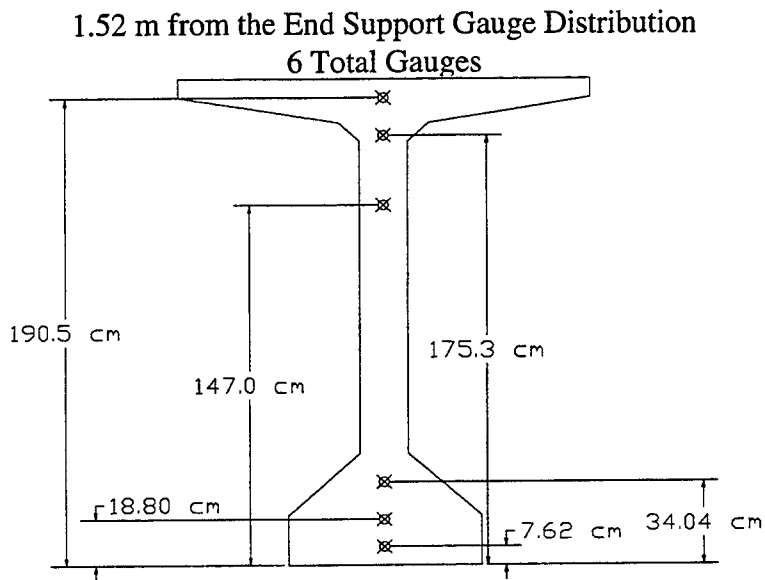


Figure 2-8 Gauge distribution for Beams 1 and 4 at 1.52 m from the end support.

84.07 cm (33.1 in) at the quarter-span and 147.1 cm (57.9 in) at the point located 1.52 m (5 ft) from the support. These two cross-sections can be seen in Figure 2-7 for the quarter-span and Figure 2-8 for the point 1.52 m (5 ft) from the end support.

2.3.3 Gauge Placement Along Strand

In addition to the cross-sectional variation of prestress, another area of interest was how the stress would vary directly along the strands. To determine this, an additional six vibrating wire strain gauges were placed in Beam 1. These gauges were placed at 22.86 cm (9 in) from the bottom at the midspan, and the other three were placed at 17.78 cm (7 in) from the bottom at the point 1.52 m (5 ft) from the support. These gauges were directly attached to the steel tendons at these locations, to secure them from shifting during casting.

2.4 Composite Slab Instrumentation

2.4.1 Introduction

On top of the girders of the Westbound Gandy Bridge, a 20.32 cm (8 in) continuous reinforced concrete deck slab was placed over each three-span unit. This deck causes the girder-deck combination to act as a single unit. Although this concrete deck is not prestressed, it would be interesting to see how and if the prestress losses occurring in the girders below it would effect the slab's stress distribution. Figure 2-9 contains a top

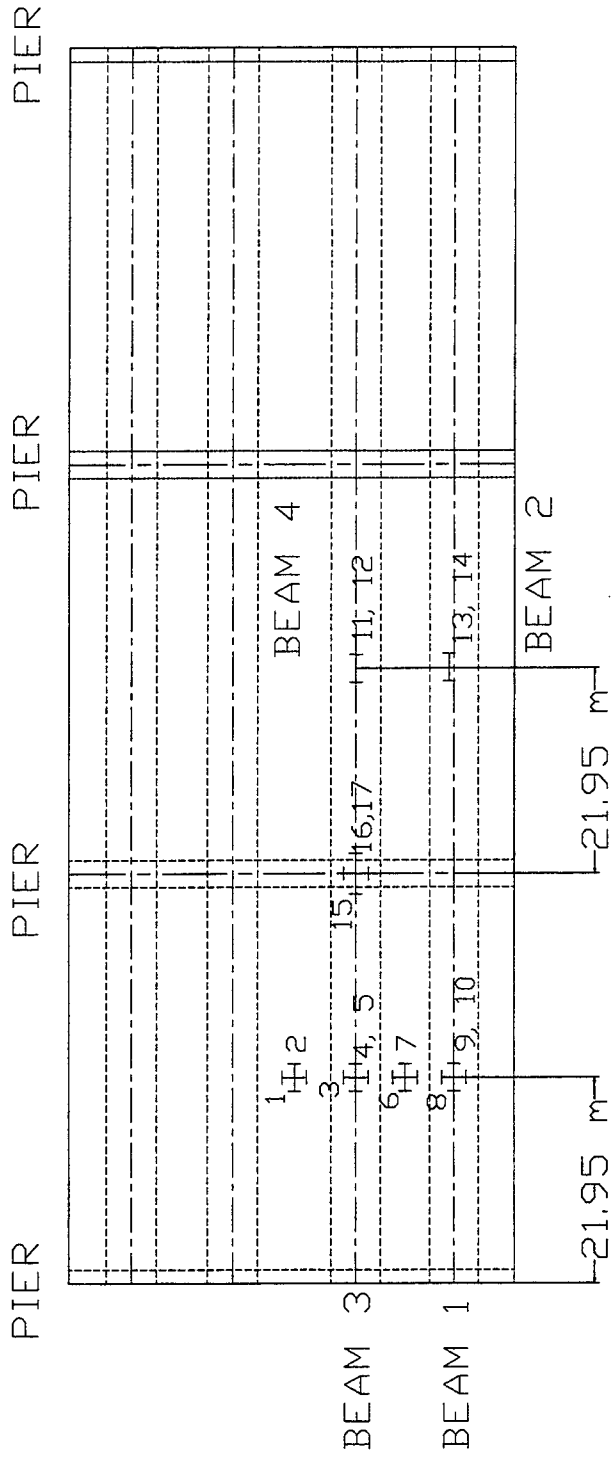


Figure 2-9 Slab gauge distribution for Westbound Gandy Bridge.

Table 2-2 Detailed information about composite slab gauges.

Slab Gauge #	Depth (measured from top of beam)		Location	Orientation (with respect to beam direction)
1	7.62 cm	3.0 in	Midspan of Slab between Beam 3 and North Beam	Perpendicular
2	10.16 cm	4.0 in	Midspan of Slab between Beam 3 and North Beam	Parallel
3	11.43 cm	4.5 in	Midspan of Beam 3	Perpendicular
4	10.16 cm	4.0 in	Midspan of Beam 3	Parallel
5	1.27 cm	0.5 in	Midspan of Beam 3	Parallel
6	13.97 cm	5.5 in	Midspan of Slab between Beam 1 and 3	Perpendicular
7	11.43 cm	4.5 in	Midspan of Slab between Beam 1 and 3	Parallel
8	10.80 cm	4.25 in	Midspan of Beam 1	Perpendicular
9	10.16 cm	4.0 in	Midspan of Beam 1	Parallel
10	2.54 cm	1.0 in	Midspan of Beam 1	Parallel
11	10.16 cm	4.0 in	Midspan of Beam 4	Parallel
12	0.76 cm	0.3 in	Midspan of Beam 4	Parallel
13	12.7 cm	5.0 in	Midspan of Beam 2	Parallel
14	1.27 cm	0.5 in	Midspan of Beam 2	Parallel
15	13.97 cm	5.5 in	At support between Beam 3 and 4	Perpendicular
16	12.7 cm	5.0 in	At support between Beam 3 and 4	Parallel
17	1.27 cm	0.5 in	At support between Beam 3 and 4	Parallel

view of the instrumented deck. Table 2-2 contains information about the depth, location, and orientation of each gauge labeled in Figure 2-9.

2.4.2 Gauge Placement Along the Slab Longitudinal Axis

The choice of points along the slab in which gauges were placed was important, especially since the results obtained would have to work in conjunction with those from the girders. The midspan of each girder would be a natural place for gauges to be placed. Here they would allow a complete stress distribution from the bottom portion of the girder to the top portion of the slab to be determined. Other locations of interest are the points of maximum positive and negative moment in the continuous deck.

2.4.3 Gauge Placement Across Depth of Slab

In the case of the girder, the gauges were placed parallel with the span of the girder in order to obtain stresses in the axial direction. In the concrete deck, however, it is important to obtain stress distributions in both the longitudinal and perpendicular directions of the slab. This is necessary because applied loads create moments, which in turn induce stresses in both directions within the deck.

The gauges were placed at approximately two depth locations within the slab. These two depths are 0 and 10.16 cm (4 in), measured from the top of the girder. The gauges placed at 0 represent the location where the interface between the girder and the slab occurs. There should be a stress discontinuity occurring at this location. The point at 10.16 cm (4 in) was chosen because it is the mid-depth of the 20.32 cm (8 in) thick

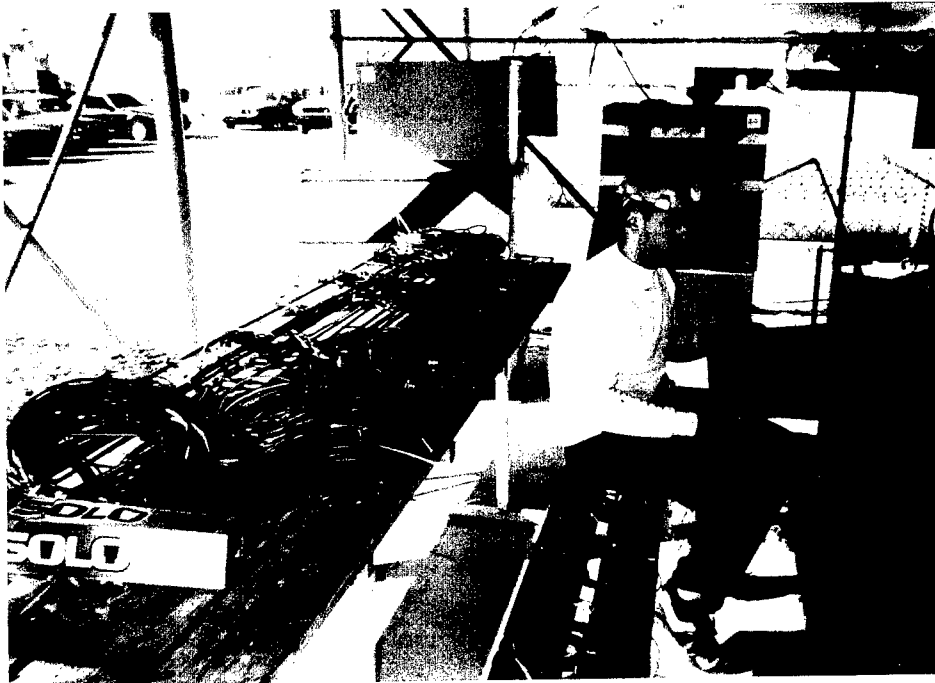
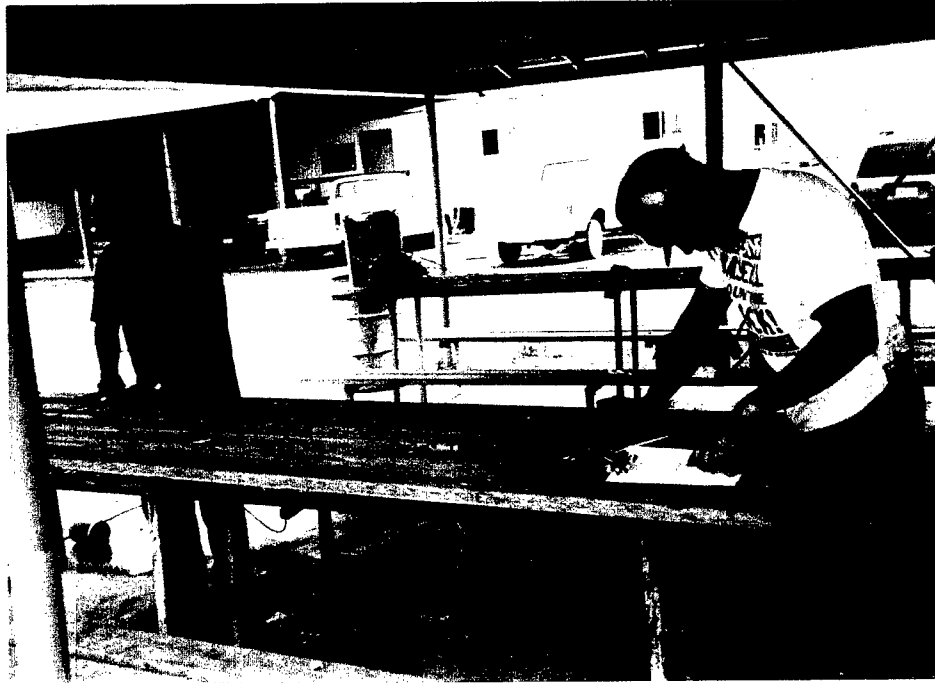
slab. In addition to this 10.16 cm point allows for a determination of the stress distribution between the 20.32 cm point and the 0 cm point.

2.5 Installation of Strain Gauges

2.5.1 Girder Strain Gauges

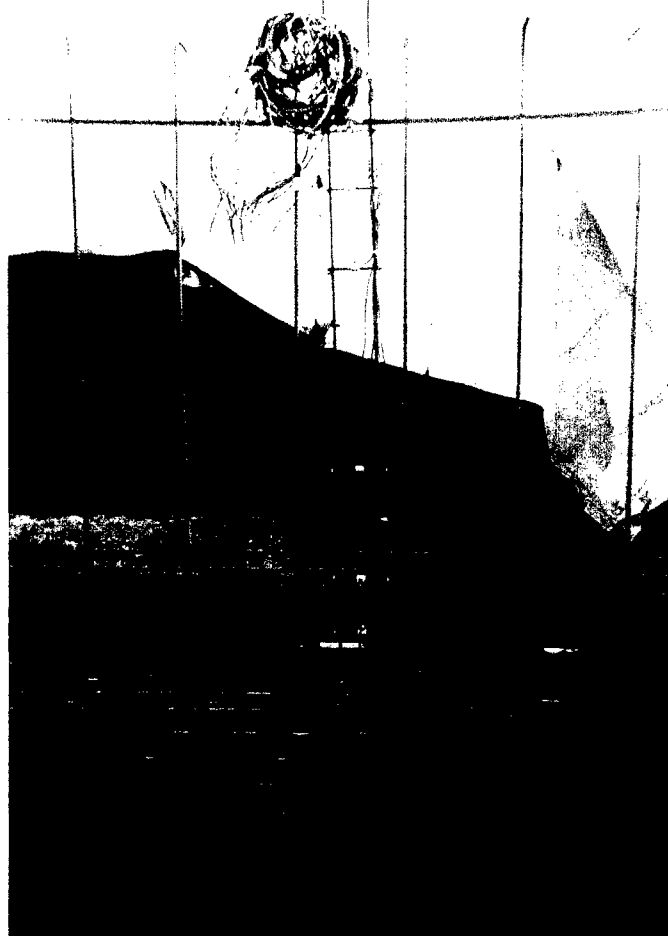
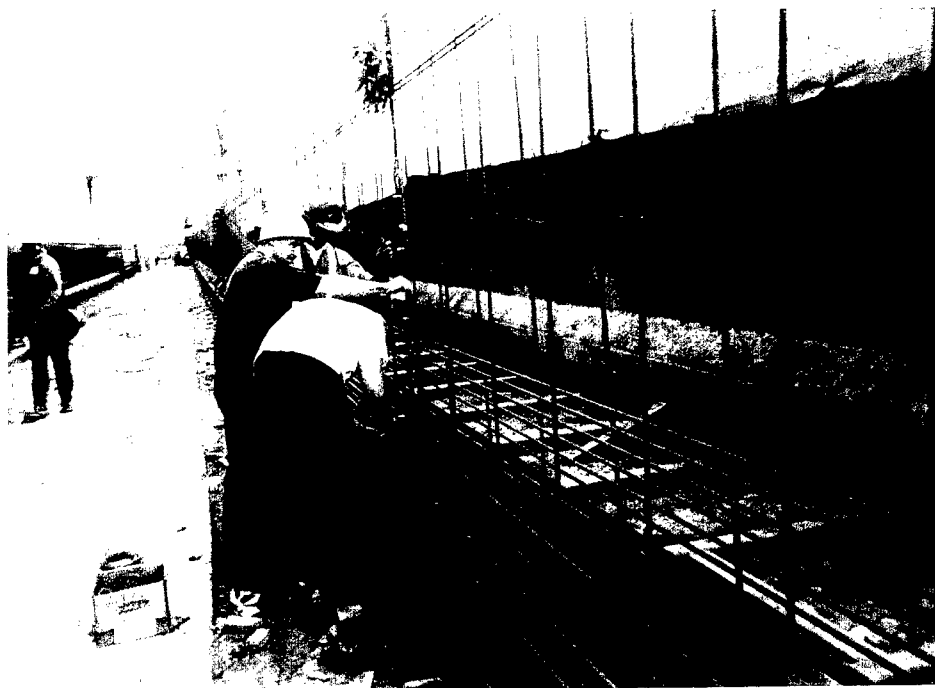
Effective installation of the vibrating wire strain gauges was imperative for this research project to be successful. The strain gauges had to be installed securely, so that they would not shift during the casting of the beams. Secure installation achieved by attaching the gauges to two Number 2 steel rebars. These two rebars were separated by a distance slightly smaller than the width of the gauge, and then these rebars were welded together by two pieces of steel. The location of gauges were marked with chalk on the rebars, and then the gauges were attached with steel tie wire. Finally, the gauge-rebar combination was tied securely to the prestressed steel tendons to keep it in place.

Each of these strain gauges has a wire with a connector attached to its end. It was very important to keep the connectors dry, so they would not be damaged during casting of the concrete. This was achieved by running the wires along the rebar and placing them in several plastic bags above the top flange of the beam. After casting and vibration of the concrete, the wires were removed from the bag and connected to the multiplexers. Then, these multiplexers were connected to the data acquisition system before data collection began. The photographs shown in Figures 2-10(a-d) depicts the gauge installation process for the girders and bridge instrumentation



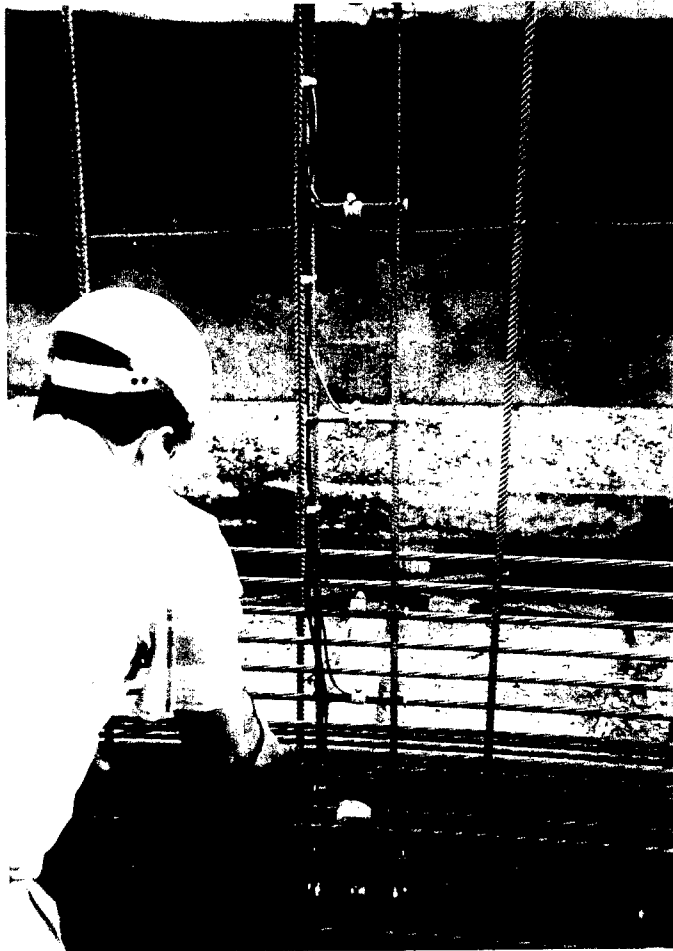
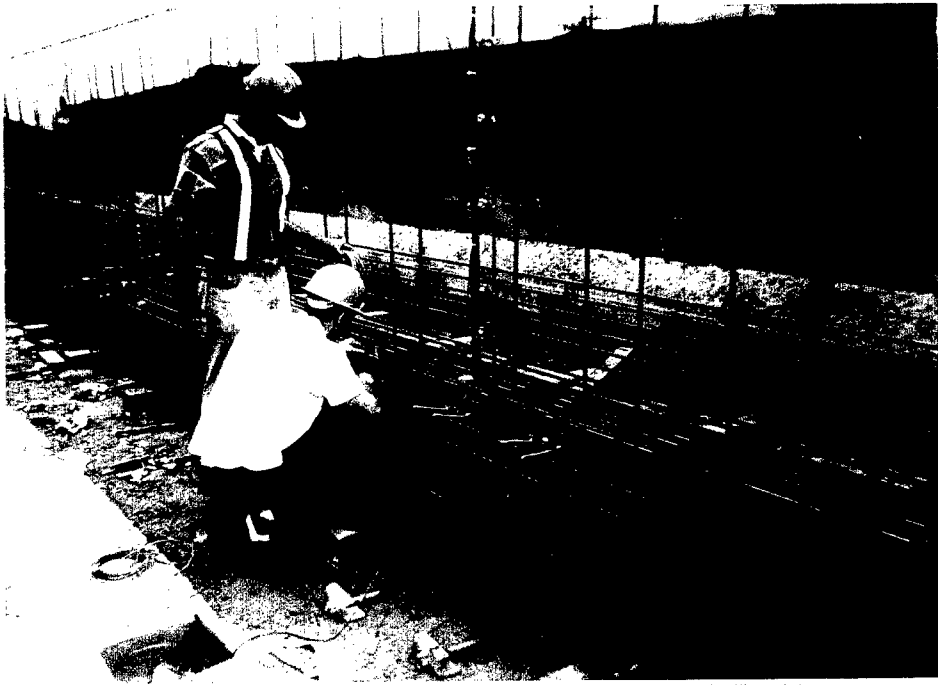
Reproduced from
best available copy.

Figure 2-10a Preparation of strain gauges for placement in girders.



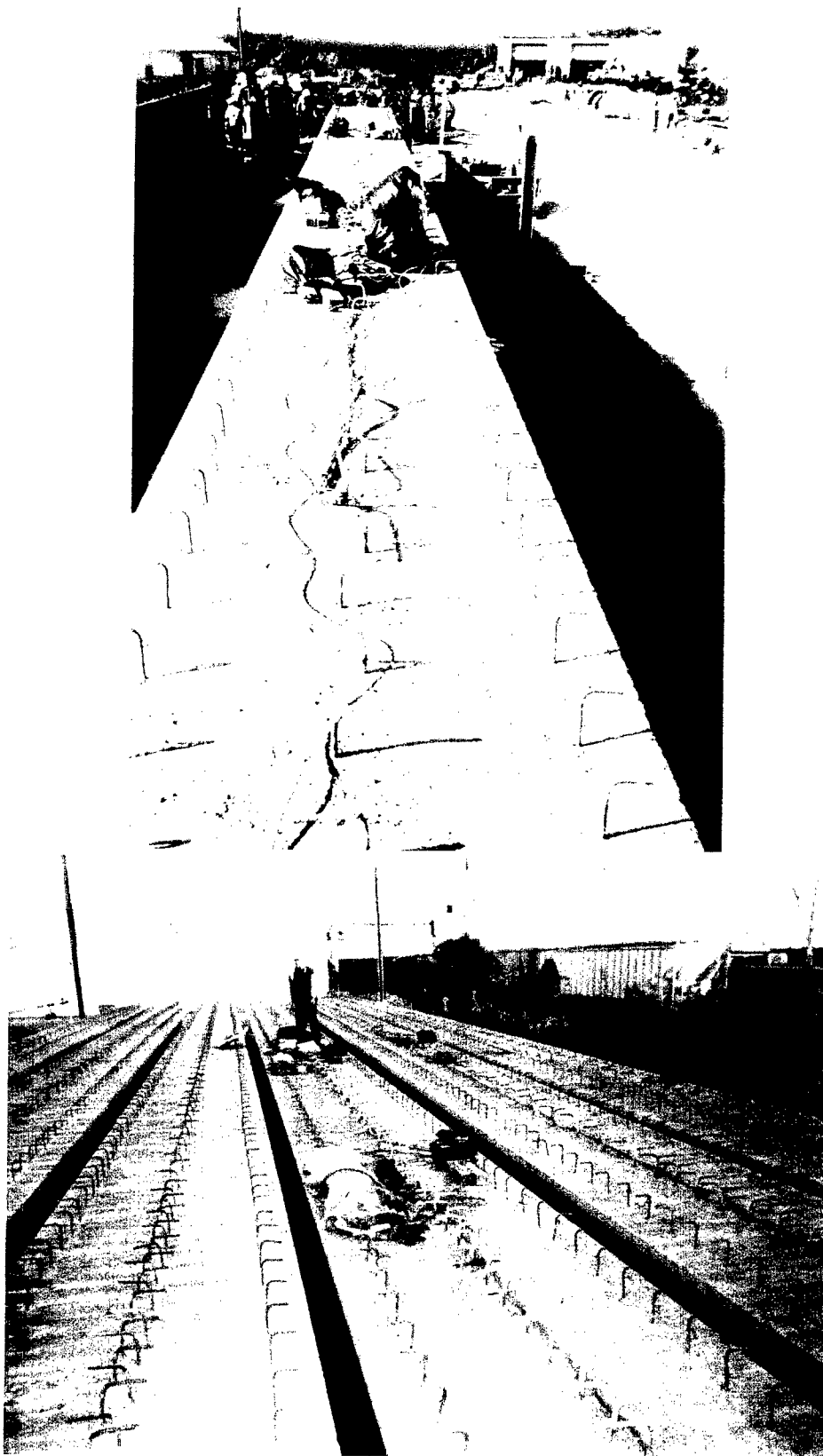
Reproduced from
best available copy.

Figure 2-10b Shows placement of strain gauges within the girders.



Reproduced from
best available copy.

Figure 2-10c Attachment of strain gauges along the steel strands.



Reproduced from
best available copy.

Figure 2-10d The instrumented girders in the staging area awaiting shipment to the bridge site.

2.5.2 Slab Strain Gauges

Instrumentation of the slab gauges promoted a different kind of problem, because the slab forms and steel reinforcement were in place before the gauges could be installed. The strain gauges could not be placed any time earlier because they could have been damaged during the placement of the steel reinforcement for the slab. Hence, the strain gauges were attached to the steel rebar after the slab reinforcement was in place at the specified locations using steel tie wire.

The connecting wire lengths were increased by cutting and soldering longer wires to them. Since the workers walk directly on the reinforcement during casting, the wires could not be placed on top of the reinforcement. (If the wires had been caught between the workers' feet and the rebar, they could have been damaged.) Therefore, all the wires needed to be fed below the steel reinforcement in the slab.

To enable the connection of the gauges to the multiplexers which were attached to the web (see Section 2.6), it was necessary to cut holes in the bottom of the forms, and to pass the wires through to the multiplexers.

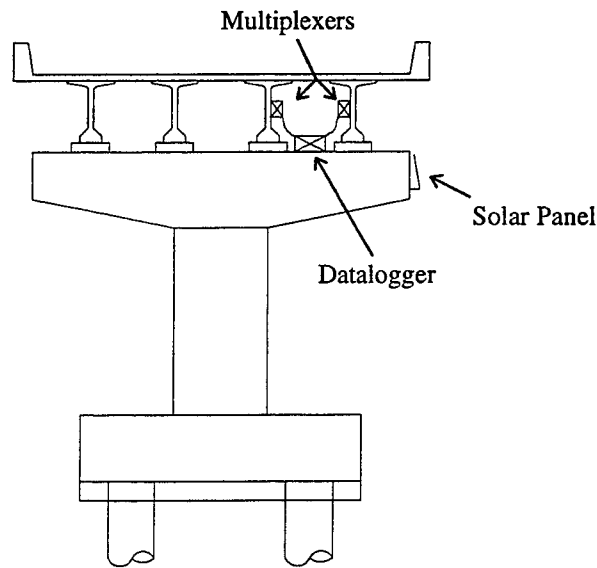


Figure 2-11 Bridge cross-section with equipment.

2.6 Equipment Attachment to Bridge

Once the girders were moved to the bridge, all the equipment had to be permanently secured to the bridge. The multiplexers were directly attached to the web of the girders. A schematic of this can be seen in Figure 2-11. These multiplexers were attached with 5.72 cm (2-¹/₄ in) concrete bolts and a hammer drill. The strain gauge wires and multiplexer wires connected to the data acquisition system required some sag, which had to be accounted for. Attaching clips to the girder webs accounted for the excess sag.

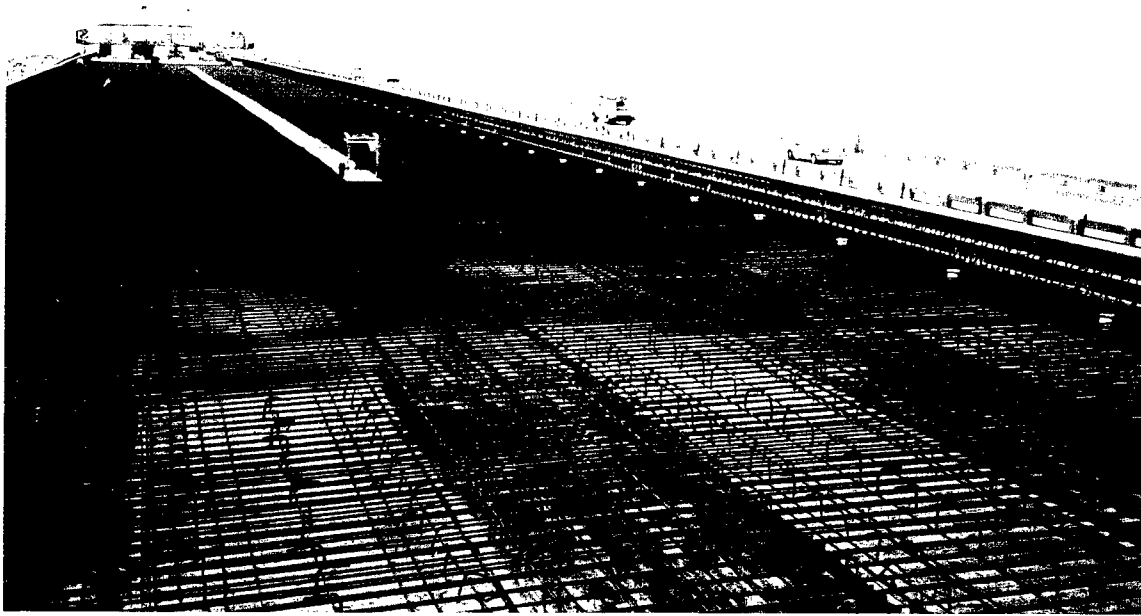
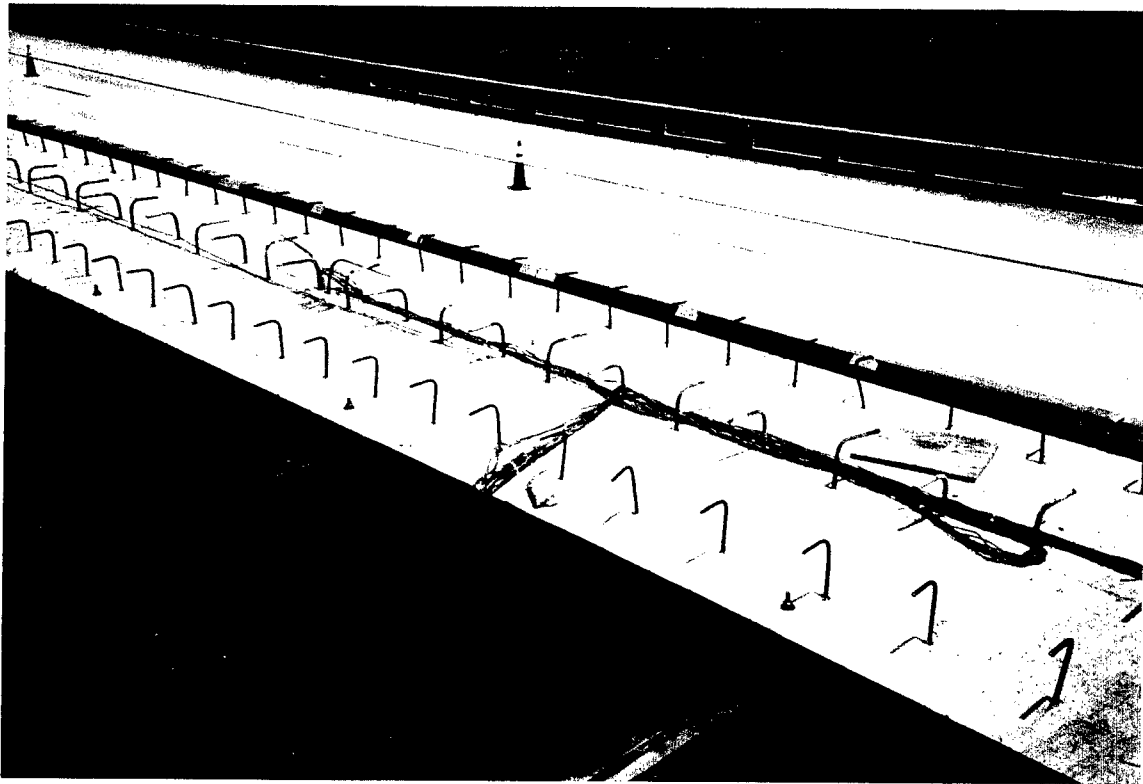
The location of the data acquisition system was important because it had to be easily accessible in case of a problem. The location selected was the pier between the four instrumented beams. Along side of the datalogger is the 12-volt battery, both of which are bolted using concrete bolts. This location allows for the datalogger to be accessed by a ladder placed at the footer.

It was important to get the solar panel in an area where it would be directly exposed to sunlight, to allow it to recharge the battery effectively. The relative humidity and ambient temperature probe, and cellular phone antenna had to be in a location where their readings or waves would not be inhibited. Hence, all of these three pieces of equipment were attached to the outside of the pier. Figures 2-12(a-c) shows pictures of the equipment attachment at the bridge site, and views of the bridge girder & deck reinforcement before the deck was poured.

2.7 Shrinkage Cylinders

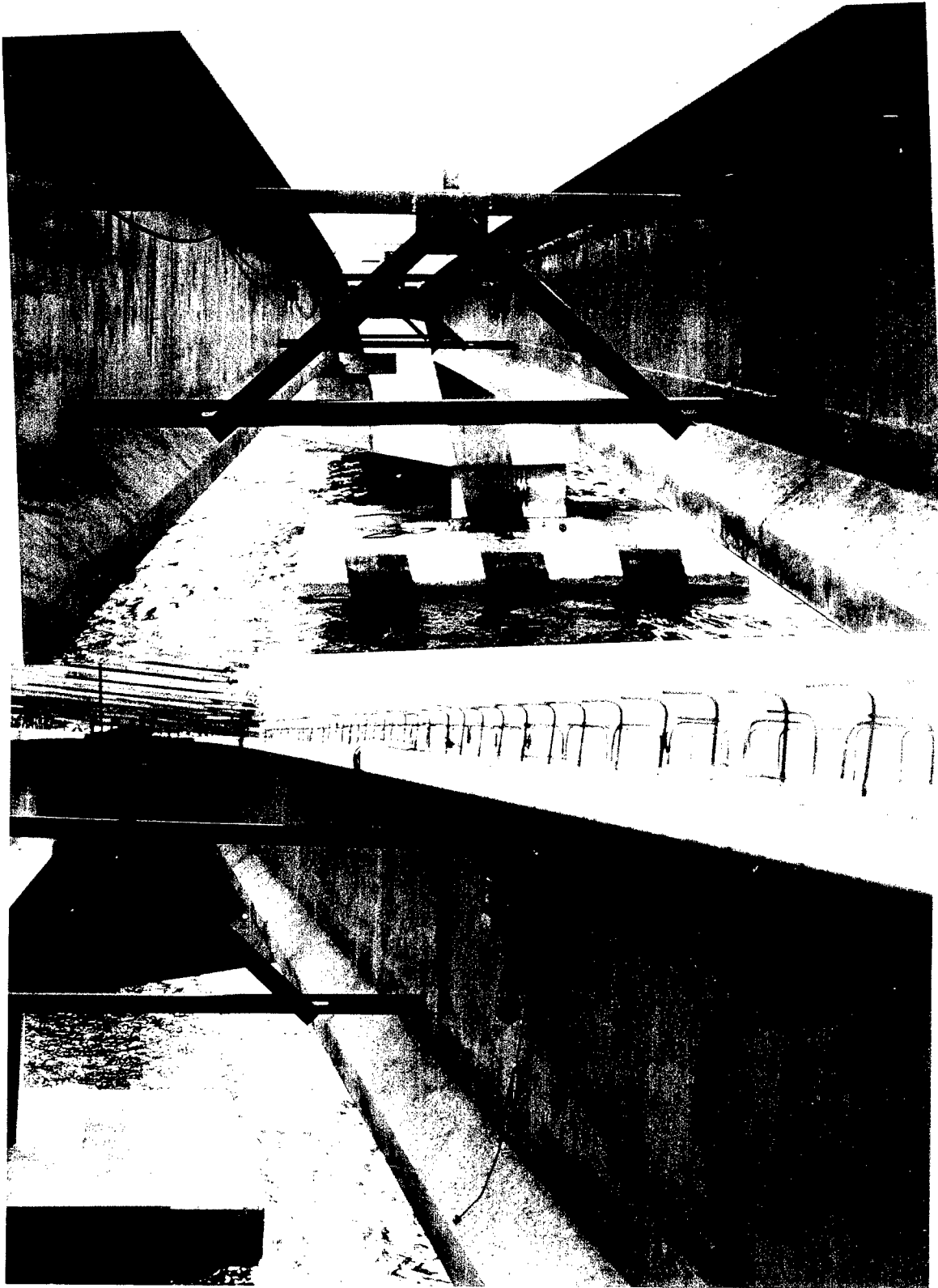
In trying to extract the components of the time-dependent prestress loss, it is important to get as much information about the concrete as possible. It was decided that five 15.24 cm by 30.48 cm (6 in by 12 in) cylinders would be cast for the purpose of determining shrinkage strains in concrete. These cylinders were made from the same concrete batch as used for the girders, and exposed to the same environmental conditions as the girders.

Each of these shrinkage cylinders are instrumented with similar vibrating wire strain gauges that were used in the girders and the deck. The gauge was placed in the center of the cylinder mold, and held in place by three steel tie wires to allow measurement of axial strain. These tie wires pass through small holes in the mold, and are taped to the outside of the mold to hold it in place. A slit on the top of the mold was left so the wire could be connected to the multiplexer.



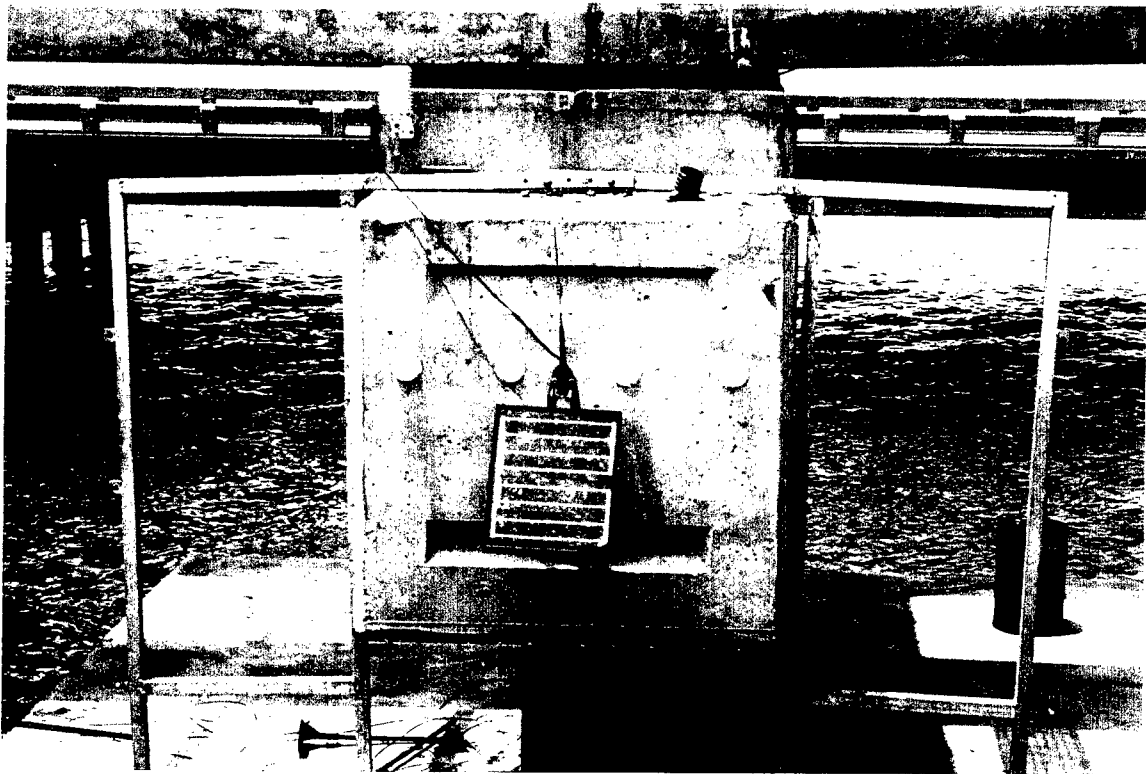
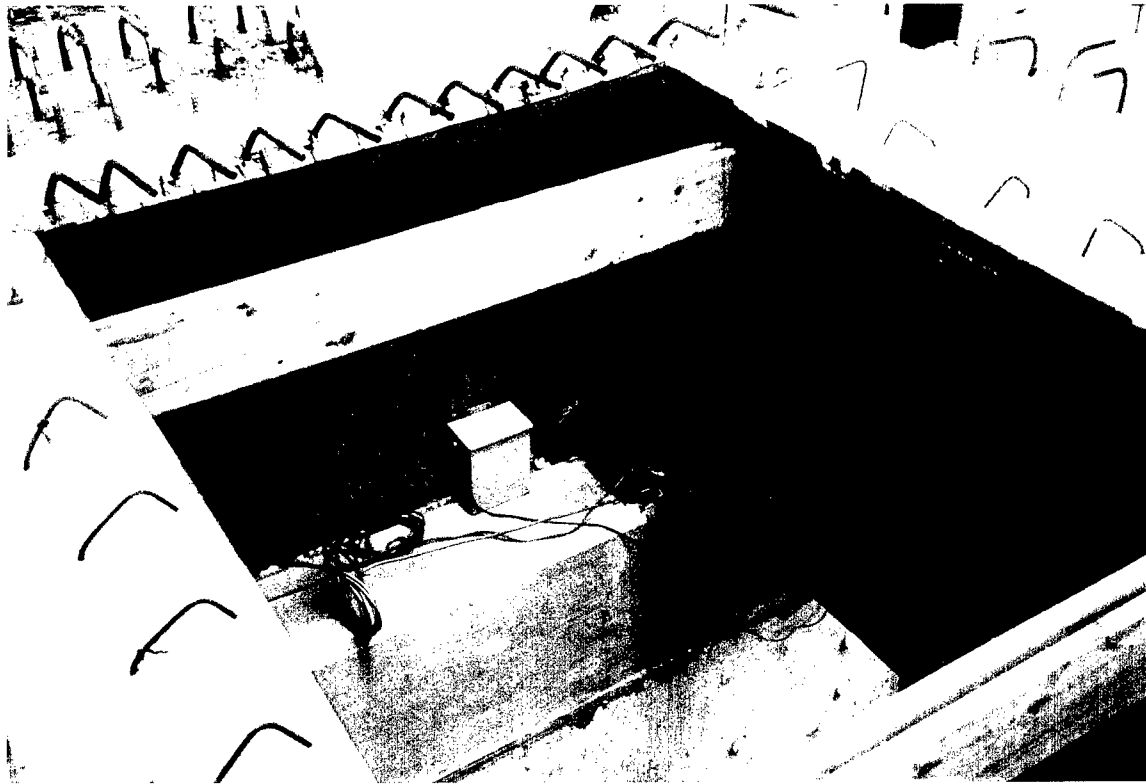
Reproduced from
best available copy.

Figure 2-12a Placement of girder on bridge pier and bridge deck with reinforcement in place.



Reproduced from
best available copy.

Figure 2-12b Multiplexers attached to girder web with slack in the connecting wires.



Reproduced from
best available copy.

Figure 2-12c Location of data acquisition system and battery (top) and solar panel, cellular phone antenna, and relative humidity probe (bottom).

The girders and cylinders were cast at the same time. The cylinders were exposed to the same conditions as the girders from conception to the bridge site. Once at the bridge site, the cylinders were placed on an adjacent pier to that where the datalogger is located. The wires from the cylinders are attached to the side of the girders, similar to those of the multiplexers and girder gauge wires. The photographs in Figure 2-13a shows the preparations of a typical shrinkage cylinder mold before casting. Figure 2-13b, the shrinkage cylinders are shown on the girder in the staging area, and at their final locations when moved to the bridge site.

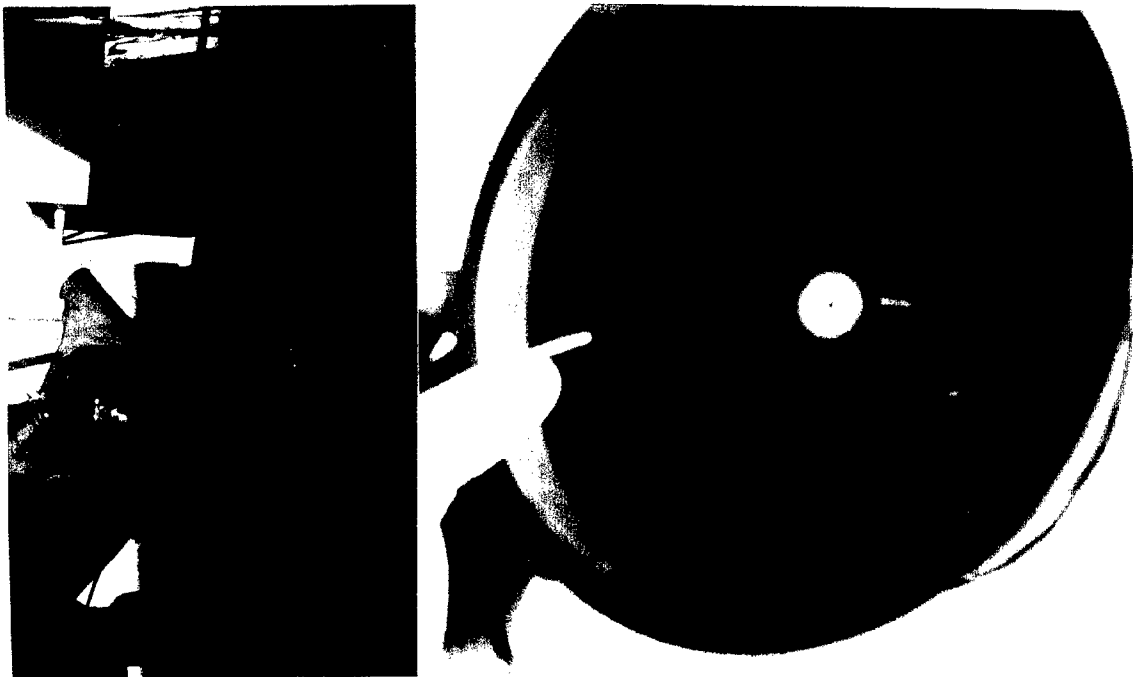


Figure 2-13a A Preparation of shrinkage cylinder mold with strain gauge.

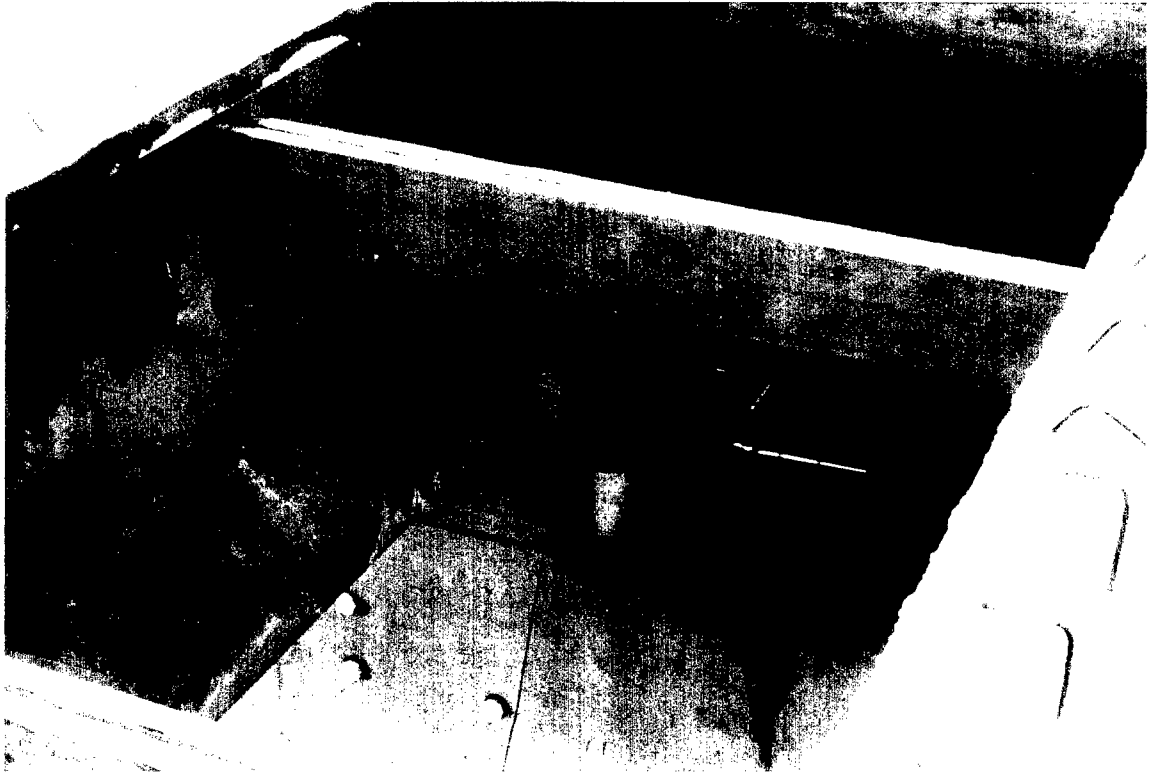


Figure 2-13b Shrinkage cylinders on top of the girder and at the bridge site.

Reproduced from
best available copy. 

2.8 Modulus of Elasticity

2.8.1 Introduction

The modulus of elasticity of any material directly relates the stress to the strain according to Hooke's Law, which is $\sigma = E \cdot \epsilon$. The symbols σ , E , and ϵ , are the stress, modulus of elasticity, and strain for a given material, respectively. For concrete, this linear relationship holds true initially, but becomes nonlinear after a certain point.

2.8.2 ACI 318-95 Definition of E_c

The American Concrete Institute Building Code Requirements for Reinforced Concrete of 1995 (ACI 318-95), defines the modulus of elasticity of material as the ratio of the normal stress to its strain for either tensile or compressive stresses under the proportional limit of that material as described in Section 2.1 of the Code. For concrete, the 95 Code states in Section 8.5 Commentary that the modulus of elasticity of concrete, E_c , is the slope of the line drawn from 0 to $0.45f'_c$ on a stress strain curve, where f'_c is defined as the 28-day compressive strength of concrete. It also states that measured E_c values may range from 80 to 120 percent of the calculated value.

The equation suggested by the ACI to determine E_c is based on w_c and f'_c . Where w_c is the specific weight of the concrete in lb/ft^3 and f'_c is in psi. For w_c ranging from 90 to 155 lb/ft^3 the equation for E_c in Section 8.5 of the Code is as follows:

$$E_c = w_c^{1.5} 33\sqrt{f'_c} \quad (2-1)$$

This is the equation typically used in design.

2.8.3 Experimental Determination of E_c

The actual modulus of concrete tends to deviate as a function of time from the equation suggested by ACI. A more accurate modulus for concrete could give a better representation of what the actual prestress losses are. With this in mind, an additional twenty test cylinders, 15.24 cm by 30.48 cm (6 in by 12 in) were cast from the concrete batch used, so that the modulus of concrete could be determined experimentally.

The experiments were performed at the CEEFL (the Civil and Environmental Engineering Field Lab) at the University of Central Florida. The equipment used was a compressive strength machine manufactured by SATEC Systems, Inc., Grove City, Pennsylvania, and a strain measuring box borrowed from the Florida Department of Transportation Structures Laboratory, Tallahassee, Florida. The strain gauges used were attached to the outside of the cylinder being tested. From the testing, the following measurements of the compressive strength and elastic modulus were recorded. Table 2-3 contains the experimental results from this testing. The plots for the experimental determined modulus of elasticity can be found in Appendix A.

Table 2-3 Experimental results using concrete collected during casting of Beams 1 and 4.

Experiment Results for f_c' and E_c Conducted at CEEFL, UCF				
Time	f_c'		E_c	
Days	MPa	psi	GPa	ksi
1	27.983	4058.5	30.097	4365.1
2	35.981	5218.5	23.772	3447.8
3	39.170	5680.9	29.275	4245.9
5	43.603	6323.9	36.215	5252.4
7	45.777	6639.1	27.625	4006.5

The values E_c were obtained using a linear regression with the stress-strain curves data generated by the testing upto $0.45f_c'$. In this report, another method of calculating E_c is used in order to avoid including large experimental errors in the values obtained. The elastic modulus is an essential component in this study and is needed to be computed as a function of time.

2.8.4 CEB-FIP Model Code 1990 Method for Determining $E_c(t)$

In the text “Concrete Structures: Stresses and Deformations,” by Ghali and Farve[4], it suggests a few different methods for determining the time-dependent modulus of elasticity of concrete. The method used here is that which was suggested by the

CEB-FIP Model Code 1990 [5]. This committee suggests the following equation for determining the 28-day modulus of elasticity:

$$E_c(28) = 21500 \left(\frac{f_{cm}}{f_{cm0}} \right)^{\frac{1}{3}} \quad (2-2)$$

In Equation 2-2, f_{cm} is the mean compressive strength at 28 days in MPa, and f_{cm0} is equal to 10 MPa. The mean compressive strength, f_{cm} , is related to the characteristic strength, f_{ck} , as follows:

$$f_{cm} = f_{ck} + \Delta f \quad (2-3)$$

In Equation 2-3, the quantity Δf is equal to 8 MPa. The characteristic strength, f_{ck} , is obtained performing compression tests on 15.0 cm by 30.0 cm (6 in by 12 in) cylinders stored in water at 20 ± 2 °C and tested 28 days after casting. So Equation 2-2 can now be rewritten as follows:

$$E_c(28) = 21500 \left[\frac{(f_{ck} + \Delta f)}{f_{cm0}} \right]^{\frac{1}{3}} \quad (2-4)$$

The time-dependent modulus $E_c(t)$ is estimated by the following equation:

$$E_c(t) = \beta_E(t) E_c(28) \quad (2-5)$$

where

$$\beta_E = \sqrt{e^{\left[s \left(1 - \sqrt{\frac{28}{t}} \right) \right]}} \quad (2-6)$$

In Equation 2-6, the time t is measured in days, and s is a coefficient depending on the type of cement used. For rapid hardening high strength cements, s is equal to 0.2, as it was taken for this project.

2.8.5 Calculating $E_c(t)$ and Comparing to Design

In order for Equation 2-6 to be effective, it is necessary to have a reliable source of f_{ck} . The closest quantity available to f_{ck} is f_c' at 28 days so this was used as a substitute. The Quality Control personnel at the Hardaway Company in Tampa, Florida, measured compressive strength at the time of transfer, and at 7 and 28 days after the concrete was cast. For each beam, two tests were performed for each day mentioned. The only values needed here are those for f_c' at 28

Table 2-4 Values of the 28 day compressive strength tests for the girders (Courtesy of Hardaway Company, Prestress Division, Tampa, Florida).

f _c ' Values that will used as f _{ck} in Equation 2.4 for E _c (28)			
Beam 1 and Beam 4		Beam 2 and Beam 3	
MPa	psi	MPa	psi
57.316	8313	54.879	7959

days. Since Beams 1 and 4 were cast on the same day using the same concrete batch, their compressive strengths were averaged to come up with one value. Similarly, the procedure was done for the compressive strengths of Beams 2 and 3. The results obtained can be seen in Table 2-4. It is interesting to note that the original design was

done on the assumption of f_c' of 44.8 MPa (6500 psi), but the strength achieved in the field was much greater. With the quantities in Table 2-4, it is now possible to obtain values of $E_c(t)$. These values will be included in Table 2-5 and compared to those from the original design.

Now that all the parameters have been established, the calculation of $E_c(t)$ can proceed. The calculated values E_c' for Beams 1 and 4 and Beams 2 and 3 versus the design-calculated values are shown in Table 2-5. As mentioned earlier, the results using another method, the ACI Committee 209 method for determining $E_c(t)$ can be found in Appendix B. The actual design was based on the CEB-FIP Method, hence it was used over the ACI Committee Method in this study.

These E_c values according to CEB-FIP were used in determining the prestress loss of the members analyzed in this project. Additional days, which were between those values reported in Table 2-5, were calculated and used in the loss calculations as well. All the calculated E_c values were multiplied by 0.9 in accordance with FDOT guidelines for concrete using limerock aggregate.

Table 2-5 Design $E_c(t)$ versus $E_c(t)$ calculated by CEB-FIP Model Code 1990 Method.

Design and Calculated Values for E_c						
Time	Design		Beams 1 and 4		Beams 2 and 3	
	E_c		E_c		E_c	
Days	GPa	ksi	GPa	ksi	GPa	ksi
3	29.138	4226	25.0326	3630.51	33.7185	3584.97
7	30.892	4480.3	27.8181	4034.52	27.4689	3983.85
14	31.637	4588.4	29.4966	4277.88	29.1258	4224.24
28	32.03	4656.4	30.744	4188.87	30.3579	4403.34
40	32.151	4662.8	31.2498	4532.22	30.8574	4475.34
60	32.246	4676.7	31.7331	4602.42	31.3353	4544.64
80	32.293	4683.5	32.0256	4644.72	31.6233	4586.4
100	32.322	4687.7	32.2254	4673.79	31.8213	4615.11
120	32.341	4690.5	32.3748	4695.39	31.968	4636.44
400	32.409	4700	33.0894	4799.07	32.6745	4738.86
2000	32.432	4703.7	33.5772	4869.81	33.156	4808.7
10000	32.437	4704.4	33.7977	4901.76	33.3738	4840.2

CHAPTER 3

CODE TREATMENT OF PRESTRESS LOSS

3.1 Introduction

There are several different methods for determining the prestress loss of a member. The accepted methods are defined by various legal bodies. The American Association of State Highway and Transportation Officials (AASHTO) is the legal body that sets the standards for bridge design. The Prestressed Concrete Institute (PCI) suggests the methods of design for both prestressed and precast concrete. The standards for both prestressed and conventional concrete are specified by the American Concrete Institute (ACI).

Although these bodies have different methods for determining the prestressed loss for various types of members, the ACI and PCI methods stem from the same article and will be combined as one. In the sections that follow, a brief overview of how these bodies determine prestress loss will be presented and discussed. At the end, a spreadsheet program will be used to calculate the results for the methods presented.

The units specified for the equations in this chapter are based on the English system of units.

3.2 AASHTO-LRFD Method for Determining Prestress Loss

3.2.1 Introduction

The AASHTO-LRFD method defines the prestress loss for both pretensioning and post-tensioning in Section 5.9.5 [6]. The prestress loss is broken into an instantaneous portion and a time-dependent portion. The AASHTO-LRFD method offers two options for determining the time-dependent prestress loss. The first option is a lump sum based on the type of member being examined, the 28-day compressive strength of that member, and the partial prestressing ratio. The other option is a refined calculation of each of the components of the time-dependent loss.

3.2.2 Total Prestress Loss

The AASHTO-LRFD in Section 5.9.5.1 defines the total prestress loss for pretensioned members that are constructed and prestressed in a single stage as follows:

$$\Delta f_{pT} = \Delta f_{pES} + \Delta f_{pSR} + \Delta f_{pCR} + \Delta f_{pR} \quad (3-1)$$

The variables in Equations 3.1 are defined in ksi as follows:

Δf_{pT} = total loss

Δf_{pSH} = loss due to shrinkage

Δf_{pCR} = loss due to creep of concrete

Δf_{pR} = loss due to relaxation of steel

Δf_{pES} = loss due to elastic shortening

The AASHTO-LRFD also states that the portion of steel relaxation loss occurring the before transfer of stress to the concrete may be deducted from the total relaxation loss.

3.2.3 Instantaneous Losses

Section 5.9.5.2 of the AASHTO-LRFD discusses the methods for determining the instantaneous losses. These losses are comprised of anchorage set, friction, and elastic shortening.

3.2.3.1 Anchorage Set Loss

Section 5.9.5.1 of the AASHTO-LRFD states that the anchorage set loss is the larger of two possible slips. The first slip is what is measured while the anchorage is restraining the stress in the prestressing steel, before and at transfer. The other slip is the amount suggested by the manufacturer of the anchor system. The commentary to this section recommends possible values of slip, depending on the type of equipment used, if none are available. These are mainly compensated for by overstressing in pretensioning, hence it is often accounted for in post-tensioned construction only.

3.2.3.2 Frictional Losses

Section 5.9.5.2.2 of AASHTO-LRFD states that the frictional losses should be considered at the hold-down devices for pretensioned members that have draped strands.

3.3.2.3 Elastic Shortening

Section 5.9.5.2.3 of AASHTO-LRFD presents the methods for determining the elastic shortening for both pretensioned and post-tensioned members. The elastic shortening loss for pretensioned members is as follows:

$$\Delta f_{pES} = \frac{E_p}{E_{ci}} f_{cgp} \quad (3-2)$$

The variables in Equations 3-2 are defined as follows:

f_{cgp} = sum of concrete stresses at the center of gravity of prestressing tendons due to the prestressing force at transfer and the self-weight of the member at the sections of maximum moment (ksi)

E_p = modulus of elasticity of prestressing steel (ksi)

E_{ci} = modulus of elasticity of concrete at transfer (ksi)

This section also suggests that, for the usual design of pretensioned members, f_{cgp} be calculated at an assumed stress of $0.65f_{pu}$ for stress-relieved strands and high strength bars and $0.70f_{pu}$ for low relaxation strands.

3.2.4 Lump Sum Approximation for Time-Dependent Losses

Section 5.9.5.3 of the AASHTO-LRFD Code suggests the use of an approximate method for determining the total of all the time-dependent losses. This method can be

used for pretensioned members, if the compressive strength at transfer is greater than or equal to 24.1 MPa (3.5 ksi). It may also be used for post-tensioned members, if the members are non-segmental with spans up to 48.8 m (160 ft), and if the stress transfer occurs between 10 and 30 days after casting. In addition to these criteria, the following material conditions must also be true for both types of tensioning: the member must be constructed from normal weight concrete and be either steam or moist cured, and the prestressing strands or bars used within the member must have normal or relaxation properties. Average exposure conditions and temperatures must be felt by the member during its lifetime.

This approximate method is a function of f_c' and PPR (partial prestressing ratio). Table 3-1 gives a listing of the applicable equations when using this procedure. The variable PPR is defined in Section 5.5.4.2 of the AASHTO-LRFD Code as follows:

$$PPR = \frac{A_{ps} F_{py}}{A_{ps} F_{py} + A_s F_y} \quad (3-3)$$

The variables in Equation 3-3 are defined as follows:

A_s = area of non-prestressed tension reinforcement (in²)

A_{ps} = area of prestressing steel (in²)

F_y = specified yield strength of reinforcing bars (ksi)

F_{py} = yield strength of prestressing steel (ksi)

Table 3-1 Equations used for lump sum prestress loss calculation according to AASHTO-LRFD

Type of Beam Section	Level	For Wires or Strands with $f_{pu} = 235, 250, \text{ or } 270 \text{ ksi}$	For Bars with $f_{pu} = 145 \text{ or } 160 \text{ ksi}$
Rectangular Beams, Solid Slab	Upper Bound Average	29.0 + 4.0 PPR 26.0 + 4.0 PPR	19.0 + 6.0 PPR
Box Girder	Upper Bound Average	21.0 + 4.0 PPR 19.0 + 4.0 PPR	15.0
I-Girder	Average	$33.0 \left[1.0 - 0.15 \frac{f_c' - 6.0}{6.0} \right] + 6.0 \text{ PPR}$	19.0 + 6.0 PPR
Single T, Double T, Hollow Core and Voided Slab	Upper Bound Average	$39.0 \left[1.0 - 0.15 \frac{f_c' - 6.0}{6.0} \right] + 6.0 \text{ PPR}$ $33.0 \left[1.0 - 0.15 \frac{f_c' - 6.0}{6.0} \right] + 6.0 \text{ PPR}$	$31.0 \left[1.0 - 0.15 \frac{f_c' - 6.0}{6.0} \right] + 6.0 \text{ PPR}$

The values obtained from equations of Table 3-1 can be reduced if low relaxation strands are used. Box girders can be reduced by 27.6 MPa (4.0 ksi). Rectangular beams, solid slabs, and I-girders can be reduced by 41.4 MPa (6.0 ksi). Single T's, double T's, hollow core, and voided slabs can be reduced by 55.2 MPa (8.0 ksi).

3.2.5 Detailed Estimates of the Time-Dependent Losses

Section 5.9.5.4 of the AASHTO-LRFD Code discusses methods for determining the individual components of the time-dependent prestress loss. Creep and shrinkage of concrete and steel relaxation make up the total time-dependent prestress loss. The methods in this section can be applied to non-segmental prestressed members that have spans less than 76.2 m (250 ft), are made up of normal density concrete, and have a compressive strength of 24.1 MPa (3.5 ksi) at time of transfer.

3.2.5.1 Shrinkage

Section 5.9.5.4.2 of the AASHTO-LRFD Code states that the shrinkage prestress loss is only a function of one variable for both pretensioned and post-tensioned members. The average annual ambient relative humidity, H , in percent, is that variable. The shrinkage loss is as follows:

$$\Delta f_{\text{psr}} = (17.0 - 0.150H) \quad (3-4)$$

Equation 3-4 applies for pretensioned members.

3.2.5.2 Creep

In Section 5.4.5.4.3 of the AASHTO-LRFD Code, the creep loss is considered the same for both pretensioned and post-tensioned members and is defined as follows:

$$\Delta f_{pCR} = 12.0f_{cgp} - 7.0\Delta f_{cdp} \geq 0 \quad (3-5)$$

The variables in Equation 3-5 are defined as follows:

f_{cgp} = concrete stress at the center of gravity of prestressing steel at transfer (ksi)

Δf_{cdp} = change in concrete stress at the center of gravity of prestressing steel due to permanent loads, except the load acting at the time prestressing force is applied.

3.2.5.3 Steel Relaxation

In Section 5.9.5.4 of AASHTO-LRFD Code, the steel relaxation loss is broken into two portions for pretensioned members. The first portion is the steel relaxation that begins after the strands are stressed, and ends upon transfer of the stress from the steel to the concrete. This steel relaxation loss calculated at transfers is as follows:

$$\Delta f_{pR1} = \frac{\log(24.0t)}{10.0} \left[\frac{f_{pj}}{f_{py}} - 0.55 \right] f_{pj} \quad (3-6)$$

$$\Delta f_{pR1} = \frac{\log(24.0t)}{40.0} \left[\frac{f_{pj}}{f_{py}} - 0.55 \right] f_{pj} \quad (3-7)$$

Equation 3-6 applies for stress-relieved strands and Equation 3-7 applies for low-relaxation strands. The variables in Equations 3-6 and 3-7 are as follows:

t = time estimated in days from stressing to transfer (days)

f_{pj} = initial stress in the tendon at the end of stressing just before transfer (ksi)

f_{py} = specified yield strength of prestressing steel (ksi)

The second portion of the steel relaxation loss that applies for pretensioned members, takes place after the stress is transferred. The steel relaxation loss in post-tensioned members occurs only at this stage. The equations for this is as follows:

$$\Delta f_{pR2} = 20.0 - 0.4\Delta f_{pES} - 0.2(\Delta f_{pSR} + \Delta f_{pCR}) \quad (3-8)$$

$$\Delta f_{pR2} = 20.0 - 0.3\Delta f_{pF} - 0.4\Delta f_{pES} - 0.2(\Delta f_{pSR} + \Delta f_{pCR}) \quad (3-9)$$

Equation 3-8 is for pretensioned members with stress-relieved strands and Equation 3-9 for post-tensioned members with stress-relieved strands. All variables are defined as before. If low relaxation prestressing steel is used the value of Δf_{pR2} can be taken as 30% of those obtained using Equations 3-8 or 3-9.

3.3 ACI-PCI Method

3.3.1 Introduction

In Section 18.6 of the ACI 318R-95 Code, are given the types of loss that should be accounted for in prestress concrete design [3]. It also only gives equations for determining frictional losses in post-tensioned tendons. In the Commentary to this section, it suggests using the Zia et. al. for estimating the prestress losses [7].. This same report is the premise for the method described in Section 4.5 of the PCI Handbook [5]. Since the report is the basis for both the ACI and PCI procedures, they have been combined here as one method. Applicable sections from both the ACI and PCI will be presented in this section.

3.3.2 Sources of Loss from ACI Code

In Section 18.6.1 of the ACI Code, definitions of the types of losses that should be estimated when the effective prestress is being determined are given. There are many different types of losses and these lead to the eventual reduction of the jacking stress to effective prestress. The sources of loss that must be allowed for are as follows: anchorage seat loss, elastic shortening, creep, and shrinkage of concrete, and relaxation of tendon stress for pretensioned members.

3.3.3 Typical Range of Total Loss According to PCI

The PCI handbook in Section 4.5.2, suggests typical ranges of total prestress loss depending on the type of concrete being used. For normal weight concrete members the total loss may lie between 173 to 345 MPa (25 to 50 ksi). For sand-lightweight concrete members the total loss may be between 207 to 379 MPa (30 to 55 ksi).

3.3.4 Equations for Determining Prestress Loss According to PCI

In Section 4.5.3 of the PCI Handbook, the equations for determining prestress losses are presented. It is interesting to note that the PCI Handbook suggests that because anchorage seat and frictional losses are mechanical losses, that they can be made up for by overstressing. Because of this argument those two types of losses are not considered in the total loss equation of Section 4.5.3 of the PCI Handbook. The equation for total loss of prestress is as follows:

$$T.L. = ES + CR + SH + RE \quad (3-10)$$

The variables in Equation 4-10 are defined as follows:

T.L. = total loss (psi)

ES = elastic shortening

CR = creep of concrete

SH = shrinkage of concrete

RE = relaxation of tendons

The equation for elastic shortening is very similar to that which is suggested by the

AASHTO-LRFD and is as follows:

$$ES = \frac{K_{es} E_s f_{cir}}{E_{ci}} \quad (3-11)$$

The variables for Equation 3-11 are as follows:

$K_{es} = 1.0$ for pretensioned members

$E_s \equiv E_p$ in AASHTO

$f_{cir} \equiv f_{cgp}$ in AASHTO

$$f_{cir} = K_{cir} \left(\frac{P_i}{A_g} + \frac{P_i e^2}{I_g} \right) - \frac{M_g e}{I_g} \quad (3-12)$$

The variables in Equation 3-12 are defined as follows:

$K_{cir} = 0.9$ for pretensioned members

P_i = initial prestress force after anchorage seating loss

e = eccentricity of center of gravity of tendons with respect to the center of gravity of concrete at the cross-section considered

A_g = area of gross concrete section at the cross-section considered

I_g = moment of inertia of gross concrete section at the cross-section considered

M_g = bending moment due to dead weight of prestressed member and any other permanent dead loads in place at time of prestressing

The equation for creep is similar to that of the AASHTO-LRFD, except that it incorporates more variables, and it is as follows:

$$CR = \frac{K_{cr} E_s}{E_c} (f_{cir} - f_{cds}) \quad (3-13)$$

The variables in Equation 3-13 are defined as follows:

K_{cr} = 2.0 for normal weight concrete or 1.6 for sand-lightweight concrete

f_{cds} = stress in concrete at center of gravity of tendons due to all superimposed permanent dead loads that are applied to the member after it has been prestressed

E_c = modulus of elasticity of concrete at 28 days

$$f_{cds} = \frac{M_{sd} e}{I_g} \quad (3-14)$$

The variables in Equation 3-14 are defined as follows:

M_{sd} = moment due to all superimposed permanent dead loads applied after prestressing

The equation for shrinkage is dependent on many variables and is as follows:

$$SH = (8.2 \times 10^{-6}) K_{sh} E_s \times \left(1 - 0.06 \frac{V}{S}\right) (100 - R.H.) \quad (3-15)$$

The variables in Equation 3-15 are defined as follows:

$K_{sh} = 1.0$ for pretensioned members

$$CR = \frac{K_{cr} E_s}{E_c} (f_{cir} - f_{cds})$$

R.H. = percent relative humidity

The equation for steel relaxation uses values selected based on the type of tendon used, and on the ratio of initial prestress after immediate losses, f_{pi} , to the ultimate strength of the tendon, f_{pu} . The equation is as follows:

$$RE = [K_{re} - J(SH + CR + ES)]C \quad (3-16)$$

The values K_{re} and J are functions of the type of tendon used and can be found in Table 3-

2. The values of C , which is a function of the ratio f_{pi}/f_{pu} , are found in Table 3-3.

Table 3-2 Values of K_{re} and J .

Type of Tendon	K_{re}	J
270 Grade stress-relieved strand or wire	20,000	0.15
250 Grade stress-relieved strand or wire	18,500	0.14
240 or 235 Grade stress-relieved wire	17,600	0.13
270 Grade low-relaxation strand	5,000	0.040
250 Grade low-relaxation wire	4,630	0.037
240 or 235 grade low-relaxation wire	4,400	0.035
145 or 160 stress-relieved bar	6,000	0.05

Table 3-3 Values of C

f_{pi}/f_{pu}	Stress-relieved strand or wire	Stress-relieved bar or low-relaxation strand or wire
0.80		1.28
0.79		1.22
0.78		1.16
0.77		1.11
0.76	1.45	1.05
0.75	1.36	1.00
0.74	1.27	0.95
0.73	1.27	0.90
0.72	1.18	0.85
0.71	1.09	0.80
0.70	1.00	0.75
0.69	0.94	0.70
0.68	0.89	0.66
0.67	0.83	0.61
0.66	0.78	0.57
0.65	0.73	0.53
0.64	0.68	0.49
0.63	0.63	0.45
0.62	0.58	0.41
0.61	0.53	0.37
0.60	0.49	0.33

3.4 Spreadsheet Prestress Loss Results

The equations from the AASHTO and ACI-PCI were incorporated into a spreadsheet, and calculated for each girder section considered in this project. These sections are the midspan and the 1.52 m (5 ft) from the end support of Beams 1 and 4, and the midspan, and quarter-span of Beams 2 and 3. The results for all of these sections are similar. These results will be presented here in this section for the beams being

investigated. The midspan had to be done for both sets of beams because the time at transfer times, and the concrete compressive strengths were different. These results are presented in Table 3-4 and Table 3-5 of this report.

Table 3-4 Spreadsheet results for the midspan of all beams studied.

Results for Midspan of Beams 1 and 4 in MPa					
Code	ES	CR	SH	RE	TL
ACI-PCI	116.9	204.6	30.7	53.8	406.1
AASHTO	123.3	228.9	39.6	25.6	417.5
Results for Midspan of Beams 2 and 3 in MPa					
Code	ES	CR	SH	RE	TL
ACI-PCI	126.4	207.2	30.7	52.9	417.1
AASHTO	133.2	228.9	39.6	22.4	424.3

The total loss values are higher for Beams 2 and 3, than Beams 1 and 4 at the midspans.

The results for the quarter-span of Beams 2 and 3, and the 1.52 m (5 ft) from the end support of Beams 1 and 4, will be shown in Table 3-5. These results, for all points examined, will be plotted and compared with those obtained experimentally.

Table 3-5 Spreadsheet results for quarter-span and 1.52 m from the end support of the beams studied.

Results for Quarter-span of Beams 2 and 3 in MPa					
Code	ES	CR	SH	RE	TL
ACI-PCI	123.4	202.2	30.7	53.6	410.3
AASHTO	129.4	222.3	39.6	23.4	414.9
Results for 1.52 m from End Support of Beams 1 and 4 in MPa					
Code	ES	CR	SH	RE	TL
ACI-PCI	116.9	204.6	30.7	54.0	406.2
AASHTO	123.3	228.9	39.6	26.6	417.5

CHAPTER 4

DATA ANALYSIS AND EXPERIMENTAL RESULTS

4.1 Introduction

The strain readings collected from the datalogger on the Westbound Gandy Bridge, are used to determine the prestress losses within the girders. However, it is not practical to use every reading for this task of determining the losses. Portions of the readings have various fluctuations that are not consistent with adjacent measurements. In order to have smooth data to work with, the raw data was filtered to eliminate large fluctuations in the measured values.

The data file is first collected as an ASCII-DOS based file with each entry separated by commas and each row representing the readings taken at a particular time. This file is then brought into Microsoft Excel, and each data reading is placed in a separate cell. This allows the data to be easily manipulated.

A typical example of the raw data collected and imported into Microsoft Excel is shown in Table 4-1. This represents only a small portion of the file because the full version is very large. The first column represents the datalogger number. The year, Julian date, and hour of collection, which is represented in military time, are in columns 2, 3, 4, and 5, respectively. The sixth column is the battery voltage, which needs to be close to 12 Volts, in order for data to be stored and collected properly at time of collection. The remaining columns are used to report the data in pairs of strain and

temperature. In which, the first column in the pair is the strain reading, in microstrain (10^{-6} · the actual strain), and the second column is the temperature reading, in °F, for each gauge. This sequence continues until the last two columns of collected data. The last two, represent the ambient temperature, in °F, and relative humidity, in percent, (not shown in Table 4-1).

Table 4-1 Example of the raw collected data.

Col. 1	Col. 2	Col. 3	Col. 4	Col. 5	Col. 6	Strain	Temp.	Strain
113	1995	355	12/21/95	1300	12.632	2445.9	67.334	2474.2
113	1995	355	12/21/95	1400	12.631	2447.5	67.605	2465.2
113	1995	355	12/21/95	1500	12.631	2447.5	68.424	2461.3
113	1995	355	12/21/95	1600	12.631	2445.2	69.69	2455.4
113	1995	355	12/21/95	1700	12.638	2439.2	71.137	2448
113	1995	355	12/21/95	1800	12.625	2432.6	72.548	2440.1
113	1995	355	12/21/95	1900	12.624	2425.8	73.662	2434.4
113	1995	355	12/21/95	2000	12.624	2419.1	74.875	2427.8
113	1995	355	12/21/95	2100	12.619	2411.5	76.158	2421
113	1995	355	12/21/95	2200	12.625	2404.2	77.409	2416
113	1995	355	12/21/95	2300	12.618	2397.5	78.668	2415.5
113	1995	356	12/22/95	0	12.618	2397.1	78.49	2421.8
113	1995	356	12/22/95	100	12.618	2402.7	77.297	2430.4
113	1995	356	12/22/95	200	12.618	2410.1	75.767	2439.3
113	1995	356	12/22/95	300	12.619	2418.9	74.029	2448.1
113	1995	356	12/22/95	400	12.612	2428.1	72.262	2457
113	1995	356	12/22/95	500	12.619	2456.4	70.577	2465.7
113	1995	356	12/22/95	600	12.611	2445.4	69.081	2475.3

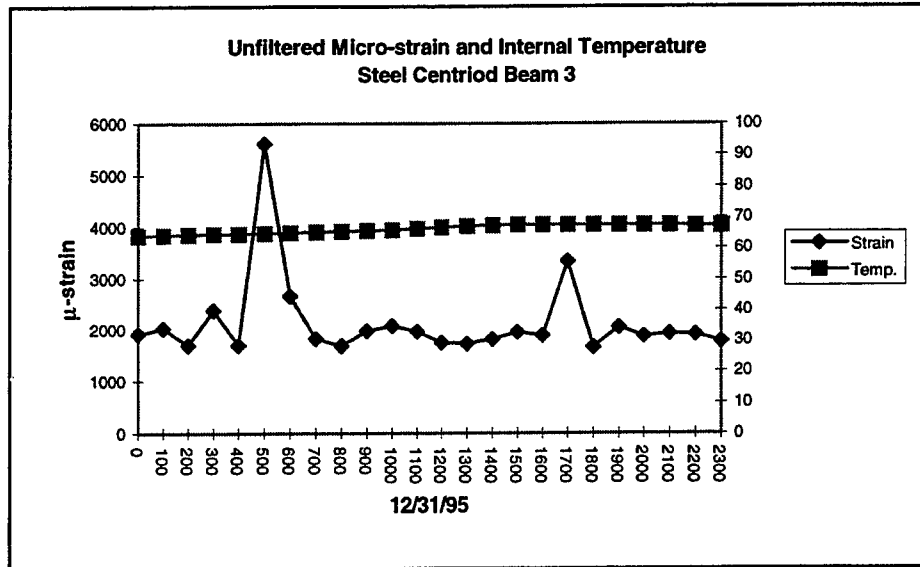


Figure 4-1 Unfiltered data plotted for December 31, 1995.

Figure 4-1 is a plot of the raw data collected from the gauge at the steel centroid, of the section at the midspan of Beam 3. This plot contains the microstrain and internal temperature versus time for December 31, 1995. Figure 4-2 shows the ambient temperature and relative humidity measured for the same time interval shown in Figure 4-1. The measurements used for these plots are raw and continuous for the interval shown. Raw in the sense that the readings are as measured, and before any has occurred. This is done to illustrate that high fluctuations do occur due to extraneous vibrations, and are not considered useful data. One suggested reason why these fluctuations might occur, is because, sudden electric noise from adjacent equipment could cause such a disturbance.

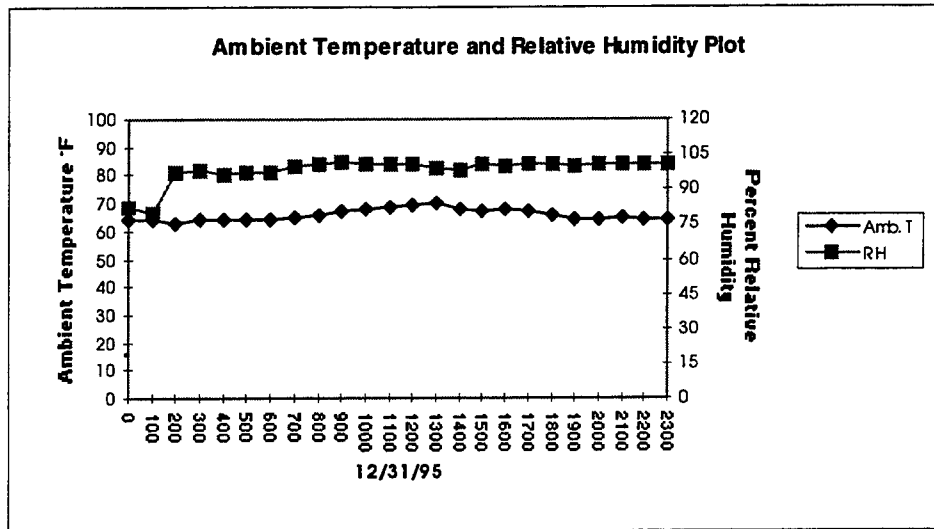


Figure 4-2 Unfiltered R. H. and ambient temperature data plotted for December 31, 1995.

4.2 Determination of Prestress Loss from Measured Data

The strain and temperature measurements used for determining the prestress losses, were taken from the most consistent data at the particular days of interest. The difference between the strain readings are what is important, because, our concern is determining the change in prestress throughout the member with time.

The measured strain reading is made up of many different components which induce strain. In order to determine the change in strain and corresponding stress that belongs to prestress loss, it is necessary to extract these other components. These components consist of temperature effects and weight effects. The temperature effects are created within the concrete and the steel of the vibrating wire in the strain gauge itself. The strain effect of the self-weight of the member is constantly changing due to the time-

dependent fluctuation of the modulus of elasticity of concrete. These effects must be removed to determine strain change due to prestress loss.

However to start with, it is necessary to determine a datum or reference to relate the change in the strain to, so that all changes refer back to the same point. Since we are dealing with two types of prestress losses (instantaneous and time-dependent), it becomes essential that there be two different reference points. The instantaneous loss, which is considered all elastic shortening, has its reference point as the last reading before the prestressing strands were cut. The last point used in determining the elastic shortening is the first reading taken after all the strands have been cut (3 hours after the first strand was cut). This point is also used as the new reference or datum for determination of the time dependent prestress losses.

The change in concrete strain due to loss of prestress for the instantaneous losses, $\Delta\epsilon_{\text{INSTANTANEOUS}}$, and time-dependent losses, $\Delta\epsilon_{\text{TIME-DEPENDENT}}$, is determined by the following equations:

$$\Delta\epsilon_{\text{INSTANTANEOUS}} = \Delta\epsilon_{\text{TOTAL}} - \delta\epsilon_{\text{TEMPERATURE}} \quad (4-1)$$

$$\Delta\epsilon_{\text{TIME-DEPENDENT}} = \Delta\epsilon_{\text{TOTAL}} - \delta\epsilon_{\text{TEMPERATURE}} - \delta\epsilon_{\text{WEIGHT EFFECTS}} \quad (4-2)$$

Equations 4-1 and 4-2 extract the prestress strain difference from the overall change in strain within the concrete. Each of the components of this equation will be explained in detail in the following paragraphs.

The change in total strain, $\Delta\epsilon_{TOTAL}$, is the difference between the strain readings, after temperature corrections of the steel in the vibrating wire strain gauges have been accounted for. This temperature correction is represented in the following equation:

$$\Delta\epsilon_{TOTAL} = (\epsilon_t - \epsilon_0) + (T_t - T_{t-1}) \times 6.78 \quad (4-3)$$

In Equation 4-3, ϵ and T represent the strain reading in microstrain and the internal temperature in °F, respectively. The subscripts, t and 0 , represent the readings at any time t and at a reference point 0 . The subscript $t-1$ is the temperature reading used from the reading taken just before t . The 6.78 multiplied with the internal temperature change is the coefficient of expansion of the steel used for the vibrating wire in the strain gauge. This number was recommended by Geokon Inc. and has the units of micro-strain/°F.

The strain created from the change of internal temperature within the concrete is $\delta\epsilon_{TEMPERATURE}$. This strain can have large effects on the overall strain in a concrete member, and must be removed to extract in the change of strain in the concrete due to loss of prestress. The equation for $\delta\epsilon_{TEMPERATURE}$ is as follows:

$$\delta\epsilon_{TEMPERATURE} = 5.5 \times (T_t - T_{t-1}) \quad (4-4)$$

In Equation 4-4, the 5.5 multiplied with the internal temperature change is the coefficient of expansion of concrete and has the units of micro-strain/°F. All the other terms in Equation 4-4 are defined as before.

Another portion of the total strain that must be removed is the strain that is created from the change in weight effects, $\delta\epsilon_{WEIGHT EFFECTS}$. The change in weight effects need to be considered after all instantaneous losses have occurred. After this time the modulus of

elasticity is constantly changing, therefore, the amount of strain that is effected by the weight is also changing. This change in weight effects can be converted into strain through its relationship with the Young's Modulus. The strain equations due to change in weight effect is as follows:

$$\delta\epsilon_{\text{WEIGHT EFFECTS}} = \frac{-M_0 \times (y - c_{\text{CONCRETE}})}{I_{\text{CONCRETE}}} \left(\frac{1}{E_{C_t}} - \frac{1}{E_{C_{t-1}}} \right) \quad \text{for } y \geq c_{\text{CONCRETE}} \quad (4-5)$$

$$\delta\epsilon_{\text{WEIGHT EFFECTS}} = \frac{M_0 \times (c_{\text{CONCRETE}} - y)}{I_{\text{CONCRETE}}} \left(\frac{1}{E_{C_t}} - \frac{1}{E_{C_{t-1}}} \right) \quad \text{for } y < c_{\text{CONCRETE}} \quad (4-6)$$

Equation 4-5 and Equation 4-6, represent the change in strain in the top and bottom portions of the member, with respect to the neutral axis, respectively. These portions are separated by the concrete centroid, c_{CONCRETE} , measured from the bottom of the member to the neutral axis with units of inches. M_0 is in k-ft and is the moment created by the self weight of the member. I_{CONCRETE} is the moment of inertia of the concrete section in in^4 . E_{C_t} and $E_{C_{t-1}}$ represent the change in the modulus of elasticity of concrete between adjacent measured readings and are measured in ksi. Both Equation 4-5 and Equation 4-6 will yield strain readings in micro-strain or 10^6 times the actual strain.

The initial prestress force and stress is based upon the force applied to the area of steel present. In determining the prestress losses of a member, it is usually customary to calculate them in terms of equivalent steel throughout the cross-section. This then makes it necessary to convert the strain changes in the concrete to equivalent stress changes in the steel. It is assumed that changes in the concrete strains and the prestressing steel, are equivalent because of the strong bond between them. The change in steel stress is

obtained by multiplying the change of strain extracted from the gauges in the concrete by the modulus of elasticity of the prestressing steel. The equation for this is as follows:

$$\Delta f_{\text{PRESTRESS}} = E_s \cdot \Delta \epsilon_{\text{PRESTRESS}} \quad (4-7)$$

The change in strain, $\Delta \epsilon_{\text{PRESTRESS}}$, could represent either $\Delta \epsilon_{\text{INSTANTANEOUS}}$, for instantaneous losses, or $\Delta \epsilon_{\text{TIME-DEPENDENT}}$, for time dependent losses, and would have a corresponding $\Delta f_{\text{INSTANTANEOUS}}$ and $\Delta f_{\text{TIME-DEPENDENT}}$ for the change in prestress, $\Delta f_{\text{PRESTRESS}}$. For the Westbound Gandy bridge the modulus of the prestressing steel, E_s , is 28,000 ksi

4.3 Ambient Temperature and Relative Humidity

Ambient temperature and relative humidity are considered important factors when examining the time-dependent behavior of prestressed concrete. This is especially true when studying shrinkage of concrete, as mentioned in Section 1.3.3.2 of this thesis. Shrinkage in turn affects the concrete creep and steel relaxation also.

In the case of the Westbound Gandy Bridge project all beams investigated were not cast on the same day. Beams 1 and 4, were cast five days before Beams 2 and 3, under different environmental conditions. Figures 4-3 and 4-4 contain the ambient temperature and relative humidity plots for Beams 1 and 4, and Beams 2 and 3, respectively. The points on these plots cover the same time intervals, selected for

determination of the change in prestress force. An average of the conditions on each day was computed and plotted.

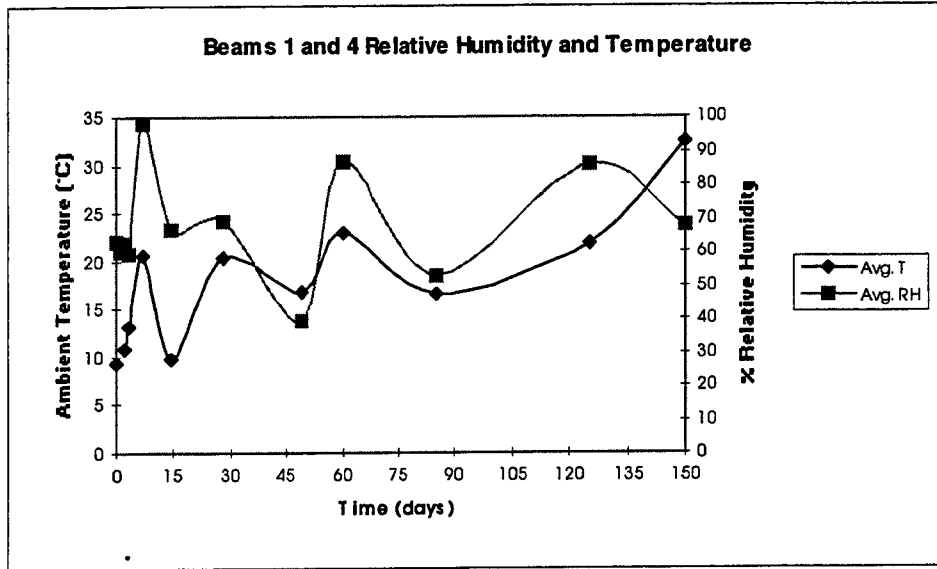


Figure 4-3 Relative humidity and ambient temperature for Beams 1 & 4.

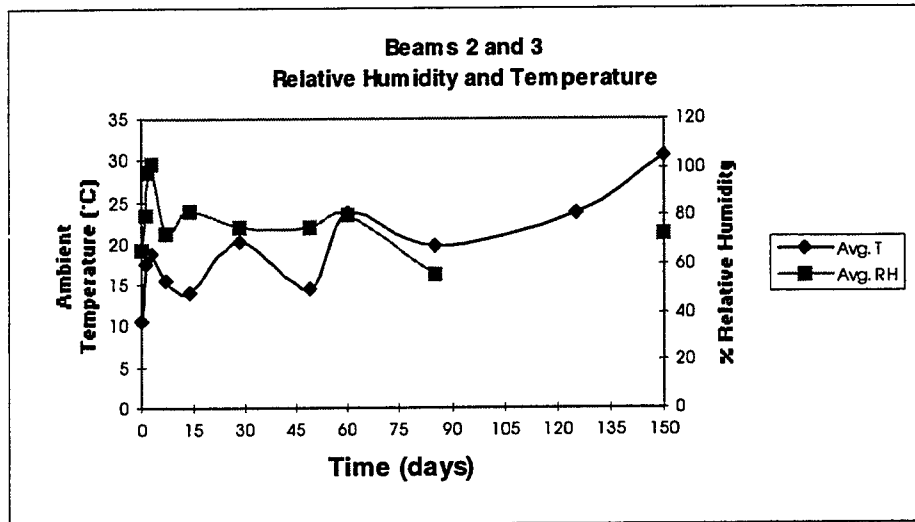


Figure 4-4 Relative humidity and ambient temperature for Beams 2 & 3.

4.4 Immediate Prestress Loss

4.4.1 Introduction

In the case of the Modified AASHTO Type VI pretensioned girders used on the Westbound Gandy bridge, it is assumed that all of the immediate prestress loss is elastic shortening. Anchorage slip and frictional losses were considered negligible in comparison to elastic shortening. The steel relaxation before the strands were cut was also considered negligible.

The portion of the prestress loss associated with elastic shortening is said to occur simultaneously, with the application of the prestress from the steel strands to the concrete. The cutting of the strands takes place approximately over a 3-hour period. Since this loss is considered a one time loss, it has an absolute start and end point. Therefore, the beginning reference point was selected just before the strands were cut. The end reference point used in the analysis was chosen at the time the cutting was finished. With this simple assumption, elastic shortening loss can be determined for all locations where data was available. Initial data for Beam 2 is unavailable and is not considered in this analysis.

4.4.2 At Midspan

The elastic shortening results obtained for midspans of Beams 1, 4, and 3, can be seen in Figures 4-5, 4-6, and 4-7, respectively. The differences between Beams 1 and 4, and Beam 3, is the age of the concrete when the prestressing strands were cut, and the ambient conditions (temperature and relative humidity). At the time the strands were cut,

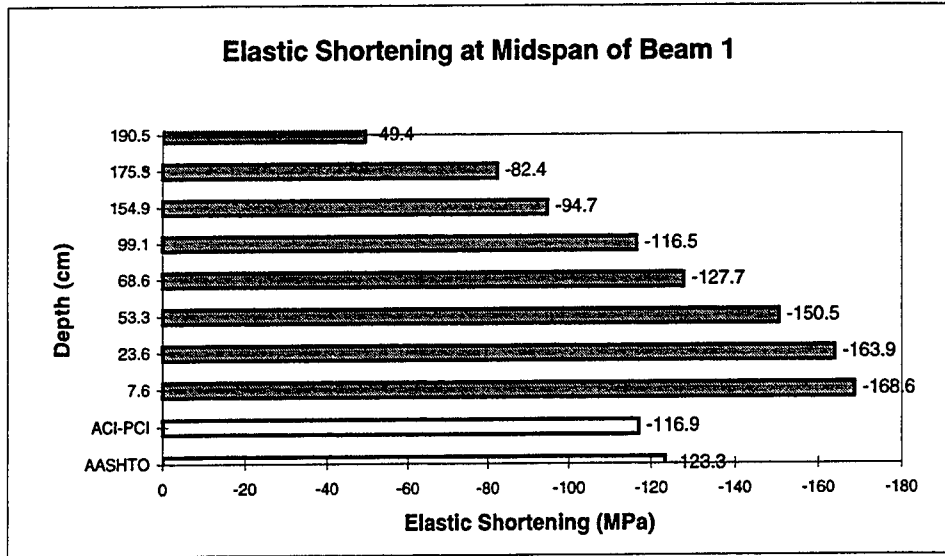


Figure 4-5 Elastic shortening loss for the midspan of Beam 1

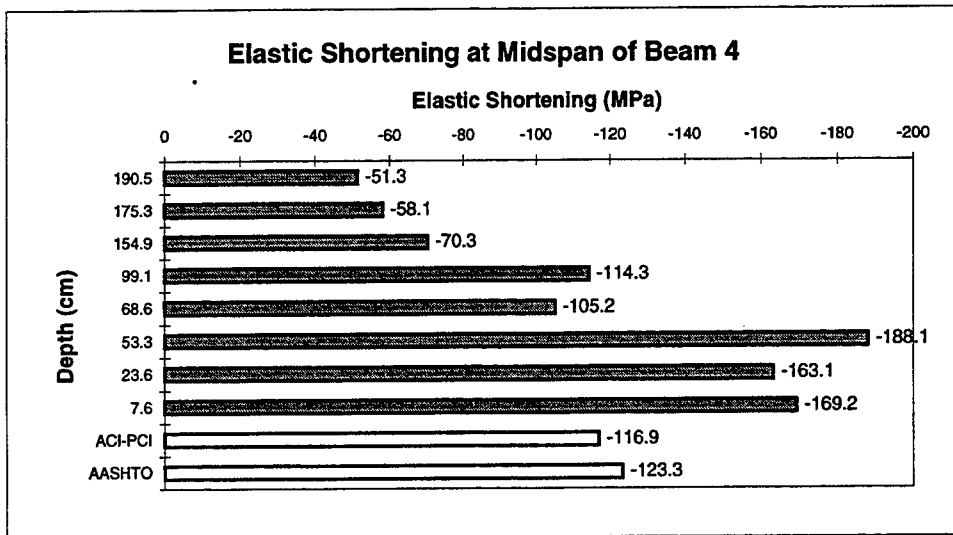


Figure 4-6 Elastic shortening loss for the midspan of Beam 4

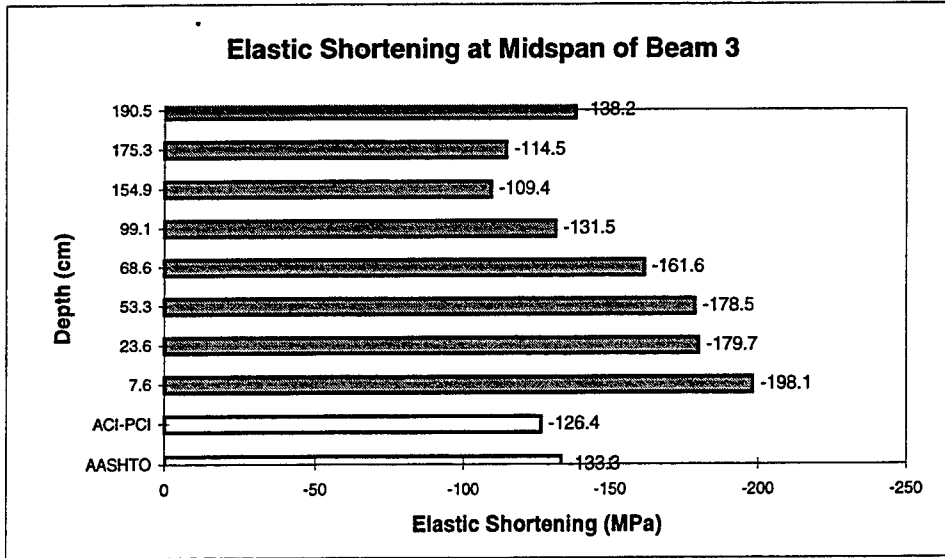


Figure 4-7 Elastic shortening loss for the midspan of Beam 3

the age of concrete for Beams 1 and 4 were five days old, while Beam 3 was three days old. Also included on the plots are the elastic shortening results calculated by the ACI-PCI and AASHTO equations of Chapter 3. In examining these plots there are clear trends, ranging from small changes in the top flange, to gradually larger changes toward the bottom flange. The elastic shortening results are larger for Beam 3, than those of Beams 1 and 4. A possible reason for this may be that the gauges were shifted during casting of the beams, causing their position not to be parallel with the span.

Figure 4-8 contains an average of the elastic shortening of the three midspans for all points within the cross-section. At the steel centroid, 23.6 cm, where the average elastic shortening loss is -168.9 MPa. Results for elastic shortening at the concrete centroid, which is at approximately 99.1 cm, is -120.7 MPa. At the future composite

centroid, 154.9 cm, the elastic shortening loss was -91.5 MPa. At 175.3 cm which is approaching the top flange, the loss is -85.0 MPa, and at 190.5 cm which is 7.6 cm from the top flange, the elastic shortening loss is -79.6 MPa. The value at the concrete centroid is quite close to that of the Code results. At the steel centroid, however, the elastic shortening loss is much larger, this may be because there is a concentration of steel there.

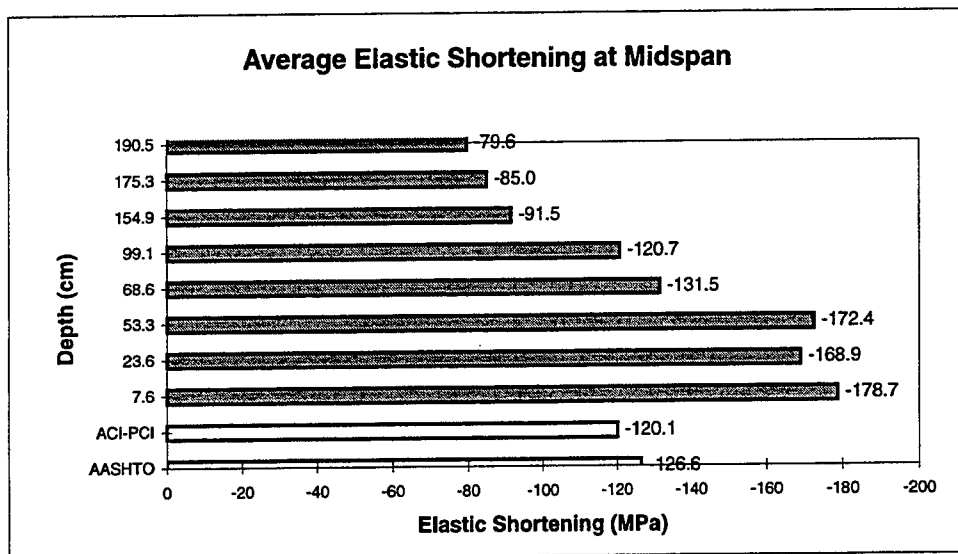


Figure 4-8 Average elastic shortening loss for the midspans

4.4.3 At Quarter-span and 1.52 m from Support

The results obtained for the quarter span of Beam 3, and at the point 1.52 m from the end support of Beams 1 and 4, can be seen in Figures 4-9, 4-10, 4-11, respectively. These three Figures follow the same trend as the midspan loss, that is the change is relatively small near the top flange, and gradually increases as you move down the cross-

section. This trend is consistent with the expectation, that greater values of loss will occur closer to the area where the prestressing strands exist. The magnitude of the loss seems to be larger, at the quarter span than at 1.52 m marks and the midspans.

For the quarter-span, four points of interest are 190.5 cm (top flange), 175.3 cm (near the future composite centroid), 84.1 cm (near the concrete centroid), and 18.8 cm (straight strand steel centroid). The results for elastic shortening at 190.5 cm, 175.3 cm, 84.1 cm, and 18.8 cm are -47.2, -46.9, -141.7, and -197.3 MPa, respectively.

For the 1.52 m mark, the four points chosen for averaging of Beams 1 and 4 data are 190.5 cm., 175.3 cm, 147.1 cm (near the future composite centroid), and 18.8 cm.

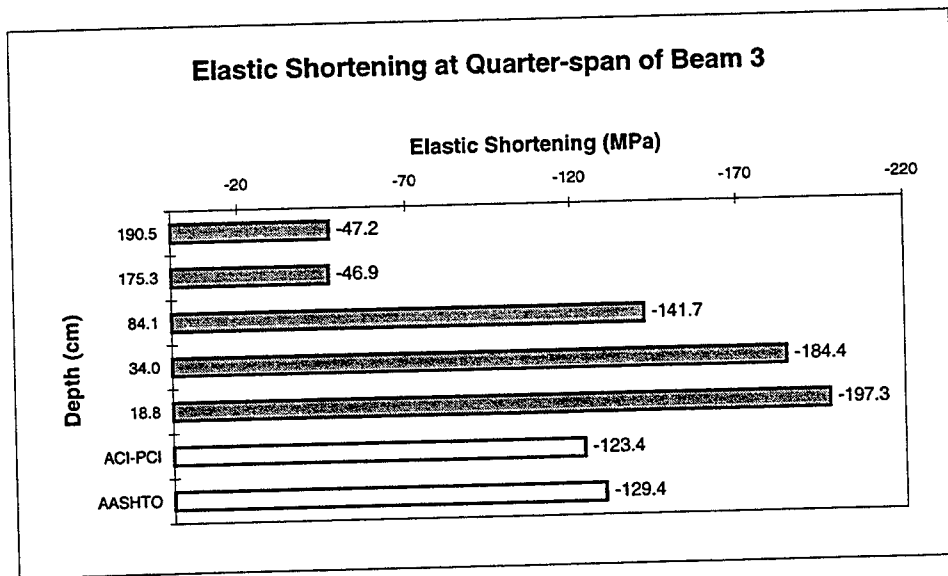


Figure 4-9 Elastic Shortening Loss for the quarter-span of Beam 3

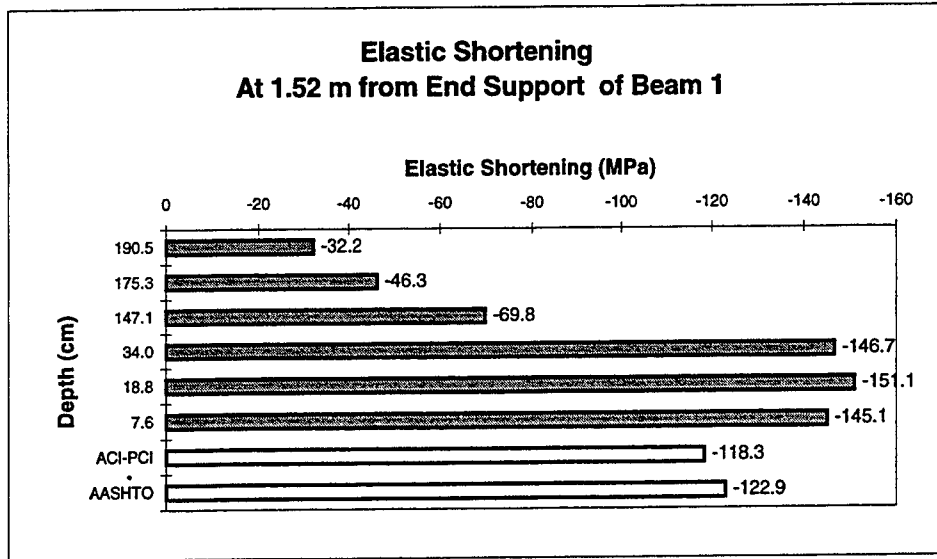


Figure 4-10 Elastic Shortening Loss for Beam 1 at 1.52 m

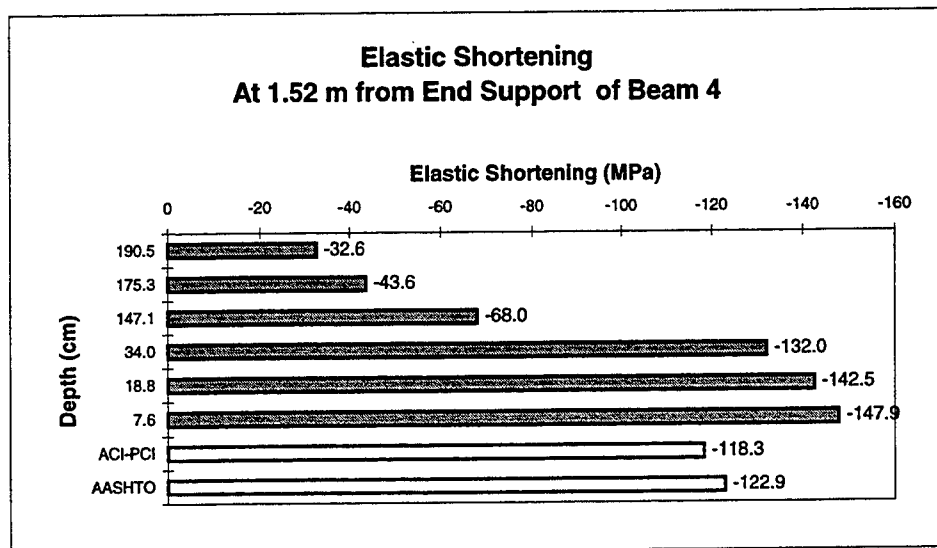


Figure 4-11 Elastic Shortening Loss for Beam 4 at 1.52 m

The results for the average of Beams 1 and 4 at the 1.52 m mark are shown in Figure 4-12. In that Figure, for 190.5 cm., 175.3 cm, 147.1 cm, and 18.8 cm, the elastic shortening loss is -32.4, -44.9, -68.9, and -146.8 MPa, respectively.

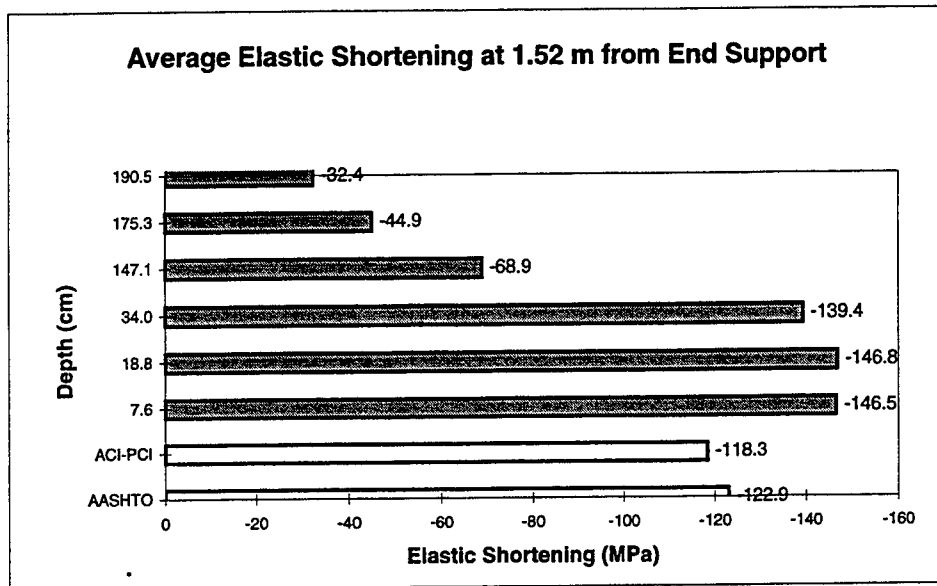


Figure 4-12 Average elastic shortening loss for the 1.52 m marks

4.4.4 Variation Along the Length of the Beam

The elastic shortening loss has been represented at points within the cross-section without any variation along the length of the beam. The average values at the points of interest will now be plotted with consideration to length as well as depth. Since at the time of this study (150 days), all beams are under similar loading, it is reasonable to superimpose data from the midspan at 21.95 m, quarter-span at 10.97 m, and the 1.52 m from the end support, in order to determine the lengthwise variation of the losses.

Figure 4-13 shows the elastic shortening variation with length for the above mentioned points. It is assumed that at this time, the loading is symmetric so the results from one side can be flipped to the other. The steel centroid loss is larger at the quarter-span than at the midspan, but much smaller at the 1.52 m mark. The concrete centroid

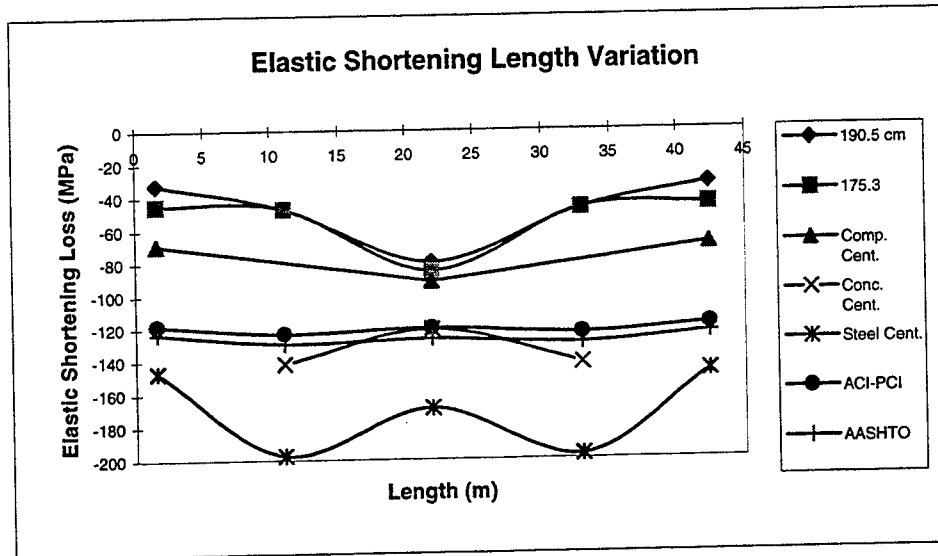


Figure 4-13 Elastic shortening loss variation along the span

loss is greater at the quarter-span, when compared with that of the midspan. The loss at the level of the future composite centroid seems be smaller at the 1.52 m mark than at the midspan points (there is no gauge at this location at the quarter-span, although the line is extended through that point). For the 190.5 and 175.3 cm points, the loss is very similar at the 1.52 m and quarter-span points but is much greater at the midspan for these points.

4.5 Time-Dependent Prestress Loss

4.5.1 Introduction

The time-dependent prestress loss is made up of creep, shrinkage of concrete, and steel relaxation. This section does not break the time-dependent prestress loss into its individual components, but it examines this loss without including the effect of elastic shortening.

It is assumed that the time-dependent portion of the prestress loss begins to occur directly after the immediate losses or when the strands are all cut. This point serves as a reference point to which all time dependent losses will be referred back to. Hence, the loss calculated at any time, t , will encompass all of the time-dependent loss up to that moment in time.

4.5.2 At Midspan

The results obtained for the time-dependent loss at the midspans of Beams 1, 4, and 3, can be seen in Figures 4-14, 4-15, and 4-16, respectively. These plots show data from all gauge locations that occur within the girder cross-sections. There seems to be little or no variation between the slopes of the time-dependent portion of the curves for all the gauges. Also shown are the calculated time-dependent prestress losses from ACI-PCI and AASHTO equations of Chapter 3.

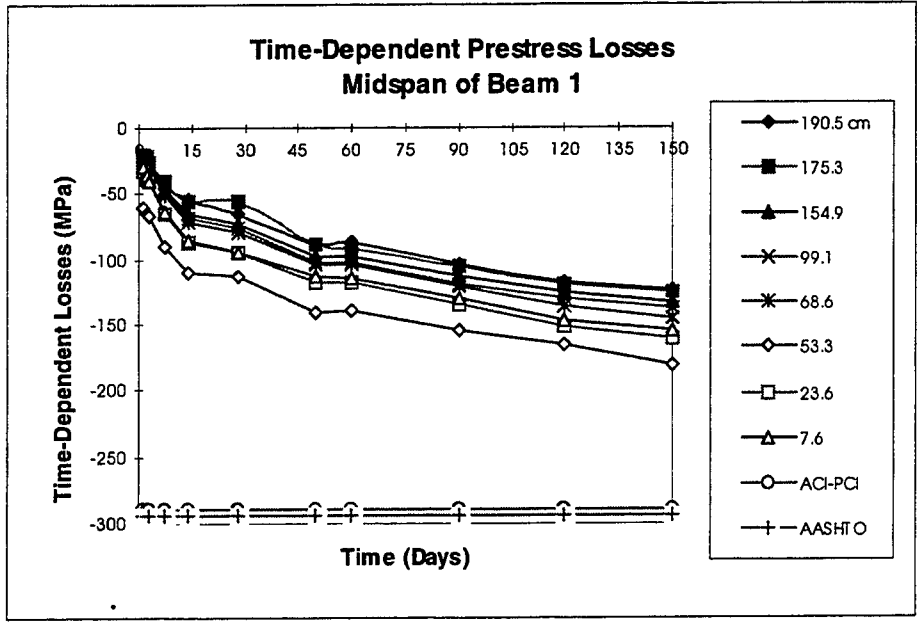


Figure 4-14 Time-Dependent loss at Midspan Beam 1

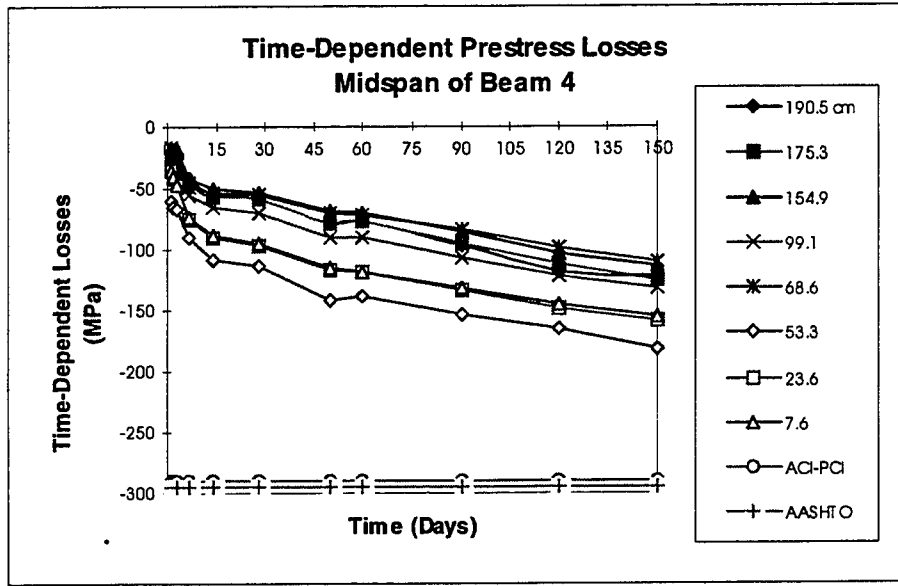


Figure 4-15 Time-Dependent loss at Midspan Beam 4

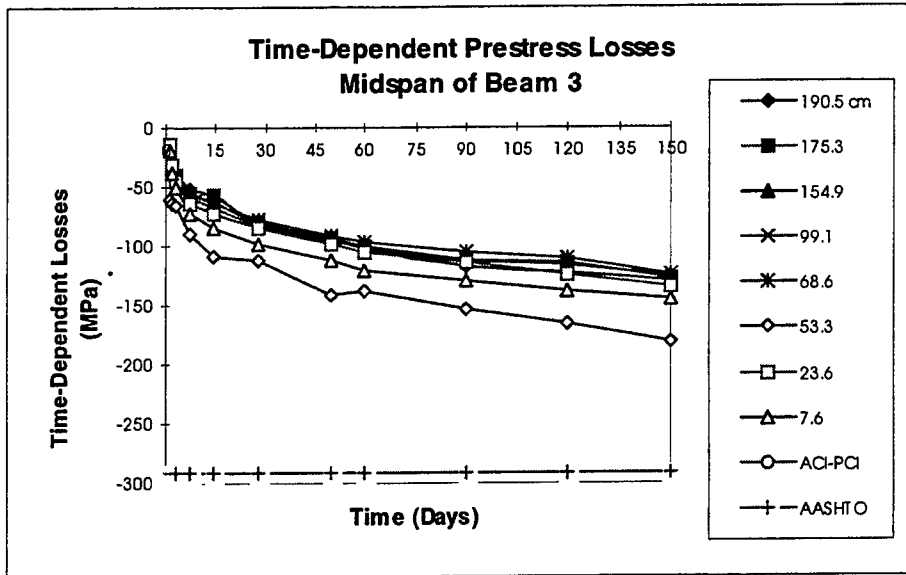


Figure 4-16 Time-Dependent loss at Midspan Beam 3.

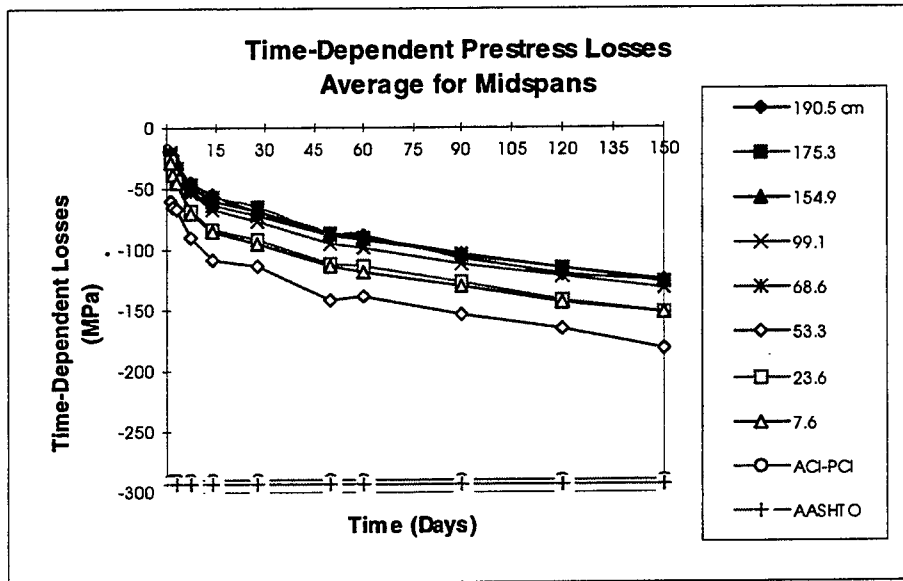


Figure 4-17 Average time-dependent loss at Midspans.

Figure 4-17 contains an average time-dependent loss over the 150 day period, for five points of interest that occur in the midspan. These points are 190.5, 175.3, 154.9, 99.1, and 23.6 cm, and the time-dependent losses are -125.1, -126.5, -124.4, -132.4, and -150.9 MPa respectively.

4.5.3 Quarter-span and 1.52 m from Support

The results obtained for the quarter span of Beam 3, and the 1.52 m points in Beams 1 and 4, are Figures 4-18, 4-19, and 4-20, respectively. They follow the same pattern, whereby they are progressively larger as you move from the top portion of the beam to the bottom.

For the quarter point of Beam 3, the time-dependent loss over the 150 day period for four points of interest are shown in Figure 4-18. For the points 190.5, 175.3, 84.1, and 18.8 cm the time-dependent losses is -116.0, -132.1, -145.7, and -162.5 MPa, respectively. These values compare well with those at the midspan.

The average time-dependent loss for Beams 1 and 4 for the selected points at 1.52 m is shown in Figure 4-21. For 190.4, 174.3, 147.1, and 18.8 cm, the losses are -91.4, -99.0, -107.8, and -148.7 MPa, respectively. The top point losses of the 1.42 m mark are smaller than those at quarter-span and midspan, and the bottom point losses are less than at the quarter-span.

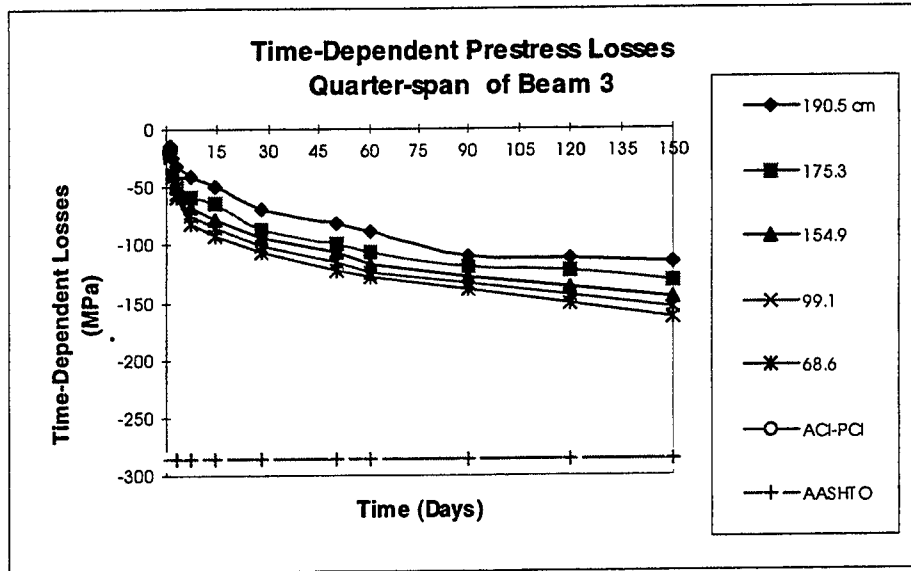


Figure 4-18 Time-dependent loss for the Quarter-span of Beam 3.

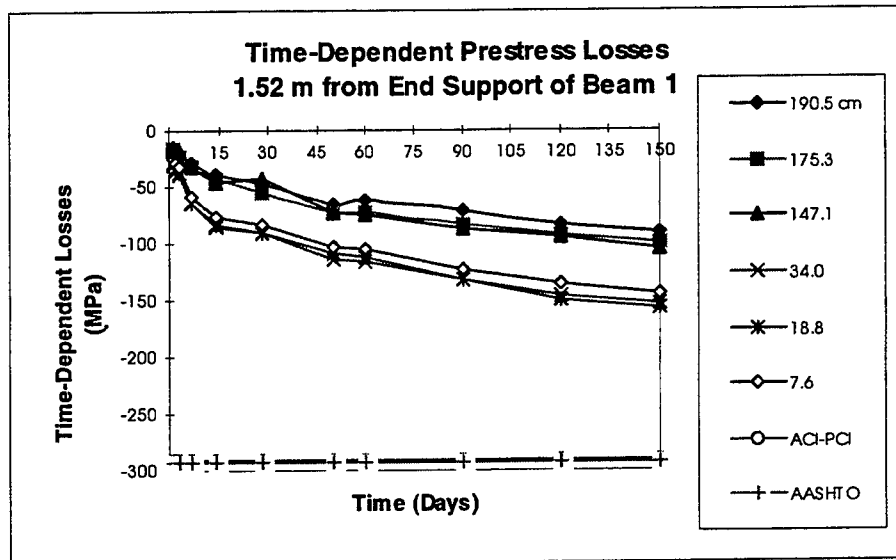


Figure 4-19 Time-dependent loss for the 1.52 m of Beam 1.

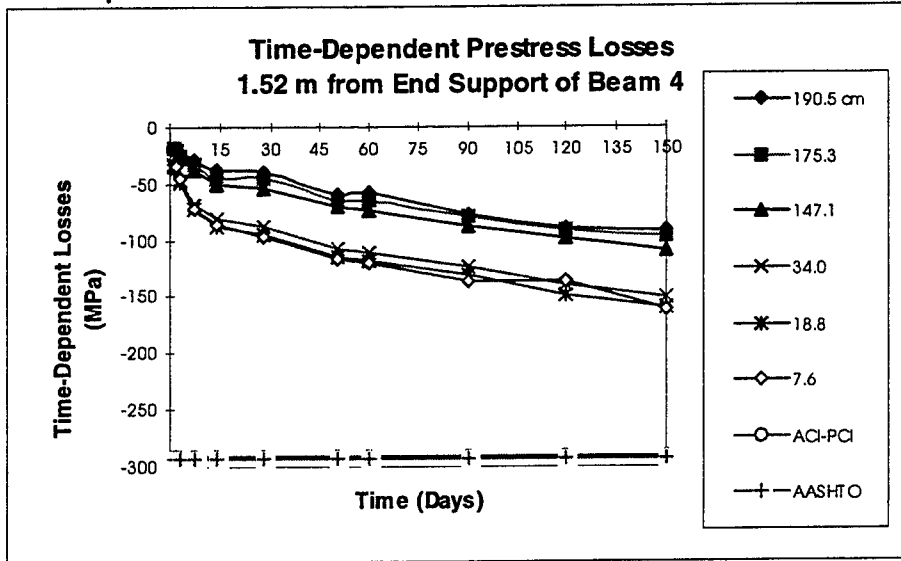


Figure 4-20 Time-dependent loss for the 1.52 m of Beam 4.

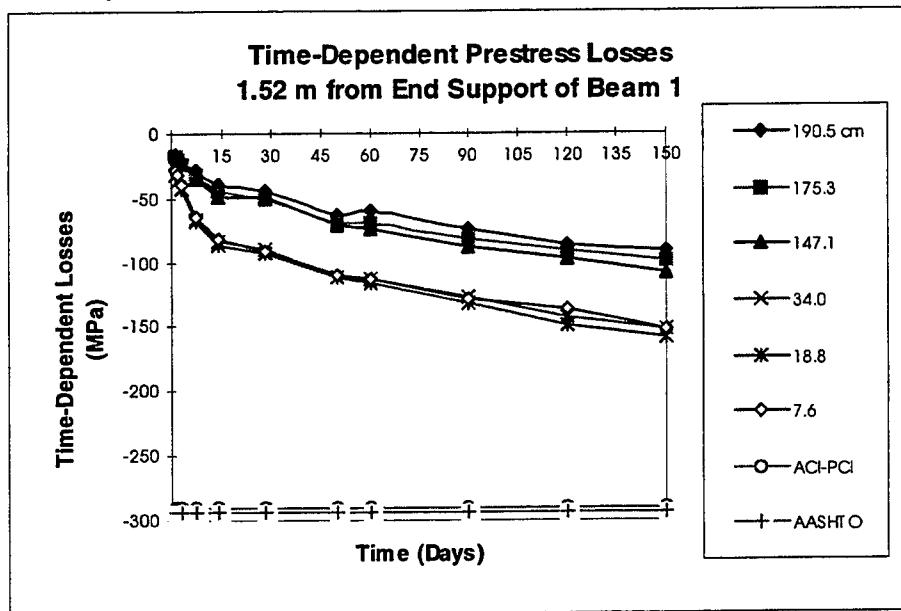


Figure 4-21 Average time-dependent loss for the 1.52 m points.

4.5.4 Variation Along the Span

The average time-dependent prestress loss variation along the span is plotted in Figure 4-22. The time-dependent prestress loss is very similar for the 1.52 m, quarter-span, and midspan, at the 190.5 cm and 175.3 cm levels. At the composite centroid, the loss is larger for the 1.52 m points than at the midspan. The concrete centroid is larger for the quarter-span than the midspan. The steel centroid level loss is larger for the quarter-span and 1.52 m points when compared to the midspan.

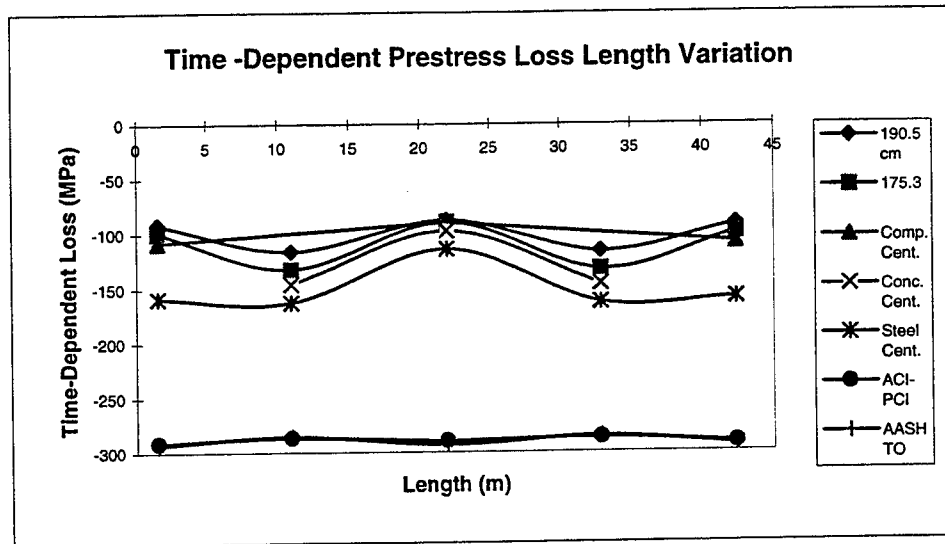


Figure 4-22 Time-dependent loss variation along the span

4.6 Lump Sum Prestress Loss

4.6.1 Introduction

The lump sum prestress loss is made up of both the immediate and time-dependent prestress loss. This is considered the total prestress loss at any time t . And for this section t is equal to 150 days.

4.6.2 At Midspan

The results obtained for the lump sum loss at the midspans of Beams 1, 4, and 3, can be seen in Figures 4-23, 4-24, and 4-25, respectively. These plots show all gauge locations that occur within the section. There seems to be little or no variation between the slopes of the time-dependent portion of the curves for all the gauges. Also shown are the calculated time-dependent prestress losses from ACI-PCI and AASHTO equations of Chapter 4.

Figure 4-26 contains an average lump sum loss over the 150 day period for five points of interest that occur in the midspan. For the points 190.5, 175.3, 154.9, 99.1, and 23.6 cm, the lump sum loss is -204.8, -211.5, -215.9, -253.1, and -319.7 MPa, respectively. All loss values have not exceeded ACI-PCI or AASHTO lump sum estimates.

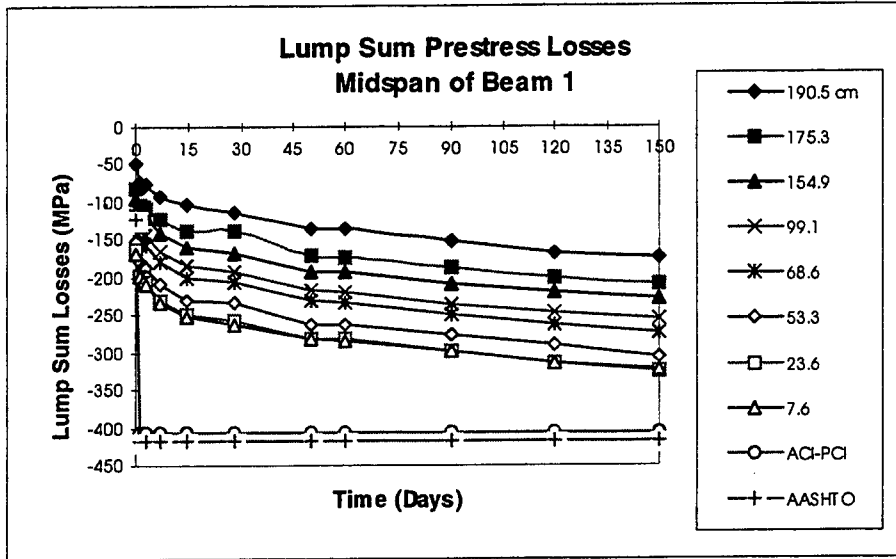


Figure 4-23 Lump Sum Loss at Midspan of Beam 1.

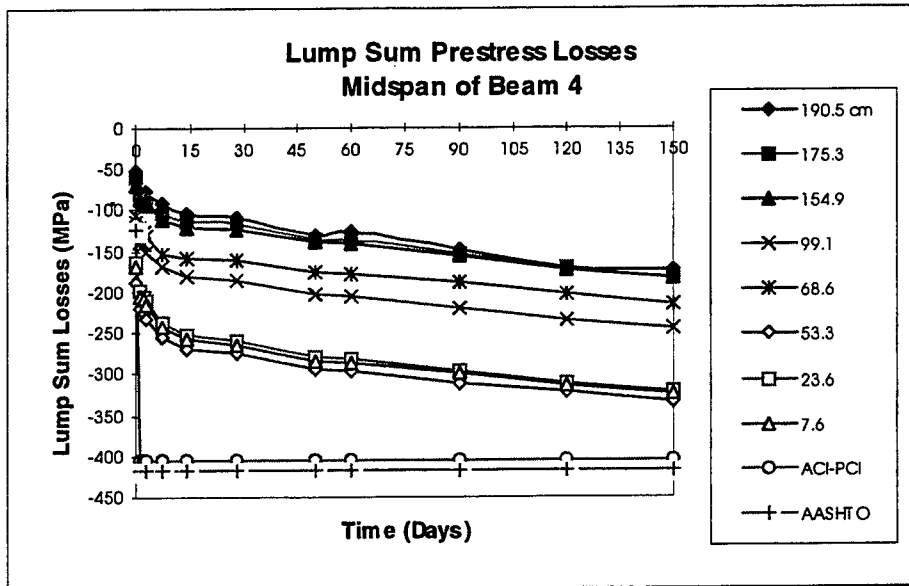


Figure 4-24 Lump Sum Loss at Midspan of Beam 4.

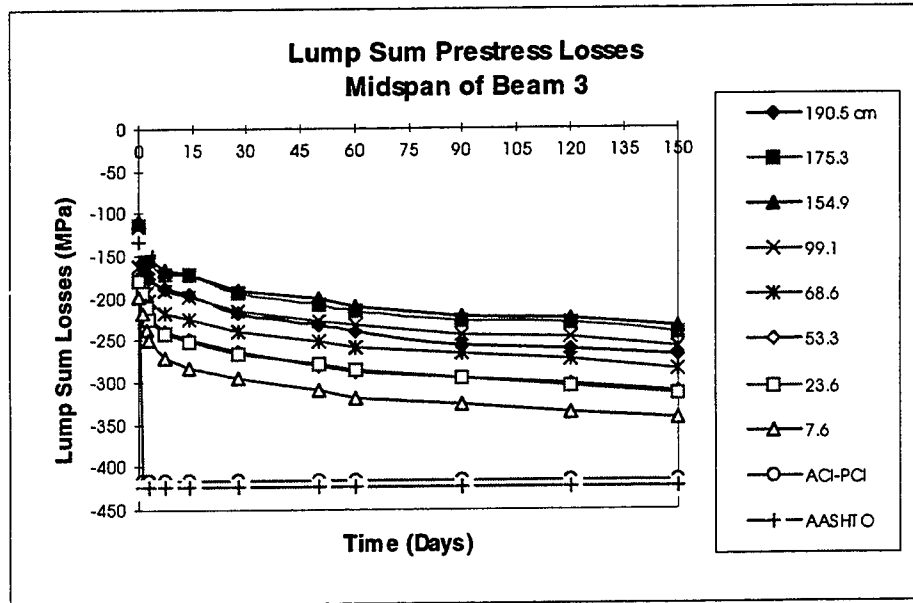


Figure 4-25 Lump Sum Loss at Midspan of Beam 3.

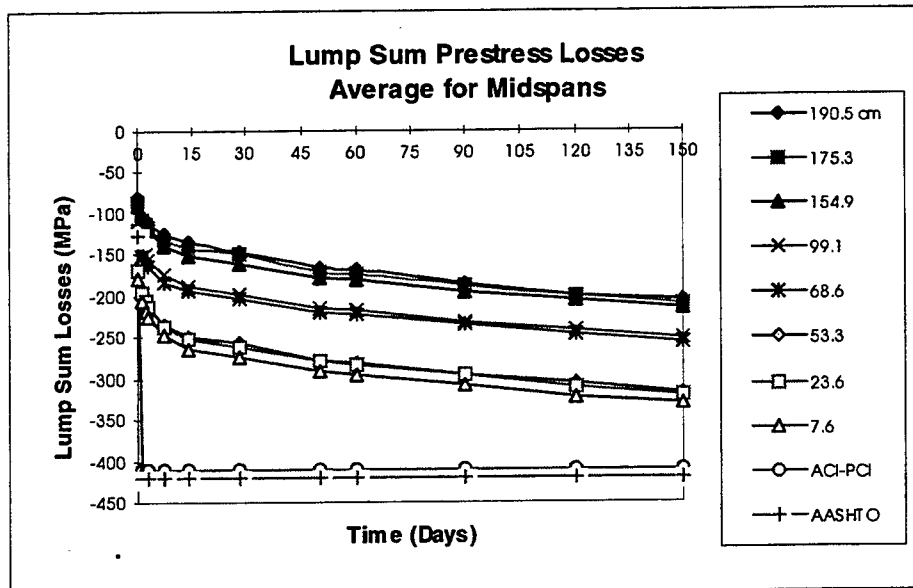


Figure 4-26 Average lump sum loss at Midspans.

4.6.3 At Quarter-span and 1.52 m from Support

The results obtained for the quarter span of Beam 3, and the 1.52 m points in Beams 1 and 4 are in Figures 4-27, 4-28, and 4-29, respectively. They follow the pattern whereby they progressively get larger as you move from the top portion of the beam to the bottom. The lump sum loss at quarter-span is greater than at 1.52 m.

For the quarter point of Beam 3, the lump sum loss over 150 day period for the four points of interest are shown in Figure 4-27. For the points 190.5, 175.3, 84.1, and 18.8 cm, the lump sum loss is -163.2, -179.0, -287.4, and -359.9 MPa, respectively.

The average time-dependent loss for Beams 1 and 4, for the selected points at 1.52 m is shown in Figure 4-30. For 190.5, 175.3, 147.1, and 18.8 cm, the losses are -123.8, -143.9, -176.7, and -305.5 MPa, respectively.

4.6.4 Variation Along the Span

The average lump sum prestress loss variation along the span is plotted in Figure 4-31. The lump sum loss increases from the 1.52 m mark to the quarter-span to the midspan for 190.5, 175.3 cm, and the composite centroid levels. At the concrete centroid and the steel centroid locations, the loss is larger for the quarter-span than the midspan.

The results observed here will be used to determine the effects of these prestress losses on prestressed concrete bridge design in the next chapter.

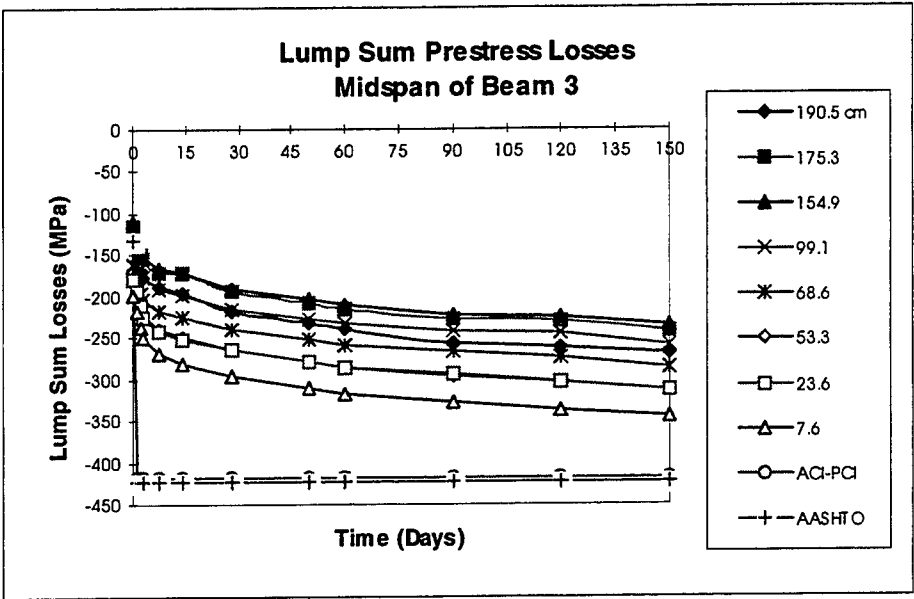


Figure 4-27 Lump Sum loss for the Quarter-span of Beam 3.

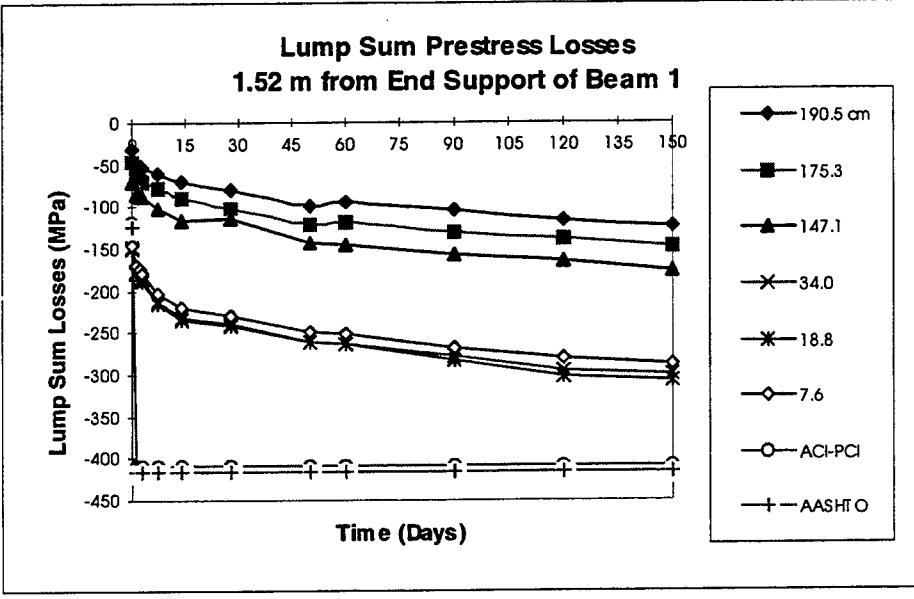


Figure 4-28 Lump Sum loss for the 1.52 m point of Beam 1.

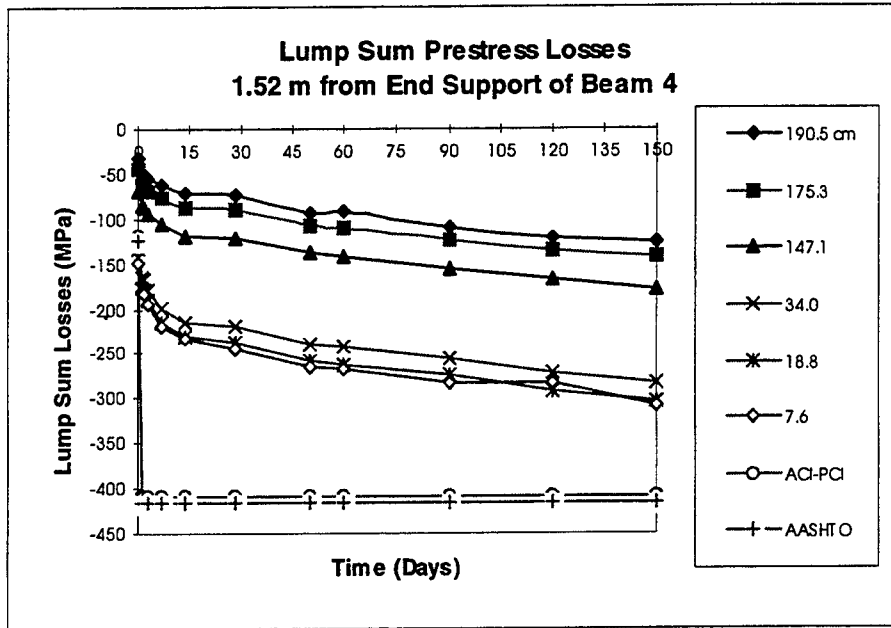


Figure 4-29 Lump Sum loss for the 1.52 m point of Beam 4.

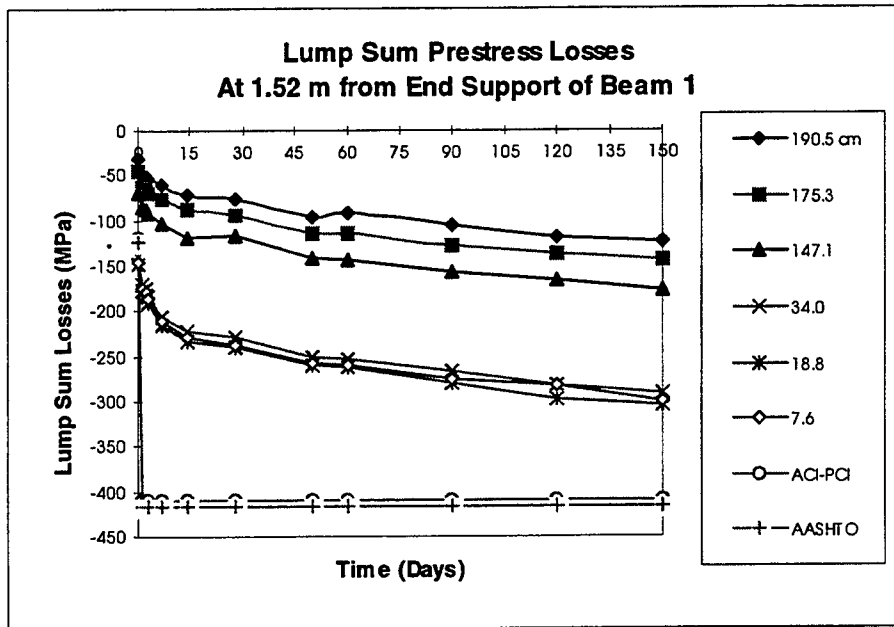


Figure 4-30 Average lump sum loss for the 1.52 m points.

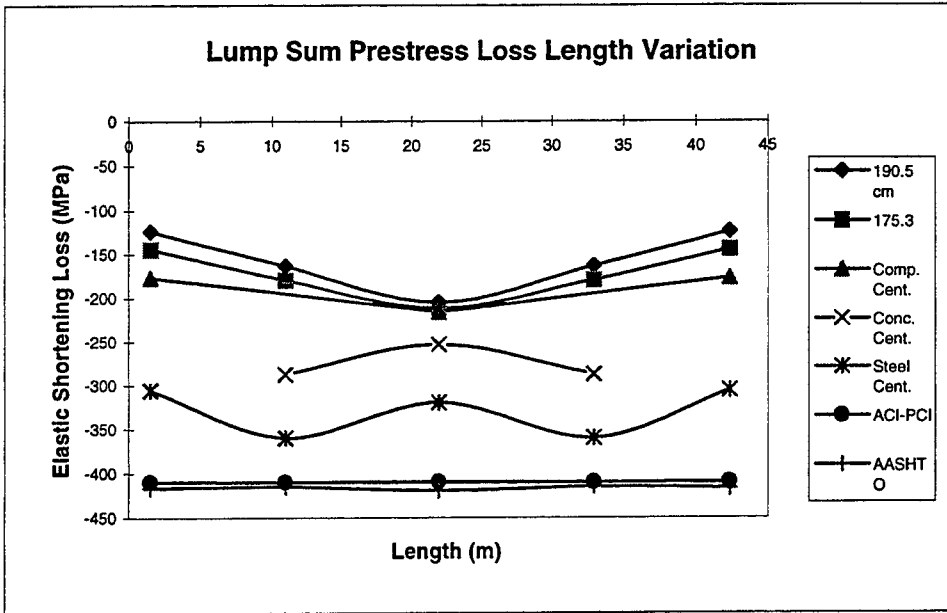


Figure 4-31 Lump sum loss variation along the span.

CHAPTER 5

EFFECTS OF PRESTRESS LOSS ON BRIDGE DESIGN

5.1 Introduction

In the previous chapter, the methods used to obtain the actual prestress losses were presented and the results shown. In this chapter, the losses are further examined to better understand their effects on bridge girder design. This is important because in design the prestress loss is generally assumed to be constant across the cross-section at any particular location being examined. Since this is not the case in reality, it is necessary to see the effect this has on other areas of design, such as, in other areas such as in the levels of concrete and tendon stresses, as well as, camber and deflection.

This chapter mainly examines three beams, using data at different locations along the span unless otherwise stated. The locations selected are the midspan of Beam 1, the quarter-span of Beam 3, and the 1.52m (5 ft.) from the end support of Beam 4. The results of the other cross-sections are similar.

To begin with, the cross-sectional prestress loss distribution on specific days are superimposed on the same plot for either 3 or 4 different days, to provide continuous time-dependent variation of the losses. Then the various ratios and percentage losses are

shown to further illustrate the effects of the losses throughout the cross-sections. Also, the stresses in both the prestressing tendons and concrete are computed and compared to their allowable values as stated in the ACI Code. Plots of relative humidity and ambient temperature versus loss at specific locations within beams studied are presented, and a regression analysis is performed to establish the level of dependency of the losses on these parameters, all things being equal. Finally, the effects of the prestress loss on the camber and deflection of the girders are studied.

5.2 Cross-sectional Prestress Loss Variation

Prestress losses are generally assumed to be uniform across the section of a member being examined during design. In reality this is not the case. The experimentally determined prestress loss varies considerable from the bottom to the top of a member. This variation appeared to be essentially linear within each specified cross-section. Therefore, having a better understanding of the prestress loss variation throughout a cross-section, allows for a more accurate determination of concrete and tendon stresses just after transfer, and under service conditions.

The cross-sectional prestress loss results are plotted for the following days: 1, 3, 7, 14, 28, 50, 60, 90, 120, and 150 days. These days are consistent with those chosen for the girder design as well. There are four plots for each cross-section examined, which will be presented in one figure per cross-section. The plots are in the following sequence: 1, 3, and 7 days, 7, 14, and 28 days, 28, 50, and 60 days, 60, 90, 120, and 150 days. The

calculated ACI-PCI and AASHTO prestress loss results are assumed uniform and are superimposed on each plot as well. Note that the days are measured from when the transfer of stress from the prestressing strands to the concrete occurs.

5.2.1 Midspan of Beam 1

The cross-sectional prestress loss versus depth for the midspan of Beam 1 is plotted in Figure 5-1(a-d). In Figure 5-1a, there is only a slight change of the cross-sectional loss between 1 and 3 days, but the gap then widens upon 7 days. In Figure 5-1b, a larger gap appears between 7 and 14 days, but there is little variation between 14 and 28 days. In Figure 5-1c, a larger variation is shown between 28 and 50 days with little or no change at all between 50 and 60 days. In Figure 5-1d, clearly indicates that the loss increases at a decreasing rate, as time elapses. This can be seen by the gradual decrement in the gaps between the days shown.

5.2.2 Quarter-span of Beam 3

The cross-sectional prestress loss versus depth for the quarter-span of Beam 3 is shown in Figure 5-2(a-d). In Figure 5-2a, the change between 1 and 3 days is larger than the change between 3 and 7 days for this cross-section. In Figure 5-2b, a smaller gap is shown between 7 and 14 days than between 14 and 28 days.

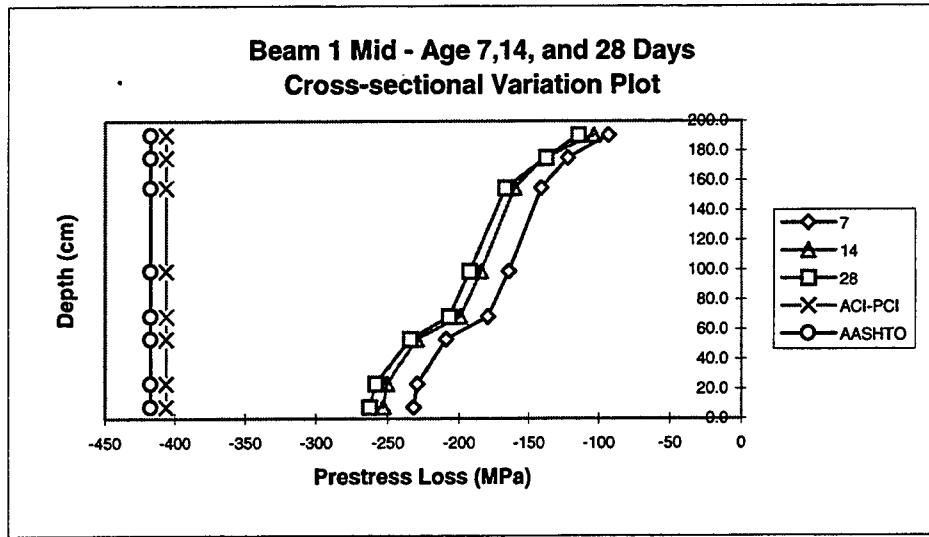
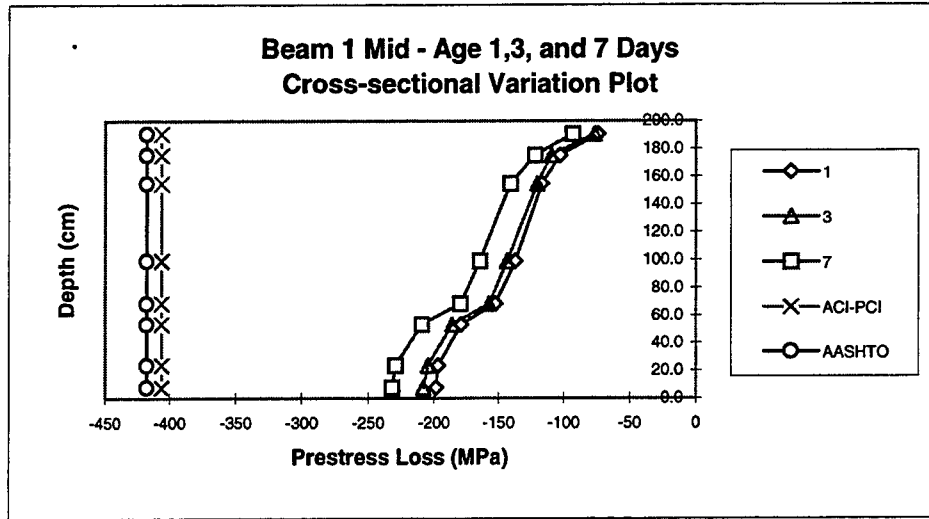


Figure 5-1(a-b) Midspan Beam 1 at (a) 1, 3, & 7 days (b) 7, 14, & 28 days

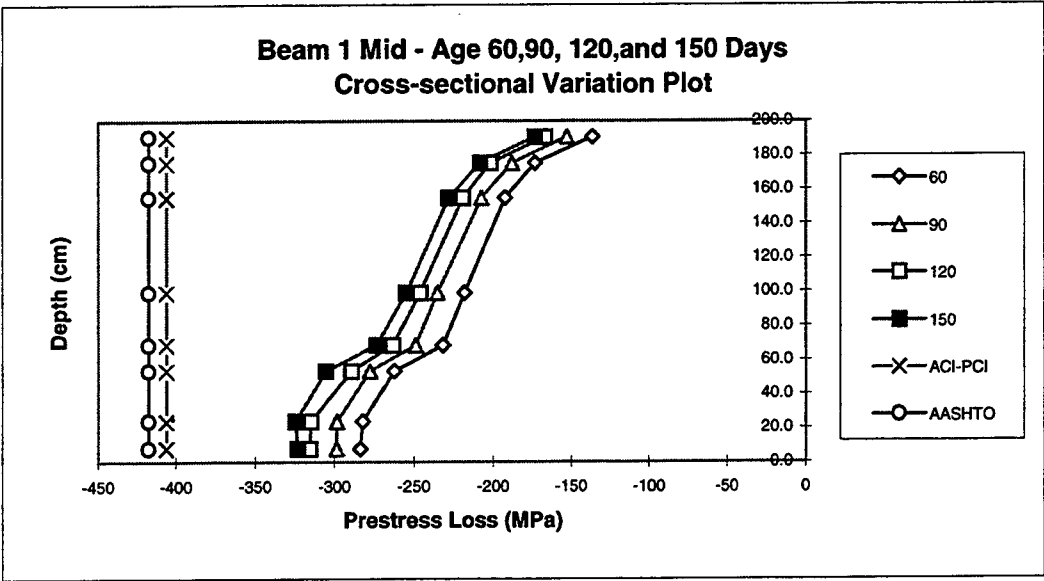
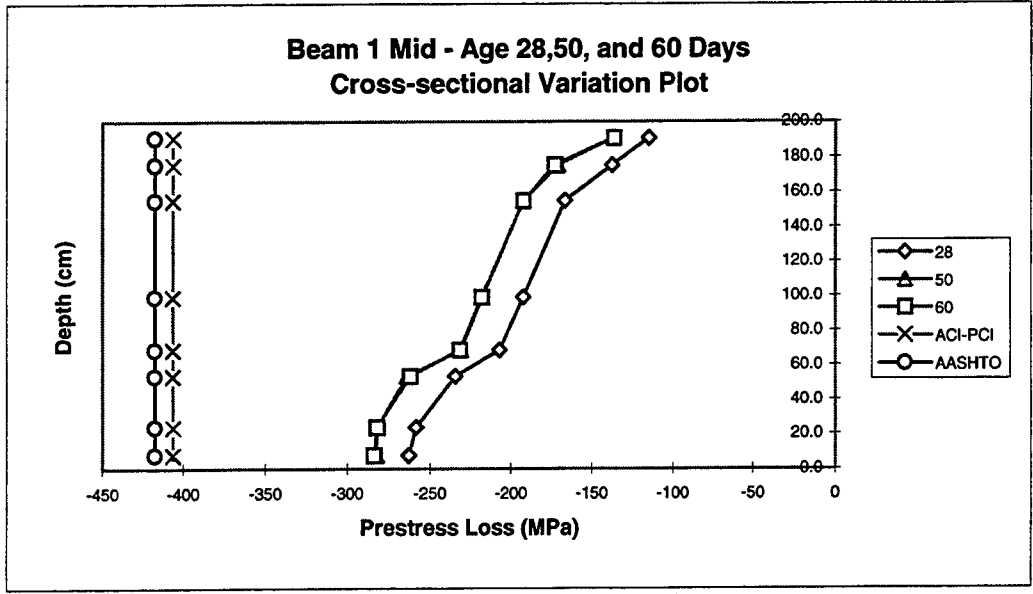


Figure 5-1(c-d) Midspan Beam 1 at (c) 28, 50, & 60 days (d) 60, 90, 120, and 150 days.

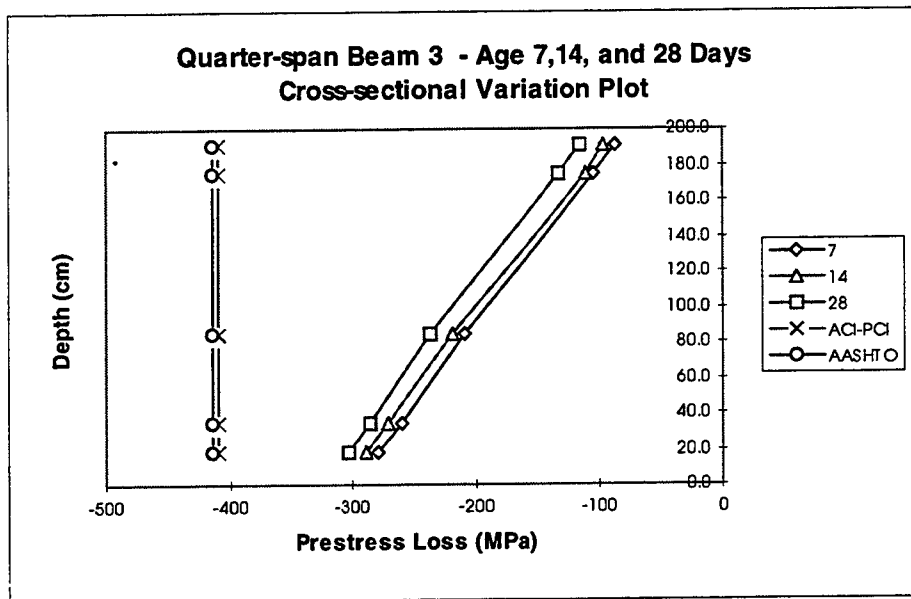
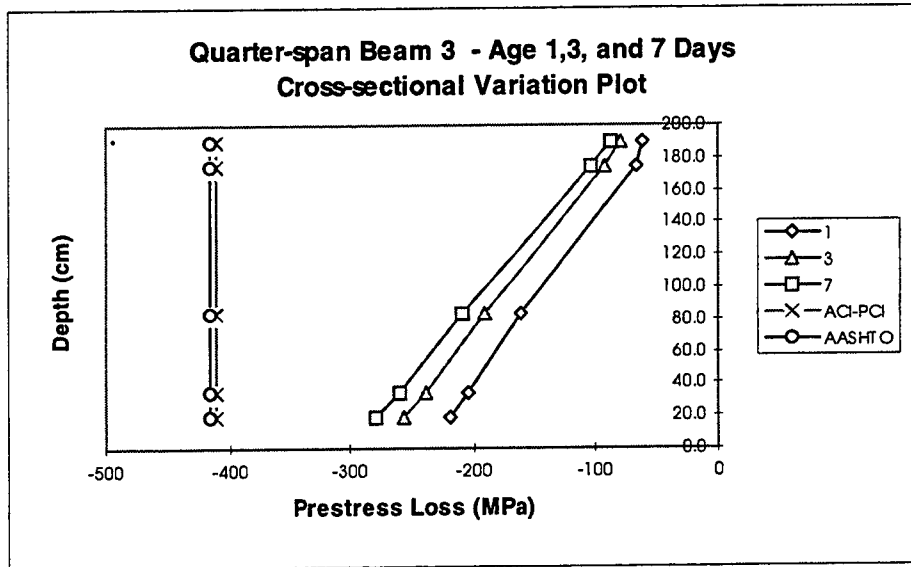


Figure 5-2 (a-b) Quarter-span Beam 3 at (a) 1, 3, & 7 days (b) 7, 14, & 28 days

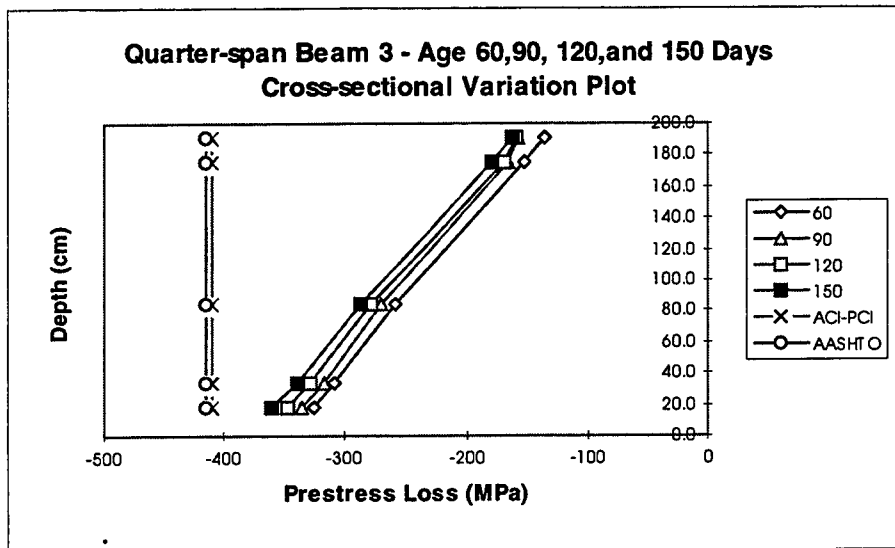
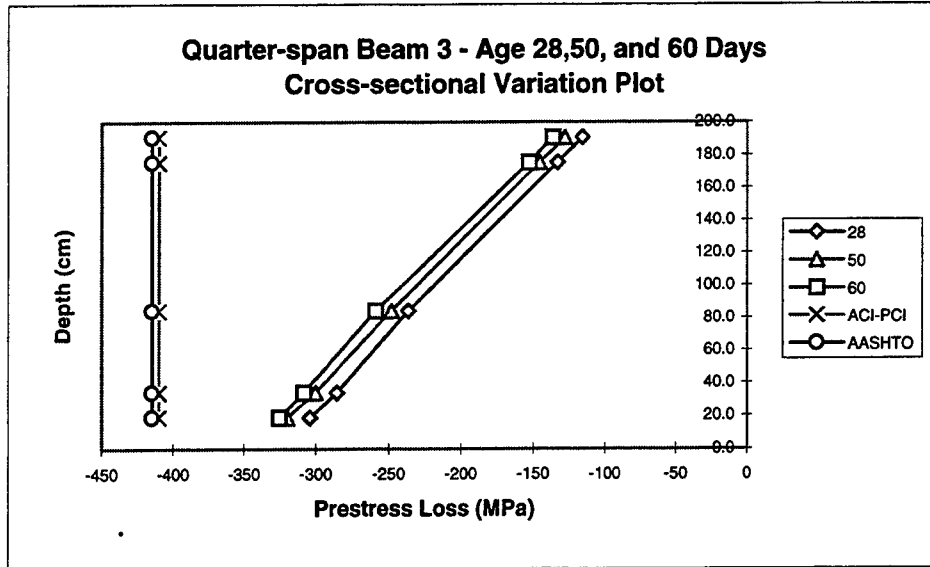


Figure 5-2(c-d) Quarter-span Beam 3 at (c) 28, 50, & 60 days (b) 60, 90, 120, & 150 days

In Figure 5-2c and d are similar to Figure 5-1d in that it shows a decreasing rate of the loss increment between the days. However, the rate at which the decrement occurs is more gradual than at the midspan. These plots for the quarter-span of Beam 3 are very similar to those of the midspan of Beam 1, but show a more linear variation of the loss over the depth of the beam.

5.2.3 From the End Support (1.52 m) Beam 4

The cross-sectional prestress loss versus depth at 1.52 m (5 ft.) from the end support for Beam 4 is shown in Figure 5-3(a-d). In the first plot, Figure 5-3a, the loss appears to be occurring at higher rate in the lower portion of the cross-section than in the upper. Figure 5-3b shows a trend towards a more uniform rate of loss between the top and bottom with little change between 14 and 28 days. However, the change between 7 and 14 days is greater. Figure 5-3c is consistent with that of Figure 5-3b except there is a larger change between 28 and 50 days while remaining relatively unchanged between 50 and 60 days. In Figure 5-3d, the loss starts showing a more consistent rate of decrement, and the separation per month going to 150 days is approximately equal.

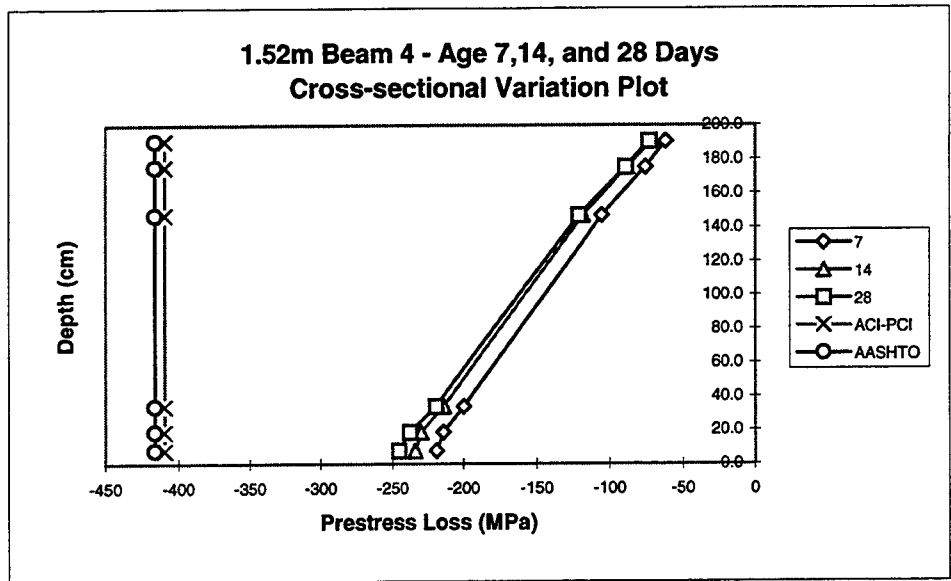
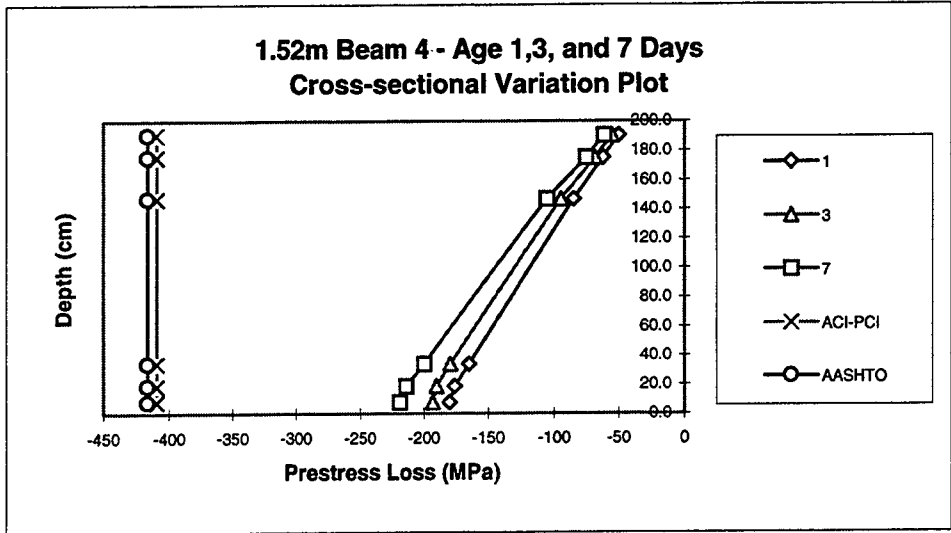


Figure 5-3 (a-b) 1.52 m Beam 4 at (a) 1, 3, & 7 days (b) 7, 14, & 28 days

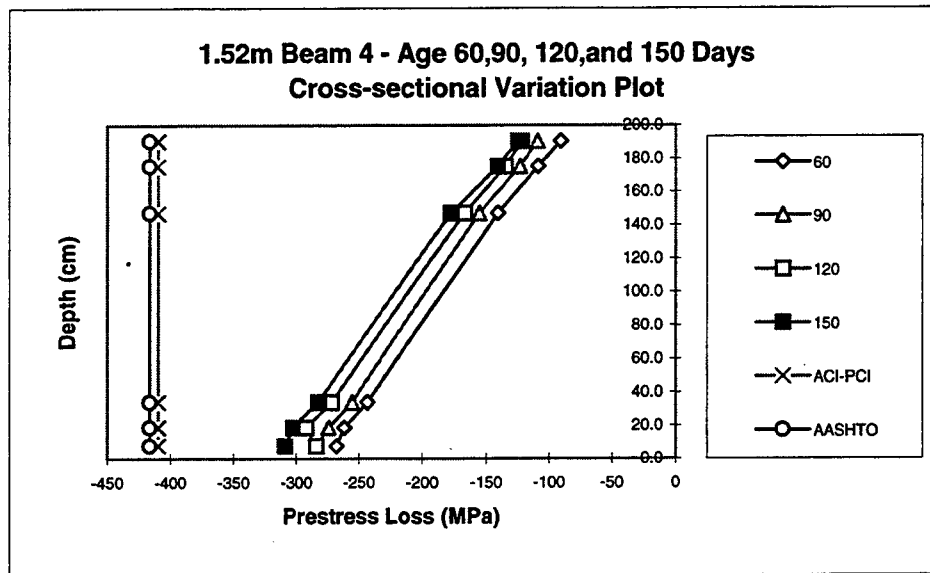
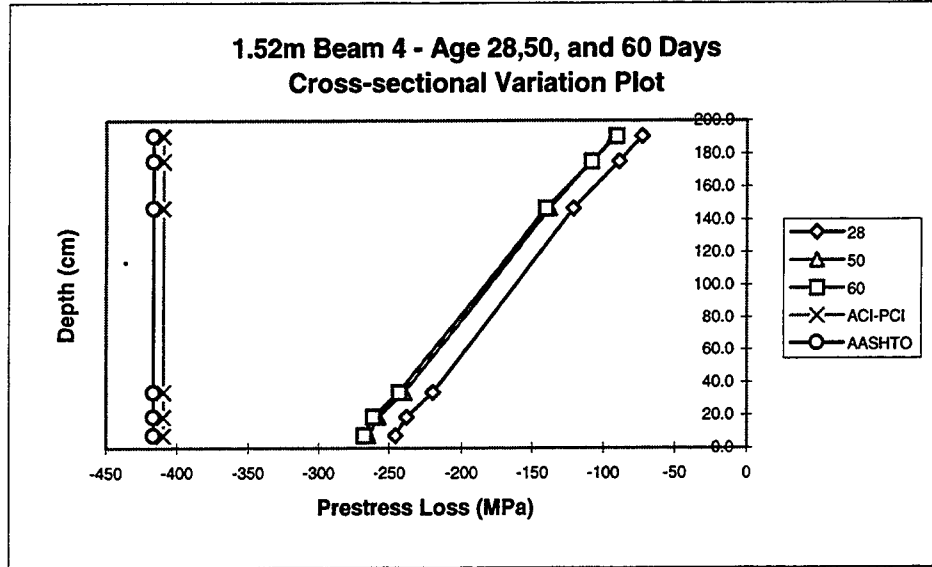


Figure 5-3 (c-d) 1.52 m Beam 4 at (c) 28, 50, & 60 days (b) 60, 90, 120, & 150 days

5.2.4 Discussion

The behavior of the cross-sectional prestress loss variation for the days mentioned is very similar for both midspan of Beam 1 and the quarter-span of Beam 3. It is interesting to note that no portions of the prestress loss have exceeded those of the Codes for any of the cross-sections shown.

5.3 Percentage Comparisons of the Prestress Loss

5.3.1 Introduction

So far the prestress loss has been represented by the value actually occurring at a specific location. An example of this is the lump sum prestress loss at the steel centroid of Beam 1 for 150 days is -324 MPa. In this section, the prestress loss is taken as defined ratios to have a better understanding of what all these numbers actually mean, with respect to prestressed concrete girder design.

5.3.2 Initial Prestress to Jacking Stress Ratio

The initial prestress, f_i , is defined as the prestress after all immediate losses have occurred. The immediate losses, in this report, are assumed to be all elastic shortening. The initial prestress can be computed as follows:

$$f_i = f_{pj} - \Delta f_{ES} \quad (5-1)$$

In Equation 5-1, f_{pj} is the jacking stress and Δf_{ES} is the loss of prestress due to elastic shortening. The jacking stress, f_{pj} , was consider uniform throughout the cross-section and was determined as follows:

$$f_{pj} = \frac{P_j}{A_{ps}} \quad (5-2)$$

In Equation 5-2, P_j represents the jacking force on one strand and A_{ps} is the cross-sectional area of one prestressing strand. For the case of the Westbound Gandy Bridge, P_j is equal to 150.4 kN (33.8 kips) and A_{ps} is equal to 1.08 cm² (0.167 in²). Applying these quantities in Equation 5-2 results for 1395 MPa (202.4 ksi), for the jacking stress.

Now that these parameters have been defined the initial prestress to jacking stress ratio is defined as follows:

$$\frac{f_{pi}}{f_{pj}} = \frac{f_{pj} - \Delta f_{ES}}{f_{pj}} \quad (5-3)$$

This ratio tells what percentage of the jacking stress is available after the immediate losses, or in this case after elastic shortening has occurred. This ratio is converted to a percent and plotted versus beam depth for the midspan of Beam 1, the quarter-span of Beam 3 and 1.52 m point for Beam 4.

Figure 5-4 shows the results from applying Equation 5-3 across the depth at the midspan of Beam 1. Also included on the plot are the ACI-PCI and AASHTO results obtained using Equation 5-3. The percentages vary with depth similarly to the plots of Section 5-2. The difference in percentages between the top gauge at 190.5 cm (75 in) to

the bottom gauge at 7.6 cm (3 in) is 8.6 %. The ACI-PCI and AASHTO Code are 91.6 % and 91.2 %, respectively. The Code results for immediate loss compare quite well with that at the girder centroid at 99.1 cm (39 in) of 91.7 % , but are smaller than at the steel centroid at 23.6 cm (9.3 in) of 87.9 %.

Figure 5-5 shows the results of initial prestress to jacking stress ratio versus depth for the quarter-span of Beam 3. The difference in percentages between the top gauge at 190.5 cm and the bottom gauge of 18.8 cm (7.4 in) is 10.7 %, which is similar to Figure 5-4. The Code results compare well with the draped steel centroid at 84.1 cm (33.1 in), which is very close to the girder centroid.

Figure 5-6 shows the results of initial prestress to jacking stress ratio versus depth for the location 1.52 m (5 ft) from the end support of Beam 4. The difference between the top gauge at 190.5 cm and the bottom gauge at 7.6 cm is 8.3 %, indicated a smaller variation of immediate prestress loss from the top and bottom in the neighborhood of the girder support. The Code results correspond quite well with those at 34.0 cm.

The girder centroid results compare well with those of the Codes at both the midspan of Beam 1 and the quarter-span of Beam 3. However, for the 1.52 m mark of Beam, the 34.0 cm location compared favorably to the Code values. The steel centroid results suggest that larger elastic shortening values than those estimated by the Codes.

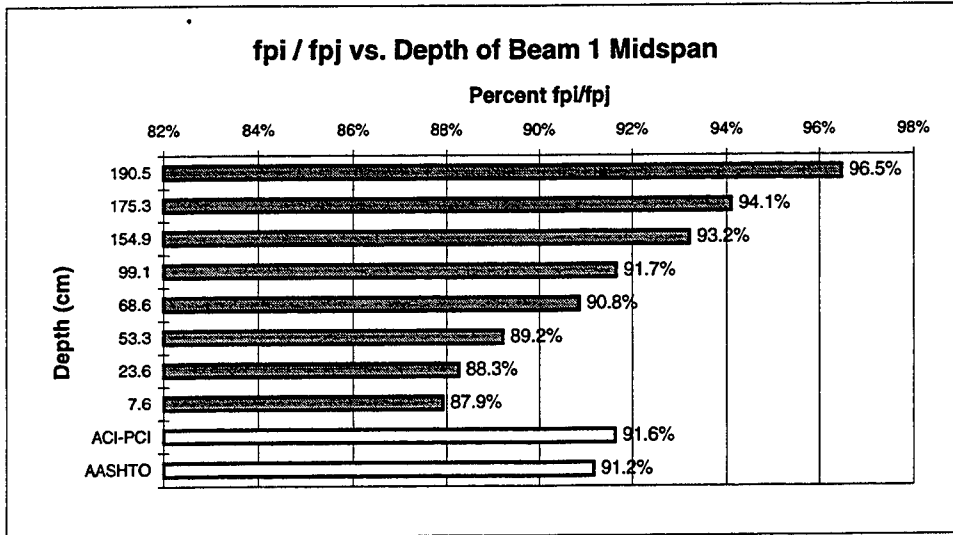


Figure 5-4 Midspan Beam 1, fpi/fpj versus depth

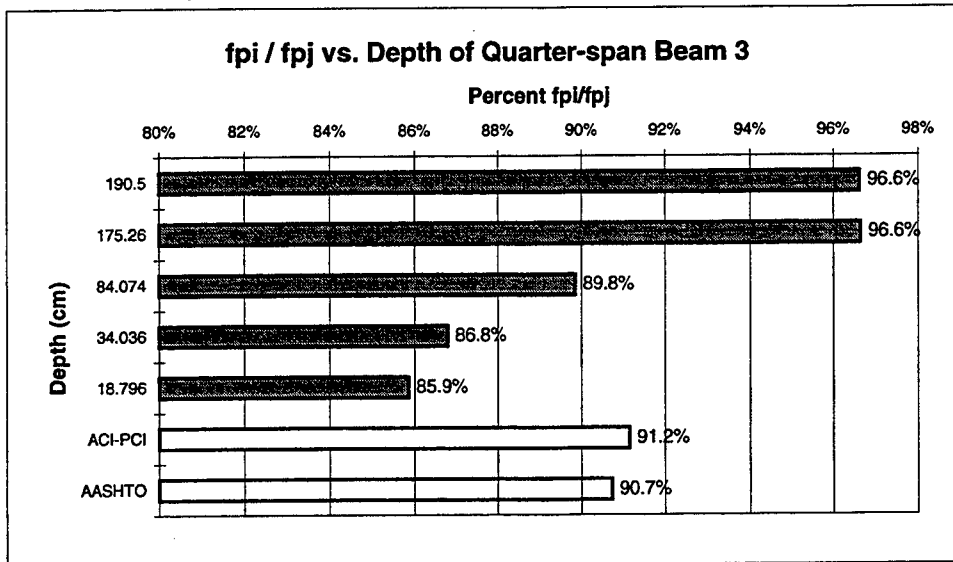


Figure 5-5 Quarter-span Beam 3, fpi/fpj versus depth

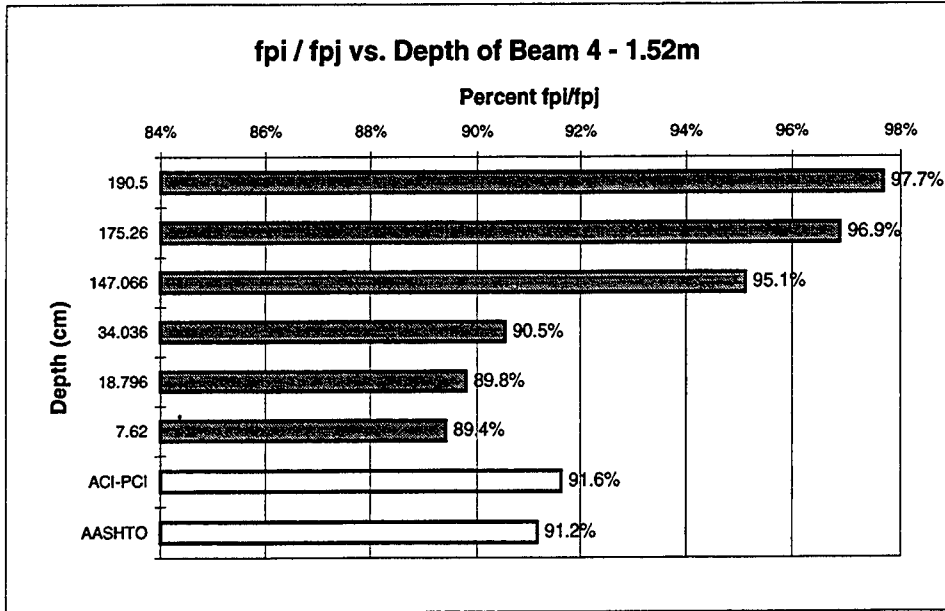


Figure 5-6 Beam 4, 1.52 m, fpi/fpj versus depth

5.3.3 The Effectiveness Ratio, R

The effectiveness ratio, R, is a parameter defined by Nilson [1] which relates the effective prestress force, P_e , at any time t to the initial prestress, P_i . The effectiveness ratio is as follows:

$$R = \frac{P_e}{P_i} \tag{5-4}$$

This ratio can easily be converted into stress by dividing P_e and P_i by the area of prestressing steel A_{ps} that corresponds to P_e and P_i . Then the effectiveness ratio takes this form:

$$R = \frac{f_{pe}}{f_{pi}} \quad (5-5)$$

In Equation 5-5, f_{pe} can be taken at any time t to determine the effectiveness ratio at that time. The effective prestress, f_{pe} is computed as follows:

$$f_{pe} = f_{pi} - \Delta f_{TD} \quad (5-6)$$

In Equation 5-6, Δf_{TD} represents the time-dependent loss occurring up to the time examined. The effectiveness ratio, describes how much prestress in terms of percent of f_{pi} is still available for the use in the girder. Nilson also suggests $(1-R)$ as another interesting quantity to investigate and is represented here in terms of stress as follows:

$$1 - R = \frac{f_{pi} - f_{pe}}{f_{pi}} = \frac{\Delta f_{TD}}{f_{pi}} \quad (5-7)$$

Equation 5-7 relates the time-dependent loss at any time t to the initial prestress. The plots in this section are set with $t = 150$ days, that means., Δf_{TD} is the time-dependent loss occurring up to this time.

Figure 5-7 contains the plots of $(1-R)$ versus depth for the midspan of Beam 1. From the 1-R plot only 9.2 % of the initial prestress for the location at 190.5 cm has been lost as opposed to 12.6 % at 7.6 cm. The ACI-PCI and the AASHTO Codes provide for 22.6 % and 23.1 % time-dependent losses, respectively.

Figure 5-8 contains the plots of (1-R) versus depth for the quarter-span of Beam 3. For the (1-R) plot, the 190.5 cm location has a time-dependent prestress loss of 8.6 % which differs from the location of 18.8 cm which has a loss of 13.6 %. These losses are smaller than the Code suggested values up to this time

Figure 5-9 represents the plots of (1-R) for the location 1.52 m from the end support. For the (1-R) plot, 6.7 % of the time-dependent prestress loss has been lost at 190.5 cm compared to 12.9 % at 7.6 cm. If the Code values are to be used as a datum, this suggests that much more time-dependent loss can be expected in the future.

5.3.4 Lump Sum Loss to Jacking Stress Ratio

The lump sum loss to jacking stress ratio tells what percentage of the applied jacking stress is lost. This is important because knowledge of this ratio can be allowed for in design and more realistic service stresses can be obtained. The lump sum loss includes immediate losses and the time-dependent losses occurring up to 150 days.

Figure 5-10 shows the lump sum loss to jacking stress ratio versus depth for the midspan of Beam 1. There are significant differences from the top of the cross-section to its bottom. At 190.5 cm, there has only been a 12.4 % loss compared to 7.6 cm, where there was a 23.2 % loss.

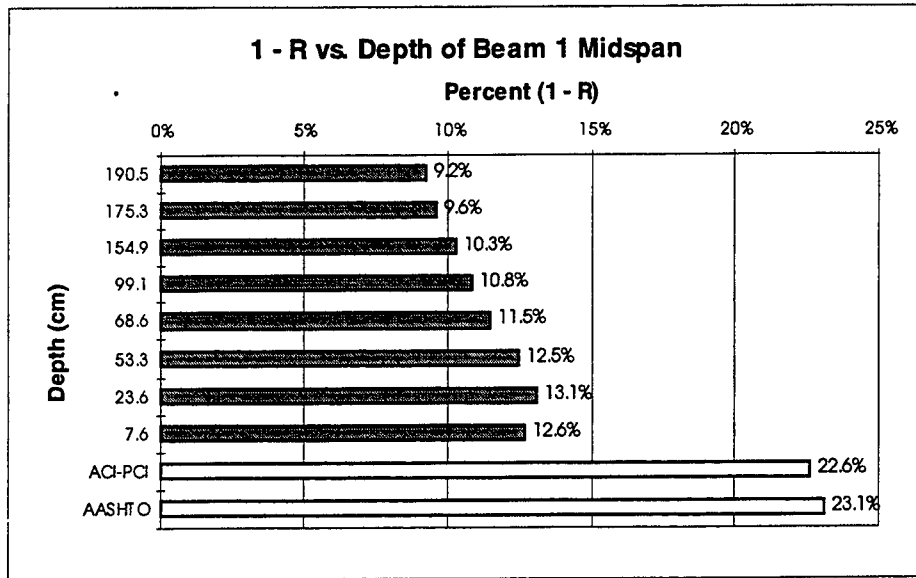


Figure 5-7 Midspan Beam 1

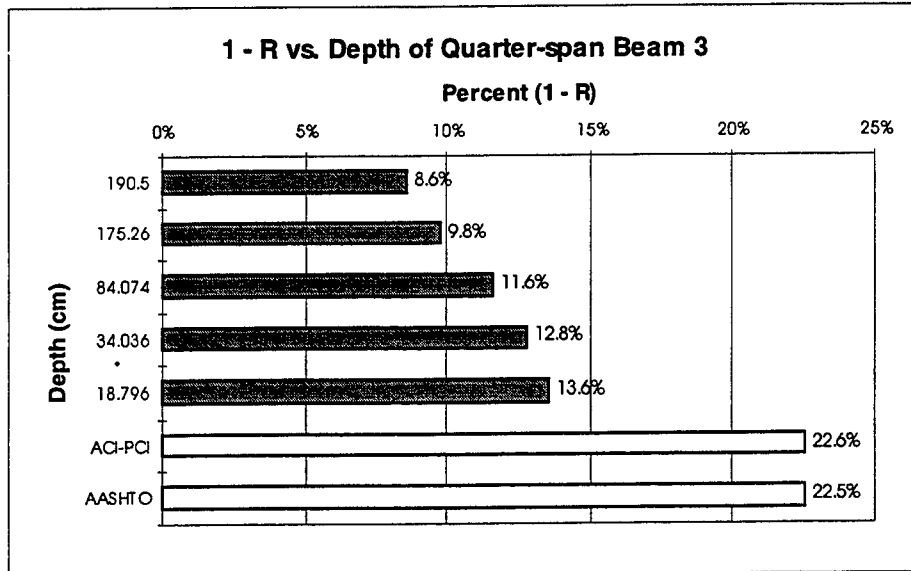


Figure 5-8 Quarter-span Beam 3

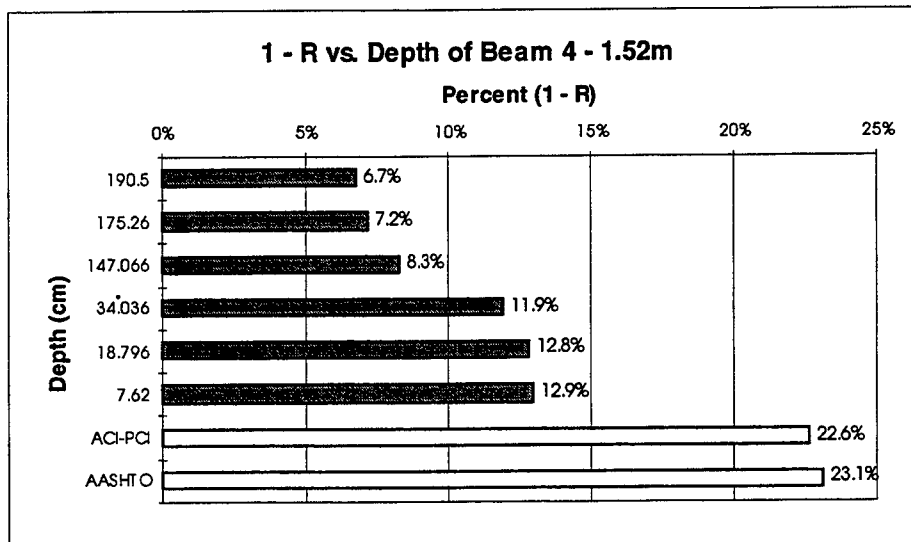


Figure 5-9 Beam 4 - 1.52 m

Figure 5-11 shows the lump sum loss to jacking stress ratio versus depth for the quarter-span of Beam 3. There also are significant differences from the top of the cross-section to its bottom. At 190.5 cm, there has only been a 11.7 % loss compared to 18.8 cm, where there is a 25.8 %..

Figure 5-12 shows the lump sum loss to jacking stress ratio versus depth for the 1.52 m mark of Beam 4. There, as well, is a significant difference between the top and bottom of the cross-sections, from 8.9 % at 190.5 to 22.1 % at 7.6 cm. This difference, however, is smaller than those of the midspan of Beam 1 and the quarter-span of Beam 3. There are no points within these cross-sections that have surpassed either the ACI-PCI or AASHTO ratios.

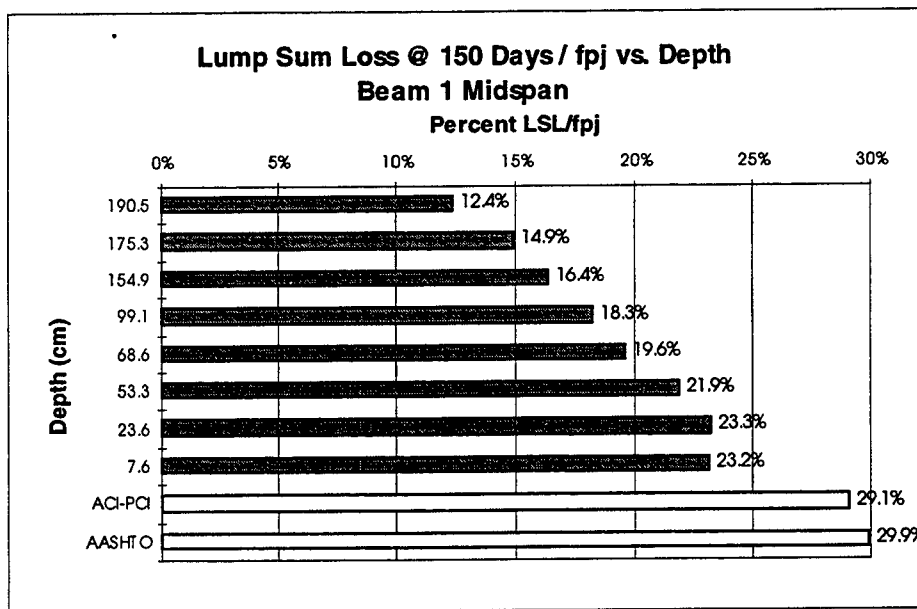


Figure 5-10 Midspan Beam 1, Lump sum loss to jacking stress

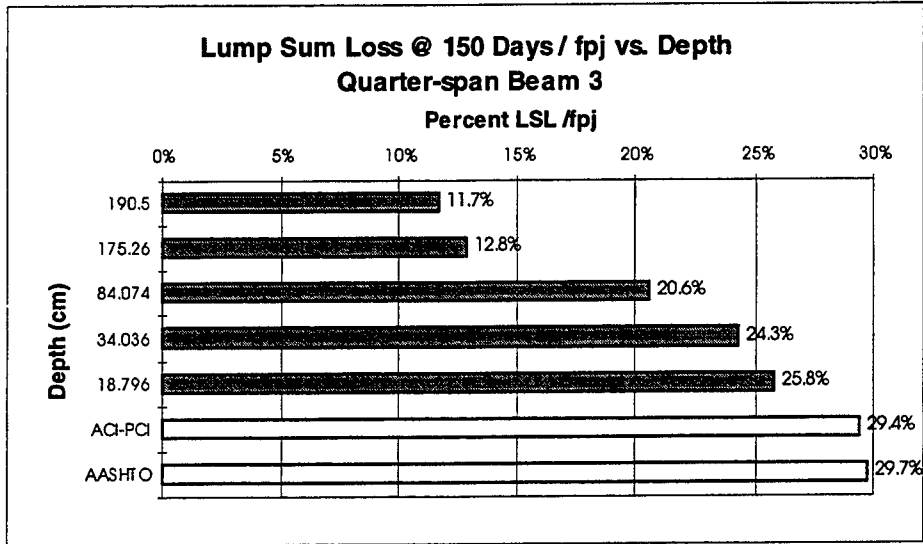


Figure 5-11 Quarter-span Beam 3, Lump sum loss to jacking stress

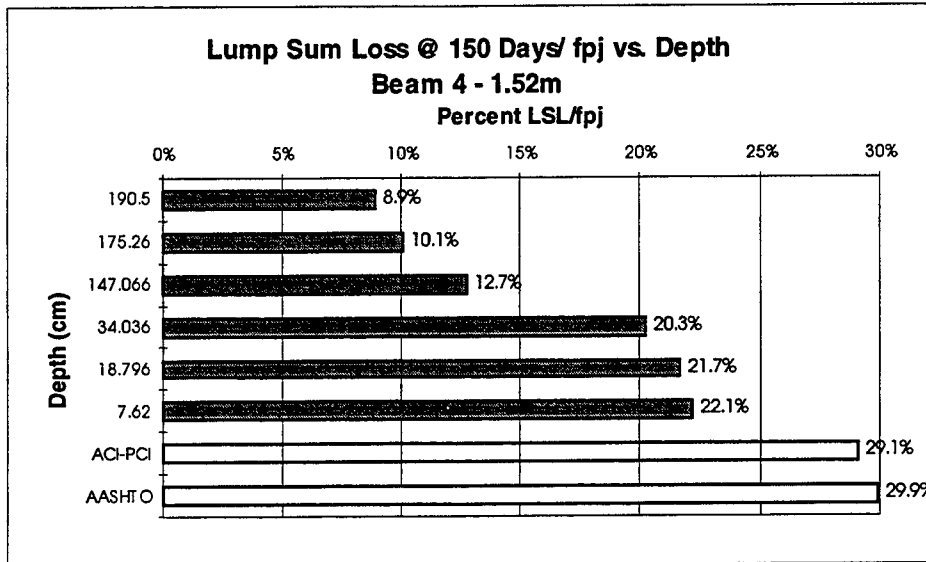


Figure 5-12 Beam 4 - 1.52 m, Lump sum loss to jacking stress

5.3.5 Elastic Shortening to Jacking Stress Ratio

Elastic shortening to jacking stress ratio is a useful quantity to a designer, because it tells how much of the jacking stress is lost initially during transfer. Actually, this ratio could be more appropriately named immediate loss to jacking stress ratio. The elastic shortening to jacking stress ratio is computed as follows:

$$\frac{\Delta f_{ES}}{f_{pj}} \quad (5-8)$$

All terms in Equation 5-8 are as defined earlier.

In Figures 5-13 through 5-15, the elastic shortening to jacking stress ratio has been converted to a percentage and is plotted versus depth for the midspan of Beam 1, the quarter-span of Beam 3, and the 1.52 m of Beam 4, respectively. For all three plots, this ratio varies considerably across the cross-section. The difference in percent between the bottom-most and top-most gauges is 8.6 %, 10.7 %, and 8.3 %, for the midspan, quarter-span and 1.52 m locations, respectively. Also included on the plots the elastic shortening to jacking stress ratio as computed by the Codes. At midspan the gauge at 99.1 cm, the concrete centroid correlates close with the Code results. The Code values are exceeded in the lower portion of the girders, with the maximum ratio of 14.1 % occurring at the quarter-span.

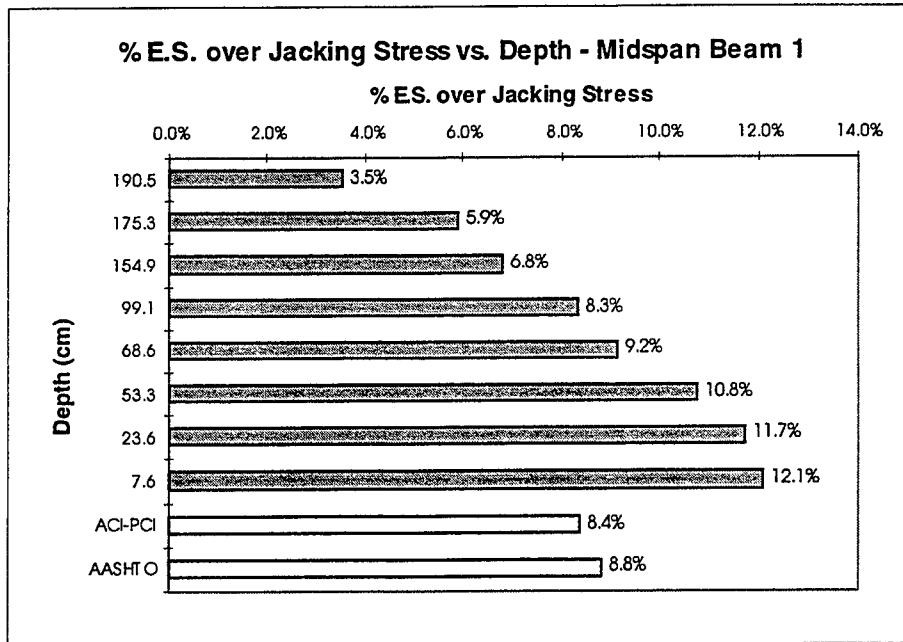


Figure 5-13 Elastic shortening to jacking stress ratio for Beam 1 midspan

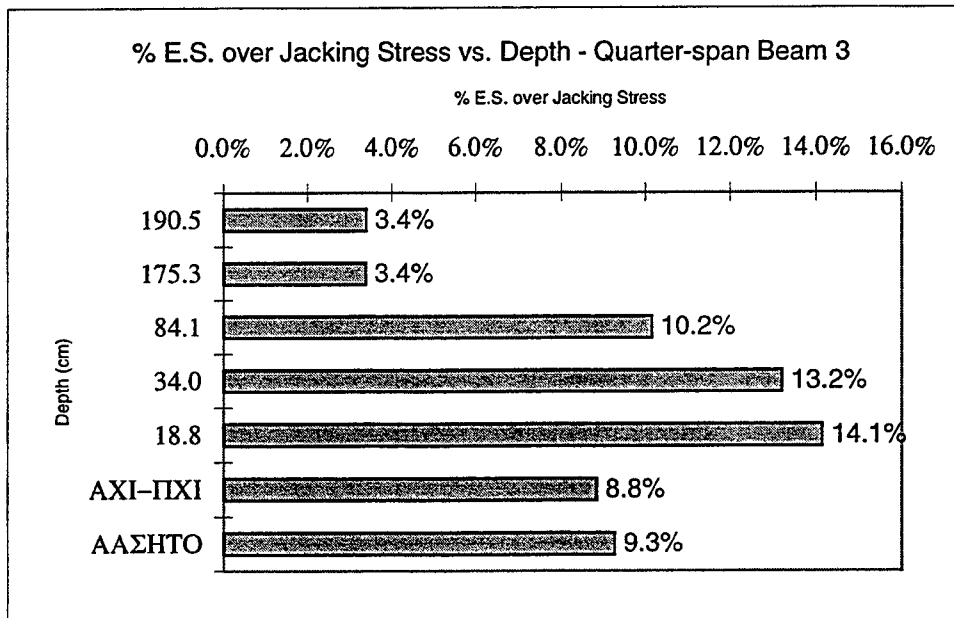


Figure 5-14 Elastic shortening to jacking stress ratio for Beam 3 quarter-span

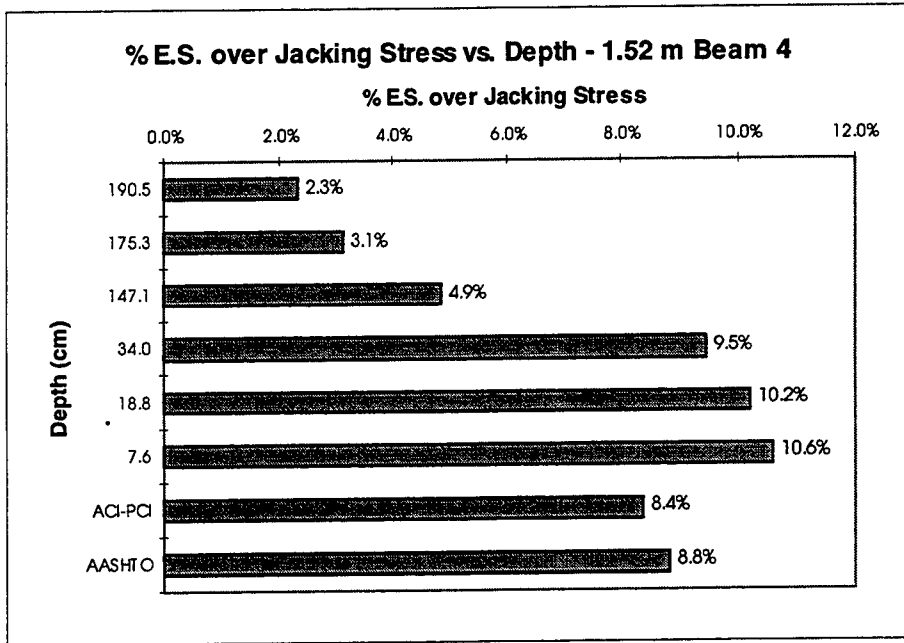


Figure 5-15 Elastic shortening to jacking stress ratio for 1.52 m mark Beam 4

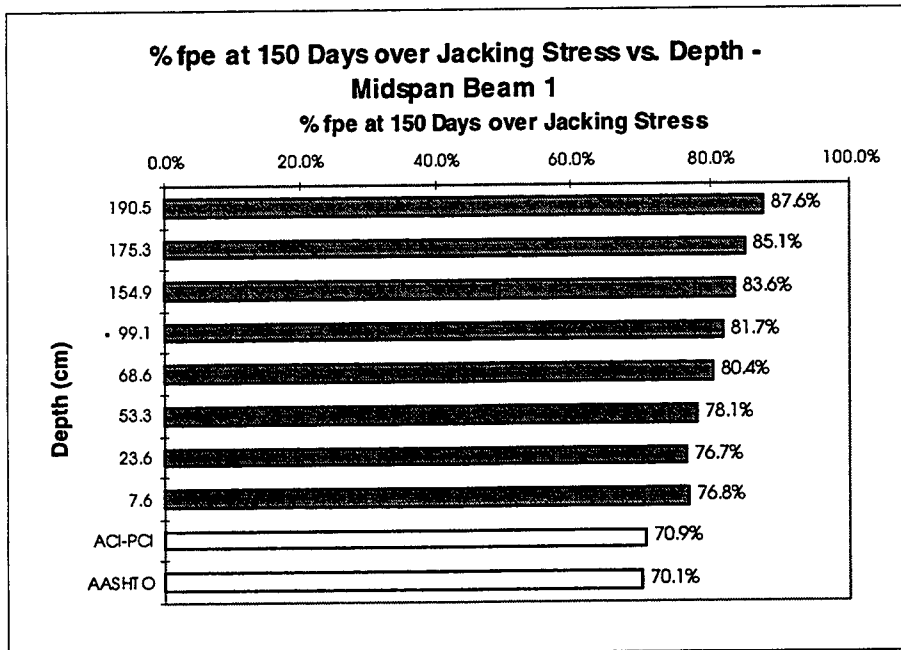


Figure 5-16 Effective stress to jacking stress ratio for Beam 1 midspan

5.3.6 Effective Stress to Jacking Stress Ratio

The effective stress to jacking stress ratio represents how much of the first applied jacking stress is still available after all losses have occurred. However, since this analysis has only taken place over the 150 days, the effective stress was computed on the basis of 150 days in this case. The effective stress at 150 days over jacking stress ratio is computed as follows:

$$\frac{f_{pe} \text{ at 150 days}}{f_{pj}} = \frac{f_{pj} - \Delta f_{\text{Lump Sum}} \text{ at 150 days}}{f_{pj}} \quad (5-9)$$

In Equation 5-9, the f_{pe} at 150 days is the effective stress at 150 days and $\Delta f_{\text{Lump Sum}}$ at 150 days is the lump sum loss occurring over 150 days.

In Figures 5-16 through 5-18, the effective stress at 150 days to jacking stress ratio has been converted to a percentage, and plotted versus depth for the midspan of Beam 1, the quarter-span of Beam 3, and the 1.52 m mark of Beam 4, respectively. Also included on these plots are the ratios computed by using the Codes. The appears to be more stress available in the upper portion the beams than at the lower portion for the three cases shown here as expected. The maximum effective stress to jacking stress ratio of 91.1 % is found at the gauge at 190.5 cm in Beam 4 at the 1.52 m mark. The minimum effective stress to jacking stress ratio of 74.2 % occurs at the 18.8 cm mark at the quarter-span of Beam 3. No values have exceeded those of the Codes for any location at this time.

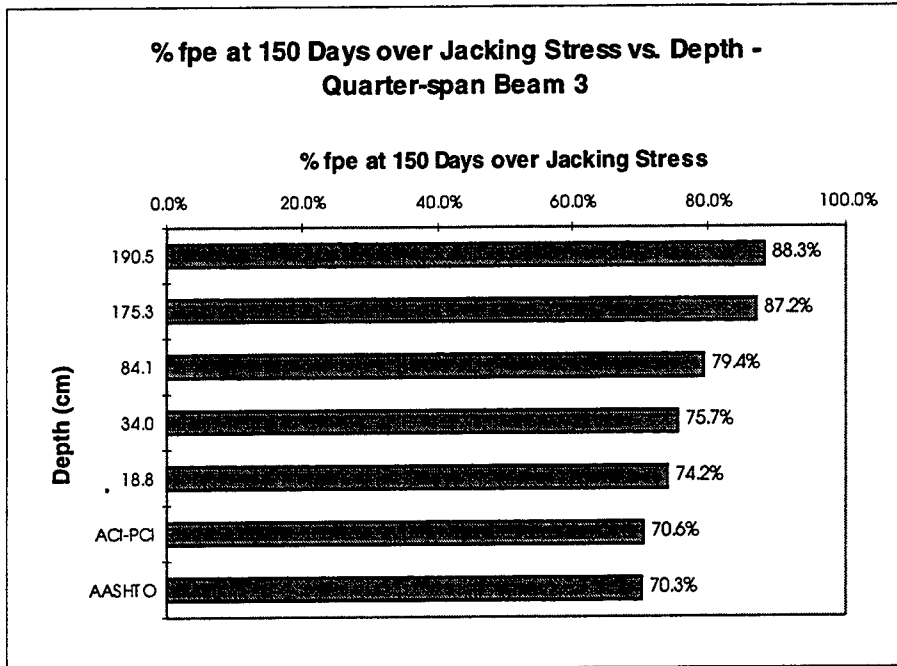


Figure 5-17 Effective stress to jacking stress ratio for Beam 3 quarter-span

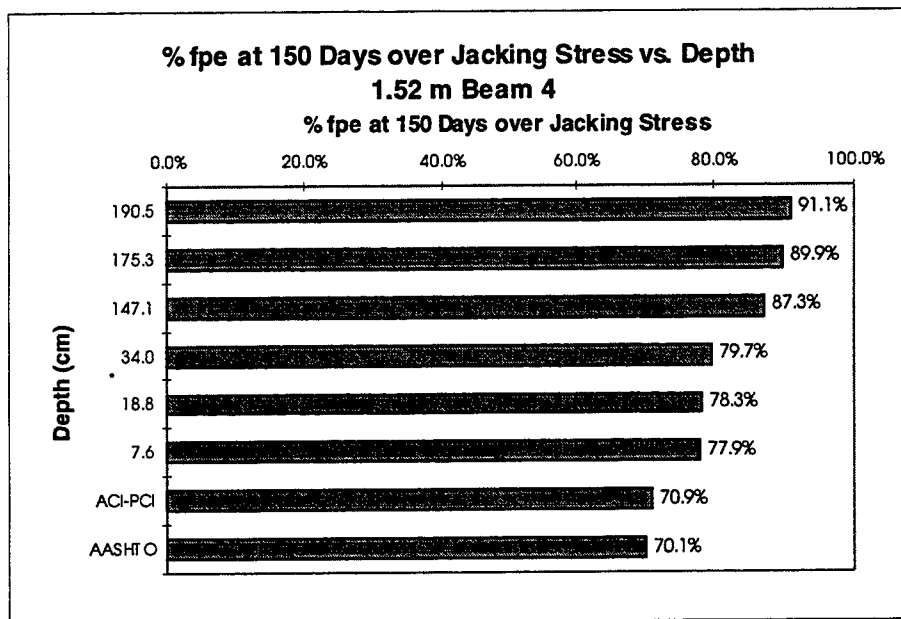


Figure 5-18 Effective stress to jacking stress ratio for 1.52 m mark Beam 4

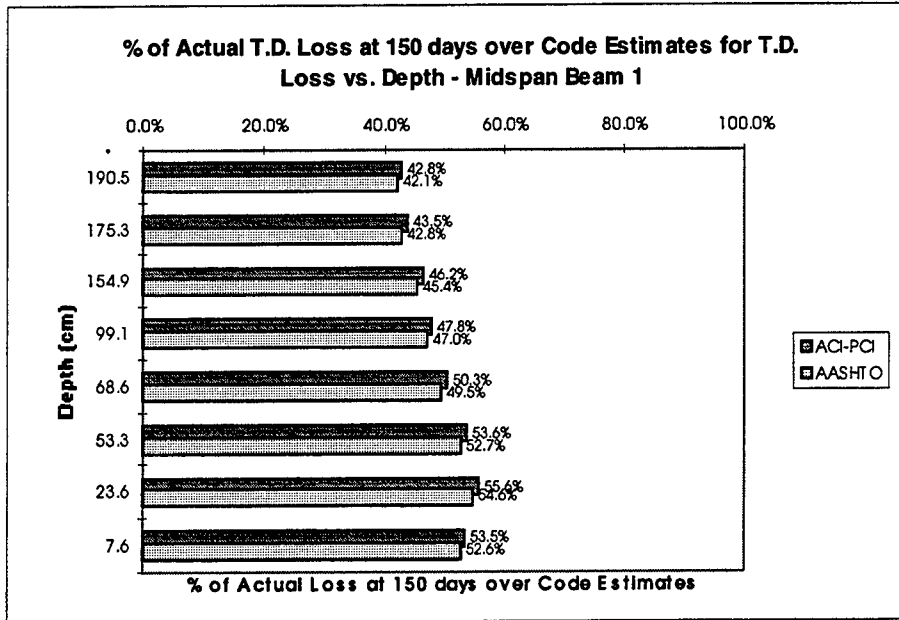


Figure 5-19 Actual T.D. loss to Code T.D. loss Beam 1 midspan

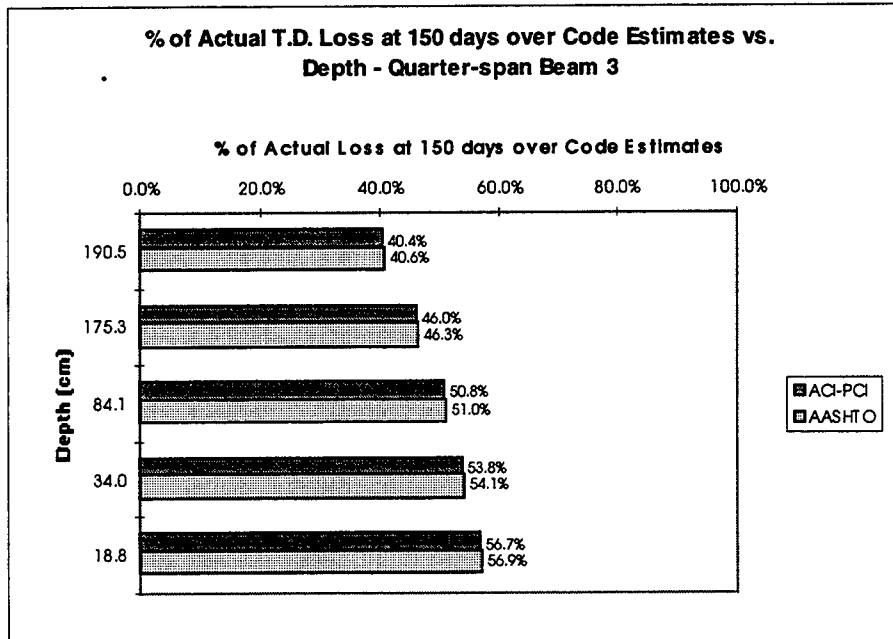


Figure 5-20 Actual T.D. loss to Code T.D. loss Beam 3 quarter-span

5.3.7 Actual Time-Dependent Loss over Code Computed Time-Dependent Loss

The actual time-dependent loss at 150 days to Code compute time-dependent loss ratio indicates how the field measured time-dependent losses compare with their Code specified counterparts. This quantity is computed as follows:

$$\frac{\Delta f_{TD \text{ ACTUAL AT 150 DAYS}}}{\Delta f_{TD \text{ CODE ESTIMATES}}} \quad (5-10)$$

In Figure 5-19 through 5-20, the this ratio expressed in percent is plotted actual versus depth for the midspan of Beam 1, the quarter-span of Beam 3, and the 1.52 m mark of Beam 4, respectively. The quantities vary within each cross-section. The largest variation occurs at the 1.52 m mark. The minimum ratios occur at the 190.5 cm gauge in the 1.52 m mark of Beam 4 and are 31.8 % and 31.3 %, corresponding to the calculations based on ACI-PCI and AASHTO computed losses. The maximum ratios occur at the 18.8 cm gauge in the quarter-span of Beam 3 and are 56.7 % and 56.9%, corresponding to the calculations based on ACI-PCI and AASHTO computed losses.

5.3.8 Actual Lump Sum Loss over Code Computed Lump Sum Loss

The actual lump sum at 150 days over Code computed lump sum loss gives a measure of where these field measured values stand against the Codes. This quantity is computed as follows:

$$\frac{\Delta f_{LS \text{ ACTUAL AT 150 DAYS}}}{\Delta f_{LS \text{ CODE ESTIMATES}}} \quad (5-11)$$

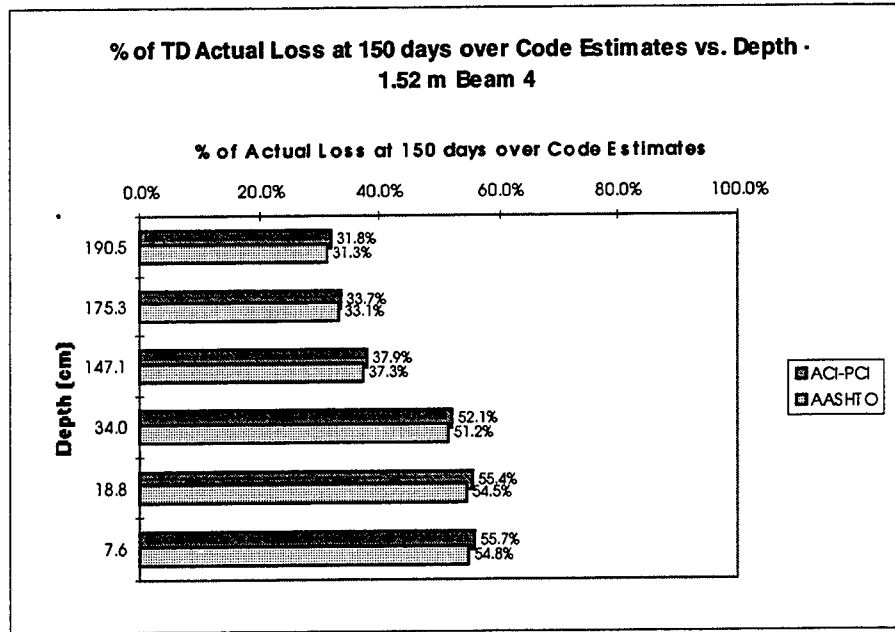


Figure 5-21 Actual T.D. loss to Code T.D. loss 1.52 m mark Beam 4

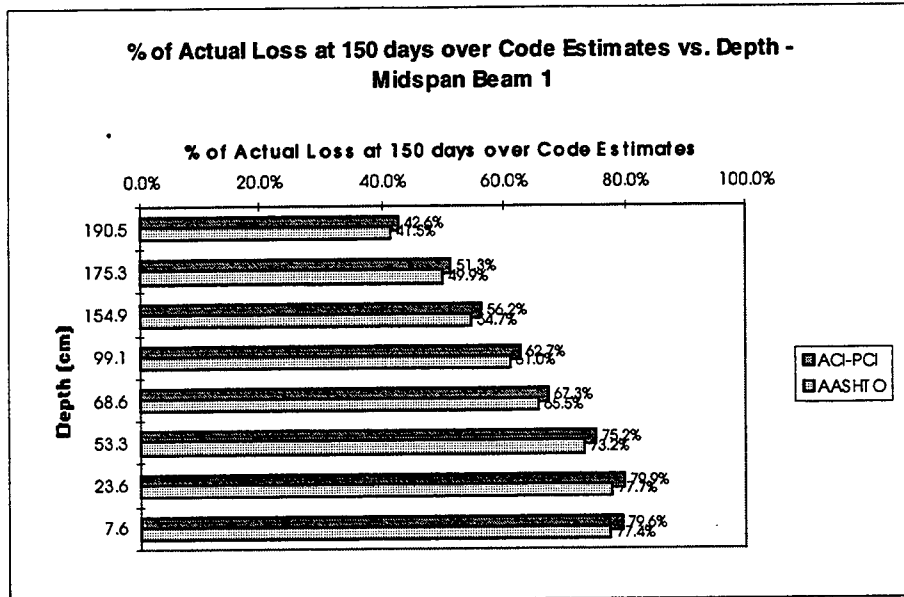


Figure 5-22 Actual L.S. loss to Code L.S. loss Beam 1 midspan

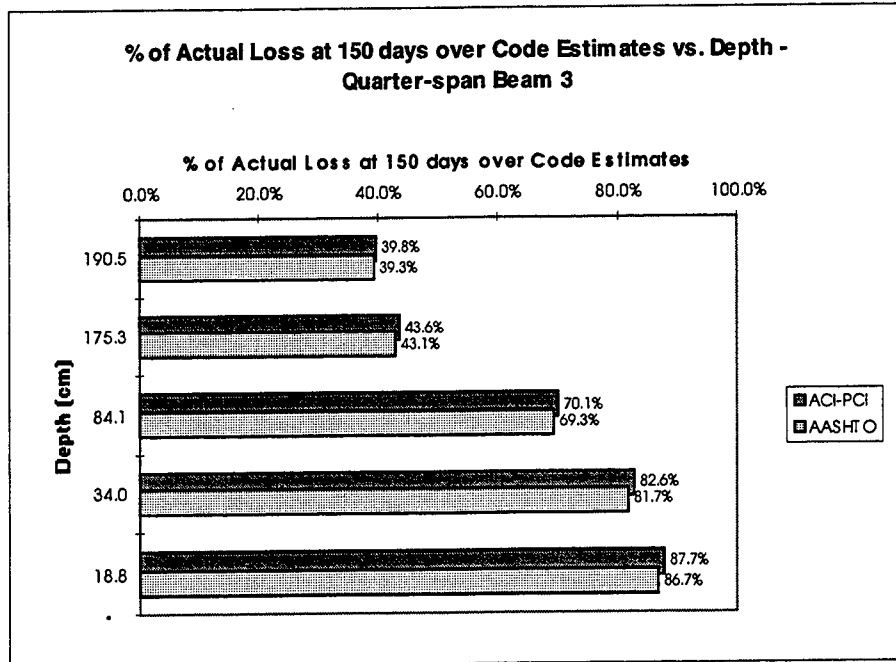


Figure 5-23 Actual L.S. loss to Code L.S. loss Beam 3 quarter-span

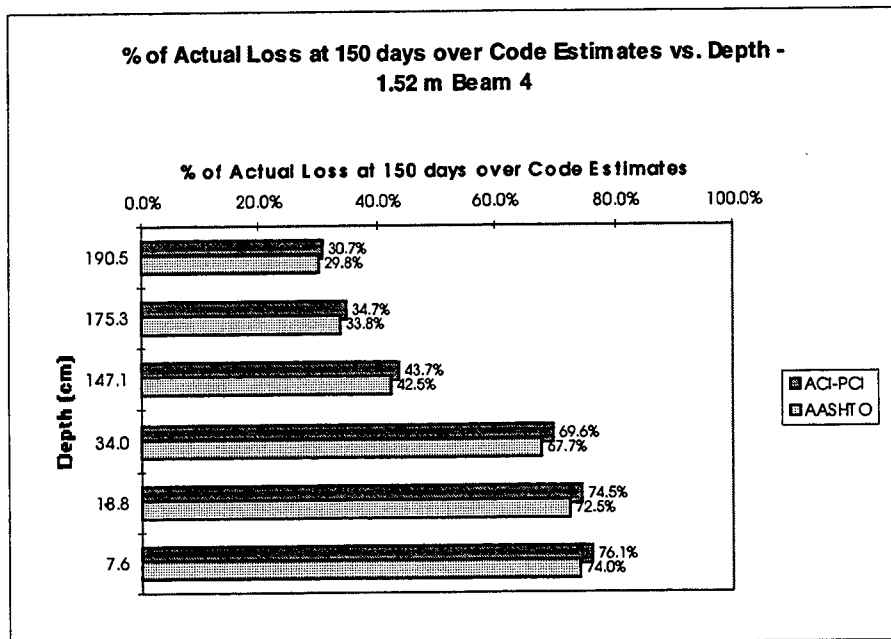


Figure 5-24 Actual L.S. loss to Code L.S. loss 1.52 m mark Beam 4

In Figure 5-22 through 5-24, these values expressed in percent are plotted versus depth for the midspan of Beam 1, the quarter-span of Beam 3, and the 1.52 m mark of Beam 4, respectively. The quantities vary within each cross-section. The largest variation occurs at the 1.52 m mark. The minimum ratios occur at the 190.5 cm gauge in the 1.52 m mark of

Beam 4, and are 30.7% and 29.8%, corresponding to the calculations based on ACI-PCI and AASHTO computed losses. The maximum ratios occur at the 18.8 cm gauge in the quarter-span of Beam 3 and are 87.7% and 86.7%, corresponding to the calculations based on ACI-PCI and AASHTO computed losses.

5.3.9 Time-Dependent Loss to Elastic Shortening Loss Ratio

The time-dependent loss to elastic shortening loss ratio relates the two types of losses. Typically, this value is in the range of 2.2 to 2.6. This range covers the Code calculated ratios. This ratio gives an indication of the influence of time-dependent behavior in a given member, at a specified location. This quantity is determined as follows:

$$\frac{\Delta f_{\text{TIME-DEPENDENT}}}{\Delta f_{\text{ELASTIC SHORTENING}}} \quad (5-12)$$

In Figure 5-25 through 5-27, time-dependent loss to elastic shortening ratio are plotted versus depth for the midspan of Beam 1, the quarter-span of Beam 3, and the 1.52

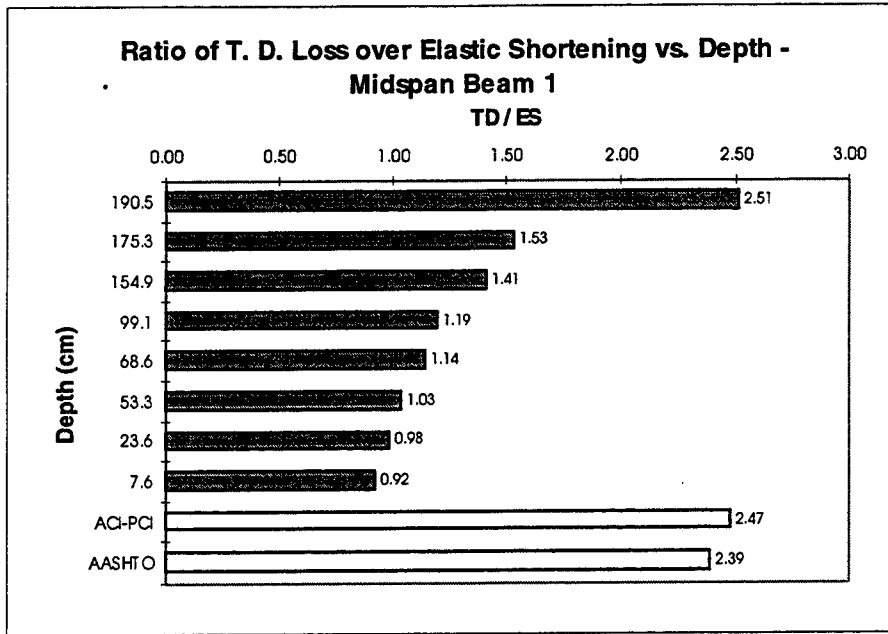


Figure 5-25 T.D. loss to E.S. loss ratio for Beam 1 midspan

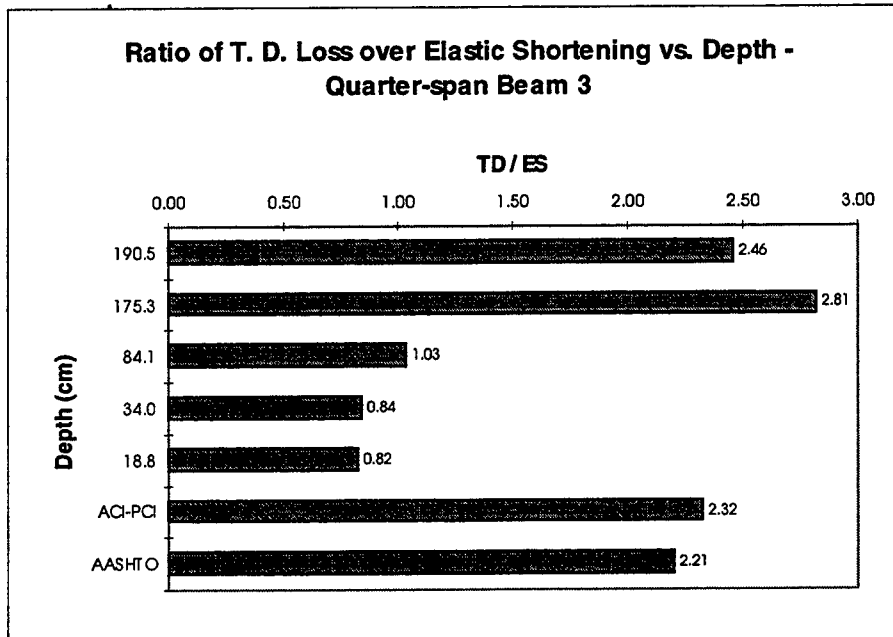


Figure 5-26 T.D. loss to E.S. loss ratio for Beam 3 quarter-span

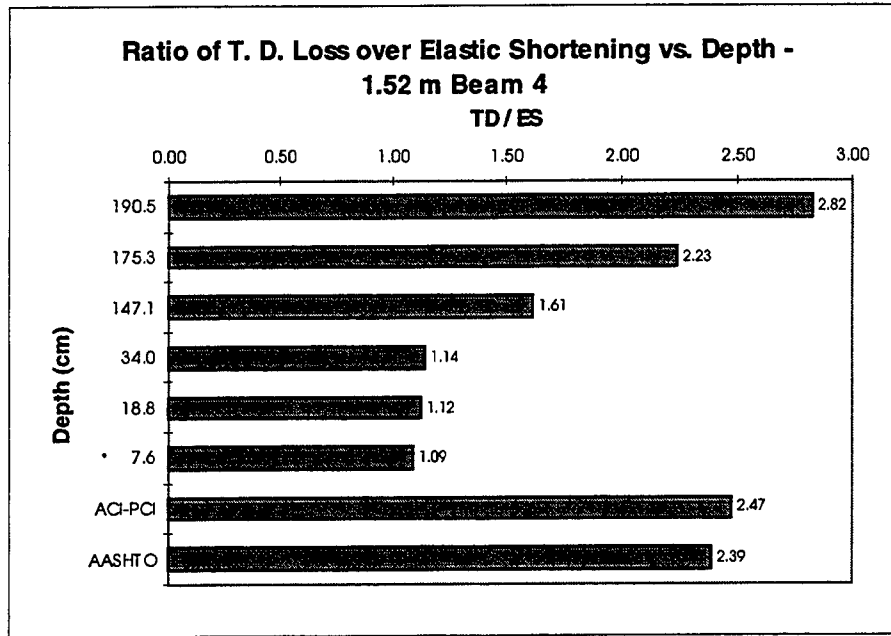


Figure 5-27 T.D. loss to E.S. loss ratio for 1.52 m Beam 4

m mark of Beam 4, respectively. The range varies from very high numbers in the upper portion of a cross-section to much lower values in the bottom portion. The greatest value of 2.82 occurs at 190.5 cm gauge location, at the 1.52 m mark of Beam 4. The lowest value of 0.82 occurs at 18.8 cm gauge of the quarter-span of Beam 3. The lower value suggests that more time-dependent losses could be expected to occur at these locations. Hence, the time-dependent behavior is more significant in this region. On the other hand, the high values in the top region suggest that the time-dependent behavior will have little or no effect in this region as time progresses.

5.4 Tendon and Concrete Stresses

5.4.1 Introduction

The ACI Code describes in Chapter 18 the limits for prestressed concrete design. In particular, Section 18.4 and 18.5 of the ACI Code, the permissible stresses in the concrete and the prestressing tendons are discussed. These limiting stresses will be applied to the Westbound Gandy Bridge in this section. In order to do this, it will be necessary incorporate the measured prestress losses in determining the tendon stresses and concrete stresses.

5.4.2 Prestressing Tendon Stresses

In Section 18.5 of the ACI-Code, the allowable tensile stresses for prestressing tendons are stated for two specific stress times. The stress due to the jacking force and the stress immediately after prestress transfer. These stress values will then be compared to those values obtained for the girders that are being investigated. Remember that the available data used in this report covers up to 150 days, which is before the slab and service loads are applicable

The prestressing tendon stress is determined at the steel centroid of the midspan of Beam 1, but for the quarter-span and the 1.52 m from the end support, the tendon stresses will be determined for two different locations. These locations will be where the draped steel centroid occurs in each section and the straight steel centroid, which is the same for both the quarter-span and 1.52 m from the end support location.

In 18.5.1(a) of the ACI-Code, it states that the tensile stress due to tendon jacking force may not be larger than $0.94f_{py}$, but not greater than the lesser of $0.80f_{pu}$ and the maximum value recommended by the prestressing tendon or anchorage manufacturer because of the jacking force. The quantity f_{py} is the specific yield stress of a prestressing tendon. In the Commentary of 18.5 of the ACI-Code, it suggests that the $0.90f_{pu}$ be used for determining f_{py} for low relaxation wires and tendons, which is the type of tendon used in the Gandy project.

In 18.5.1(b) of the ACI-Code, it states that the tensile stress may not be larger than $0.82f_{py}$, but not greater than $0.74f_{pu}$, just after the transfer of the prestressing force from the tendons to the concrete. Table 5-1 has the calculated stress limitations from Section 18.5 of the ACI-Code.

Table 5-1 Limitations on stress in the steel strands.

ACI Code Results for $f_{pu} = 1862 \text{ MPa (270 ksi)}$							
18.5.1(a) Due to Jacking Force				18.5.1(b) Immediately After Transfer			
$0.94f_{py}$		$0.80f_{pu}$		$0.82f_{py}$		$0.74f_{pu}$	
MPa	ksi	MPa	ksi	MPa	ksi	MPa	ksi
1575	228.4	1489	216	1339	194.2	1378	200

The stress limit caused by jacking force is controlled by $0.80f_{pu}$ which is 1489 MPa (216 ksi). The jacking stress f_{pj} was calculated earlier as 1396 MPa (202.4 ksi), which is below $0.80f_{pu}$, so this is okay.

The limiting stress immediately after transfer is controlled by $0.82f_{py}$, which is 1339 MPa (194 ksi). The prestressing tendon stresses for the midspan of Beam 1, the quarter-span of Beam 3, and the 1.52 m (5 ft) from the end support of Beam 3 can be seen in Table 5-2.

Table 5-2 Resulting stresses at tendon centroid locations.

Prestressing Tendon Stresses for Steel Centroid Locations				
Beam 1 Midspan	Beam 3 Quarter-span		Beam 4 Location of 1.52 m	
Overall Steel Centroid	Draped Steel Centroid	Straight Steel Centroid	Draped Steel Centroid	Straight Steel Centroid
1171 MPa	1254 MPa	1197 MPa	1327 MPa	1253 MPa
(169.8 ksi)	(181.8 ksi)	(173.7 ksi)	(192.5 ksi)	(181.7 ksi)

The steel stress of 1327 MPa (193.2 ksi) at the draped steel centroid of Beam 4 at the 1.52 m (5 ft) from the end support is dangerously close to the limiting stress of 1339 MPa (194 ksi). All other locations are well within the $0.82f_{py}$ limit.

5.4.3 Concrete Stresses

In this section, the limitations on concrete stress immediately after transfer are presented in Section 18.4.1 of the ACI-Code and will be discussed. Then the cross-sectional prestress losses presented in Section 5.2 of this project will be used to determine the concrete stresses throughout the cross-section. In addition to this, the concrete stress resulting from the uniform loss provided by AASHTO is also computed. These stresses will be determined for two different times. These times being immediately after transfer of the prestress and at 150 days. The ACI-Code limitations will also be superimposed on the plot, for limiting stresses immediately after transfer and at service loads. These plots will be done for the midspan of Beam 1, the quarter-span of Beam 3, and the 1.52 m (5 ft) from the end support of Beam 4.

5.4.3.1 ACI Code Limits on Concrete Stresses

In Section 18.4.1 of the ACI-Code, it states for flexural members the limitations of the allowable stresses in concrete for the extreme fibers immediately after transfer. The limitation in the extreme fiber stress in compression is $0.60f_{ci}'$ and for the extreme fiber stress in tension as $3\sqrt{f_{ci}'}$. The tension in the extreme fiber can be increased to $6\sqrt{f_{ci}'}$, if that section being examined is at the end of a simply supported member. For all the limitations, the value f_{ci}' is the compressive strength of concrete at the time the prestress is applied to the concrete. Beams 1 and 4 have the same f_{ci}' value, and Beams 2 and 3 have the same f_{ci}' value. Table 5-3 has the f_{ci}' values for the beams and the

computed compressive and tensile limits. The ACI-Code in the Commentary to Section 18.4 explains that these limits are concerned with serviceability conditions, and do not ensure that the flexural member will be of adequate strength. It also states that the concrete stresses should be computed after immediate losses, but before any time-dependent losses have occurred.

It is interesting to note that the girders for the Westbound Gandy Bridge were designed to have f_{ci}' of 34.5 MPa (5000 psi). Comparing this design with those in the Table 5-3, actual f_{ci}' for Beams 1 and 4 are 23 % greater, and f_{ci}' for Beams 2 and 3 are 14 % greater based upon the design value.

Table 5-3 Compressive strengths and stress limitations for Gandy bridge project.

ACI Code Results for Allowable Stress in Concrete					
Beam 1 and Beam 4					
f_{ci}'		$0.60f_{ci}'$		$3\sqrt{f_{ci}'}$	
MPa	psi	MPa	psi	MPa	psi
42.6	6191	25.6	3714	1.63	236
Beam 2 and Beam 3					
f_{ci}'		$0.60f_{ci}'$		$3\sqrt{f_{ci}'}$	
MPa	psi	MPa	psi	MPa	psi
39.2	5687	23.5	3412	1.56	226

5.4.3.2 Determination of Actual Concrete Stresses

It is now necessary to determine the concrete stresses in a section of the member, based upon the actual prestress loss which occurs within that cross-section. The actual prestress loss has been shown to vary throughout the cross-section of a member at a specified location. To get an accurate representation of the actual concrete stress this cross-sectional variation must be incorporated into the calculations.

The concrete stresses can be computed by the following equations with consistent units:

$$f_{\text{Top}} = \frac{-P(t)}{A_c} \left(1 - \frac{e(y - c_2)}{r^2} \right) - \frac{M_0(y - c_2)}{I_c} \text{ for } y \geq c_2 \quad (5-13)$$

$$f_{\text{Bottom}} = \frac{-P(t)}{A_c} \left(1 + \frac{e(c_2 - y)}{r^2} \right) + \frac{M_0(c_2 - y)}{I_c} \text{ for } y < c_2 \quad (5-14)$$

For Equations 5-13 and 5-14, the variables are defined as follows:

f_{Top} = the concrete stress at or above the girder centroid

f_{Bottom} = the concrete stress below the girder centroid

$P(t)$ = the prestressing force at any time t which varies depending on the loss

A_c = the gross area of concrete

r^2 = the radius of gyration

c_2 = is the distance from the girder centroid to the bottom most fiber

y = is the distance where the stress is being calculated

M_0 = the moment created from the self-weight of the girder

I_c = the moment of inertia of the cross-section

Equations 5-8 and 5-9 are based on an uncracked section stressed in elastic regions. Further discussion is necessary for the variable $P(t)$. This value is determined by computing the effective stress f_{pe} at any time t , and multiplying it by the area of one prestressing strand A_{ps} and the total number of strands. The value of $P(t)$ is dependent upon where along the depth of the cross-section the stress is being determined, as well as the location along the span of the girder.

The two times the concrete stresses are determined in this section of the project are immediately after transfer of the stress from the strands to the concrete and at 150 days after transfer. At transfer, only the immediate losses, in our case elastic shortening, is removed from the jacking stress to determine $P(t)$. At 150 days, the total loss, which includes both immediate and time-dependent losses, occurring at that time are removed in order to determine $P(t)$.

For the plots of concrete stress that follow, negative values are considered compressive and positive values are considered tensile. The plots for immediately after transfer contains the actual and AASHTO or design stress distributions, and shows the ACI Code tensile and compressive limits as vertical lines. The plots for 150 days after transfer contain the actual and AASHTO concrete stress distributions. The actual stress distributions take into account the varying of prestress loss along the cross-section. The

AASHTO concrete stress distribution uses the same loss throughout the depth of the cross-section.

Figure 5-28 contains the plot for immediately after transfer of stress at the midspan of Beam 1. The concrete stress is well within the limits required by the ACI Code. The entire concrete stress distribution is compressive for the actual and AASHTO according to this plot. The cross-section is much more compressive at the bottom than at the top, which is expected. The actual maximum and minimum concrete stress are -16.9 MPa occurring at 7.6 cm (3 in) and -5.1 MPa occurring at 190.5 cm (75 in). The actual concrete stress tends to be slightly more compressive in the middle portion of the cross-section, and slightly less compressive towards the top of the cross-section compared to that from the AASHTO design requirements. The actual stress distribution is essentially nonlinear as can be seen in Figure 5-28.

Figure 5-29 contains the plot for 150 days after the transfer of stress at the midspan of Beam 1. The actual maximum and minimum concrete stresses are -12.5 MPa occurring at 7.6 cm (3 in) and -5.3 MPa occurring at 190.5 cm (75 in). The actual concrete stress appears to be virtually constant for the lower portion of the beam. And, the actual concrete stress is much more compressive in the lower portion of the cross-section, and slightly less compressive in the upper portion when compared to the AASHTO results.

Figure 5-30 shows the plot immediately after the transfer of stress for the quarter-span of Beam 3. The stress limits of ACI Code are not in jeopardy at all. The entire

concrete stress distribution is compressive for both the actual and AASHTO values. The maximum and minimum actual concrete stresses are -16.5 MPa at 18.8 cm (7.4 in) and -5.0 MPa at 190.5 cm (75 in), respectively. The upper and lower portions of the actual stress agree quite well with the AASHTO values, but the actual stress is more compressive in the middle portion, as was the case at the midspan.

Figure 5-31 shows the plot for 150 days after the transfer of stress for the quarter-span of Beam 3. The results are very similar to that of Figure 5-29 for the midspan of Beam 1. The actual maximum and minimum concrete stresses are -12.5 MPa

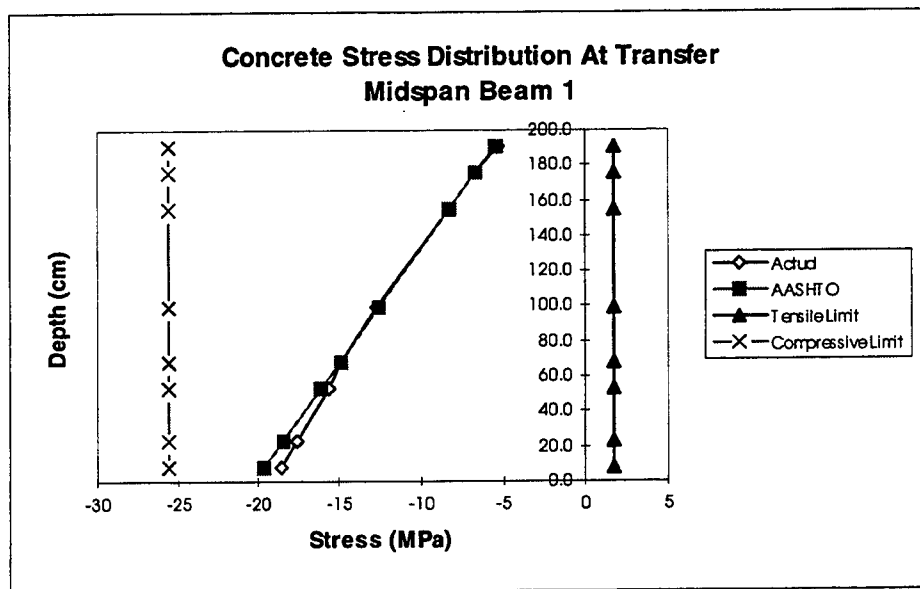


Figure 5-28 Midspan Beam 1 at transfer

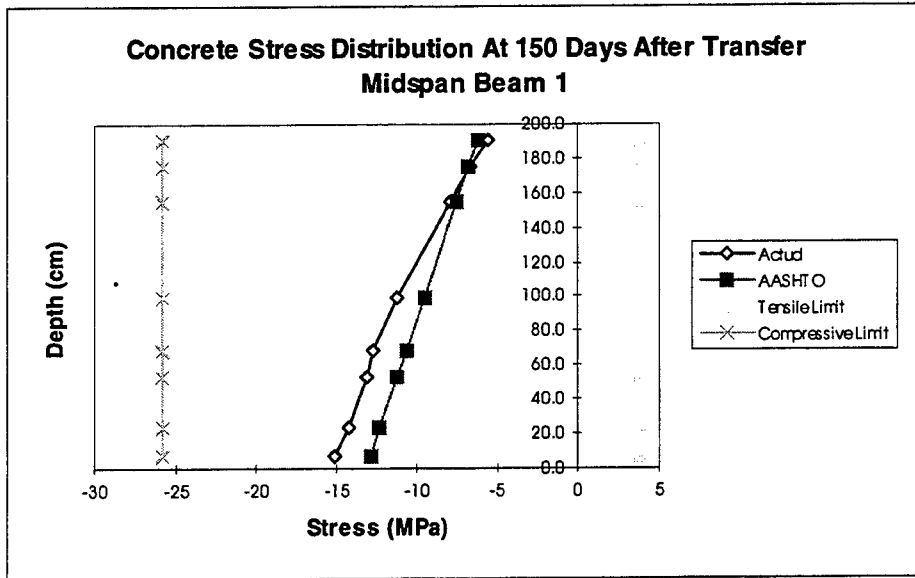


Figure 5-29 Midspan Beam 1 at 150 days

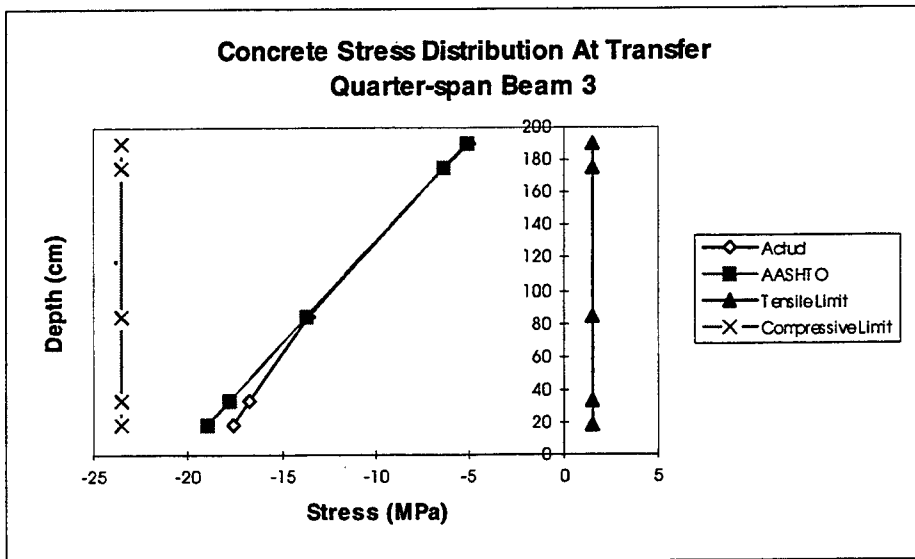


Figure 5-30 Quarter-span Beam 3 at transfer

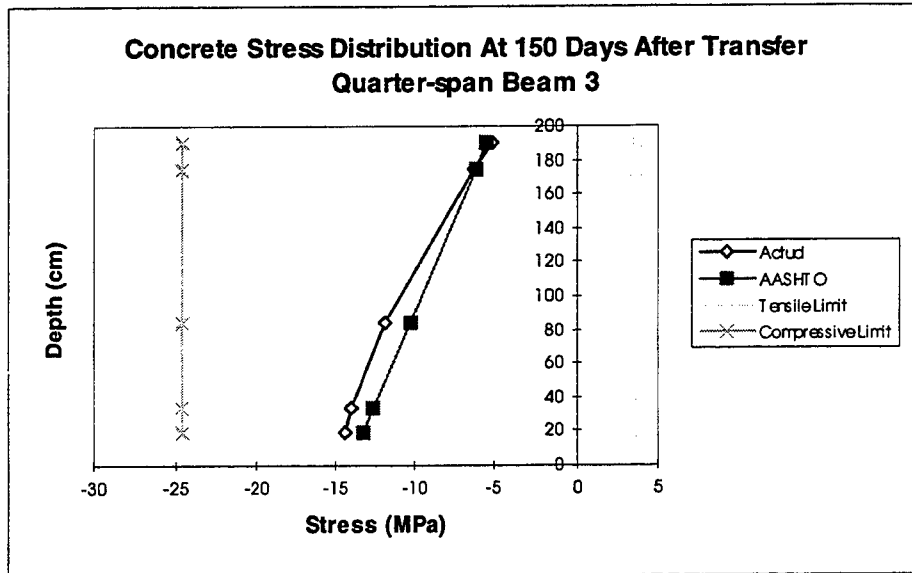


Figure 5-31 Quarter-span Beam 3 at 150 days

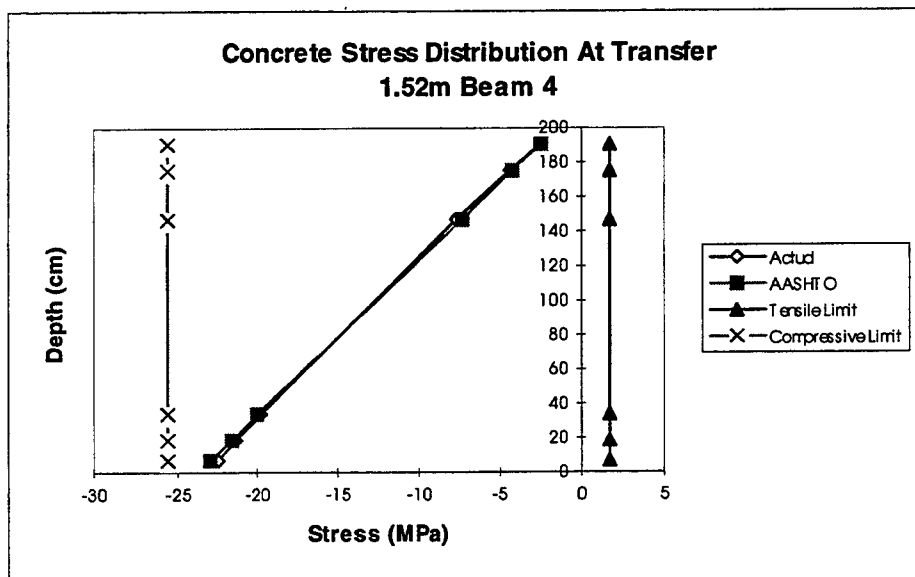


Figure 5-32 Beam 4 - 1.52 m at transfer

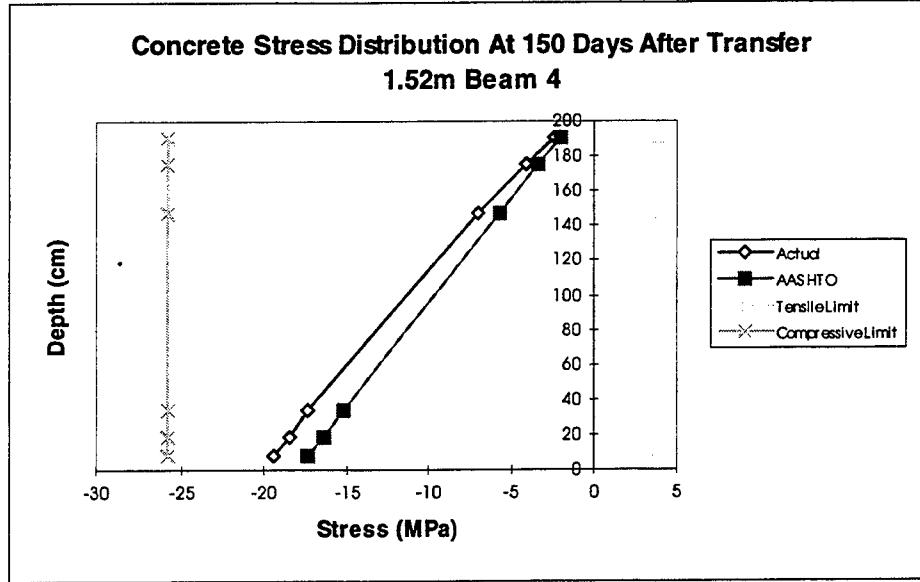


Figure 5-33 Beam 4 - 1.52 m at 150 days

occurring at 18.8 cm (7.4 in) and -5.1 MPa occurring at 190.5 cm (75 in). The actual concrete stress appears to be virtually constant for the lower portion of the beam. And, the actual concrete stress is much more compressive in the lower portion of the cross-section, and slightly less compressive in the upper portion when compared to the AASHTO results.

Figure 5-32 shows the plot of the concrete stress immediately after transfer Beam 4, at the 1.52 m (5 ft) from the end support. The results for the actual, and the AASHTO concrete stresses are similar, in that they both show almost a straight line distribution. The difference between the two is the slope of the line, the AASHTO has a higher slope. The maximum and minimum of the actual concrete stress are -22.2 MPa at 7.6 cm (3 in) and -2.5 MPa at 190.5 cm (75 in), respectively. These maximum and minimum values

come closer to the limit values than either the midspan or the quarter-span of the previous plots.

Figure 5-33 shows the plot for 150 days after transfer for the 1.52 m (5 ft) from the end support of Beam 4. The actual concrete stress values are much more compressive than the AASHTO values in the lower and middle portions of the cross-section although the gap becomes smaller near the top portion of the cross-section. The actual concrete distribution once again appears to be somewhat linear. The maximum and minimum of the actual concrete stress is -19.1 MPa at 7.6 cm (3 in) and -2.5 MPa at 190.5 cm (75 in), respectively.

5.5 Relative Humidity and Ambient Temperature Effects on Prestress Loss

5.5.1 Introduction

It is known that relative humidity and ambient temperature effect the shrinkage in a concrete member. In a prestressed concrete member, shrinkage correlates with a loss of prestress for that member. It is important to see how changes in relative humidity and ambient temperature directly relate to the prestress loss of a member. This section does not try to distinguish between what portion of the prestress loss is shrinkage and what is not. Rather, it shows plots of relative temperature and ambient versus lump sum prestress for specific locations within the girder. In addition to these points, a line is presented for each plot using a linear regression to come up with an equation relating relative humidity

and ambient temperature to lump sum prestress loss. These regression lines yield absolute value of loss in MPa for inputs of relative humidity in percent and ambient temperature in °C. Four different locations were chosen for this analysis. The midspan of both Beams 1 and 3, the 1.52 m point for Beam 4, and the quarter-span of Beam 3 were selected.

5.5.2 Selection of Points

There are three points chosen for each section. These points are varying through the depth of the section. For the midspan of Beams 1 and 3, the steel centroid at 23.6 cm, near girder centroid at 99.1 cm, and the future composite centroid of 154.9 cm were selected. For the quarter-span of Beam 3, the straight steel centroid at 18.8 cm, the draped steel centroid at 84.1 cm, and a point near the top flange at 190.5 cm were chosen. For the 1.52 m point of Beam 4, the straight steel centroid at 18.8 cm, the draped steel centroid at 147.0 cm, and a point near the top flange at 190.5 cm were chosen.

5.5.3 Relative Humidity

The relative humidity versus prestress loss for the midspans of Beams 1 and 3 are presented in Appendix C as C-1 and C-2, respectively. For the three points examined for Beam 1 midspan, the slopes are positive and less than unity. However, points for Beam 3 midspan, the slopes are negative and are larger in the absolute sense than those of Beam 1 at midspan. Beam 1 has higher average relative humidity values than Beam 3, resulting in positive slope for Beam 1 as opposed to a negative slope for Beam 3. This could mean

that less shrinkage was occurring for the days mentioned for Beam 1 than Beam 3, providing all other things being equal.

The relative humidity versus prestress loss for the quarter-span of Beam 3 is presented in Figure C-3 for the points mentioned. The slopes are negative, which is similar to Beam 3 midspan, for all three points. The slope is highest at the draped steel centroid at 84.1 cm, which is located near the girder centroid. Smaller slopes occur at the straight steel centroid of 18.8 cm and the 190.5 cm mark. These locations are located near the bottom and top flanges, respectively.

Figure C-4 shows the results of the relative humidity versus depth for the 1.52 m from the end support. The slope of the line is positive gradually increases from the top flange to the draped steel centroid to the straight steel centroid.

5.5.4 Ambient Temperature

The plots for ambient temperature versus prestress loss are presented in Appendix C as Figures C-5 and C-6, for the mid span of Beams 1 and 3, respectively. The equations for all three points for both midspans have similar slopes and intercepts. This indicates a smaller dependence of the loss variations on ambient temperature.

In Figure C-7, the prestress loss versus ambient temperature for the quarter-span of Beam 3 are shown. They have larger slopes the further away from the top of the member and all are positive.

In Figure C-8, the prestress loss versus ambient temperature is for 1.52 m from the support. Again, larger slopes prevail in the lower portion of the cross-section than the upper portion.

Within the cross-sections, the rate of change of the loss with ambient temperature (the slope) consistently higher in the lower portions of the beam, than the top portion.

These plots presented in this section can be enhanced later on to include more points, and may help in extracting the shrinkage losses from the overall prestress loss. The inclusion of more points will help define trends that may be hidden due to limited points used here. In the future, consideration should also be given to gauges located near the surface.

5.6 Effects of Prestress Loss on Camber and Deflection

5.6.1 Introduction

Camber and deflection of prestressed members are inherently affected by the amount of prestress force at any time, t . With the knowledge of what the prestress loss is at any time, t , a better estimate of the time-dependent camber and deflection can be obtained. Camber and deflection for simply-supported flexural members usually have their maximum values occurring at the midspan.

Typically, in evaluating the equations for camber and deflection of prestressed members, one loss value is assumed at any time and it is considered to be uniform across the cross-section. It has been demonstrated throughout this report, that the prestress loss

is not uniform, rather, it varies within an examined cross-section. At what level should the prestress loss within a given cross-section be used in the camber and deflection calculations? Some examples of locations where the loss should be taken are the steel centroid, concrete centroid, and composite centroid.

5.6.2 Field Measurement of Camber and Deflection

The Quality Control personnel, at the Hardaway Company Prestress Division, recorded camber and deflection calculations before the girders were moved to the bridge site. The times at which the readings were taken at the midspan are as follows: immediately after transfer, 28, 60, and 90 days. The values obtained for the midspans of Beams 1, 4, and 3, can be seen in Table 5-4. These reading will be compared with those calculated using the prestress loss at different levels at the midspan cross-sections of Beams 1, 4, and 3.

Table 5-4 Camber and Deflection Readings

Camber and Deflection Measurements Taken By QC of the Hardaway Company			
Time (days)	Beam 1 (cm)	Beam 4 (cm)	Beam 1 (cm)
Immediately After Transfer (≈ 0)	6.50	6.03	6.51
28	7.47	7.62	7.14
60	7.62	7.94	7.62
90	7.94	8.26	7.94

5.6.3 Comparing Camber and Deflection Results

The actual measurements obtained in Table 5-4 are compared with the calculated results, based on the actual losses at the steel, girder, and future composite centroids. The method used for calculating the time-dependent camber and deflection is Naaman's "Simplified C Line Approach" [5]. This approach allows for easy incorporation of the effective prestress at any time, t , and assumes uniform loss across the cross-section. The results for the midspans of Beams 1, 4, and 3 can be found in Figure 5-34 (a-c). The effective prestress was based on the losses at the steel, girder, and composite centroids, in order to see which may best model the actual measurements of camber and deflection. From all three of these plots, the camber and deflection are best modeled after the loss at the steel centroid.

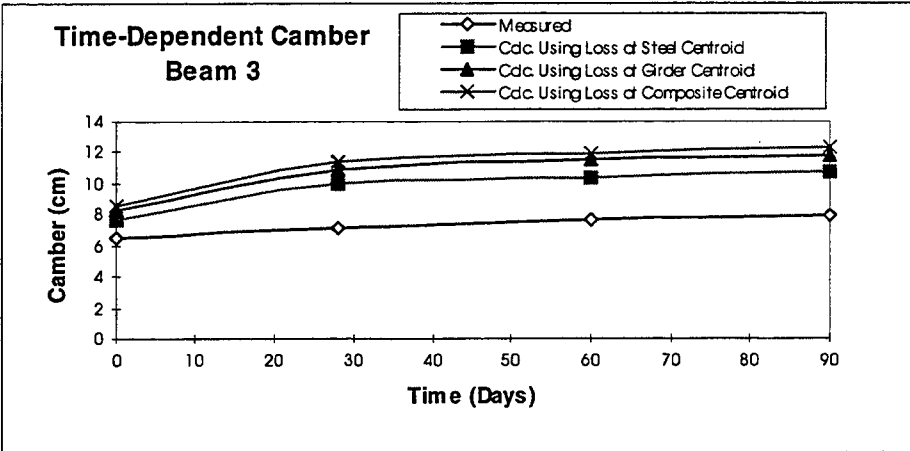
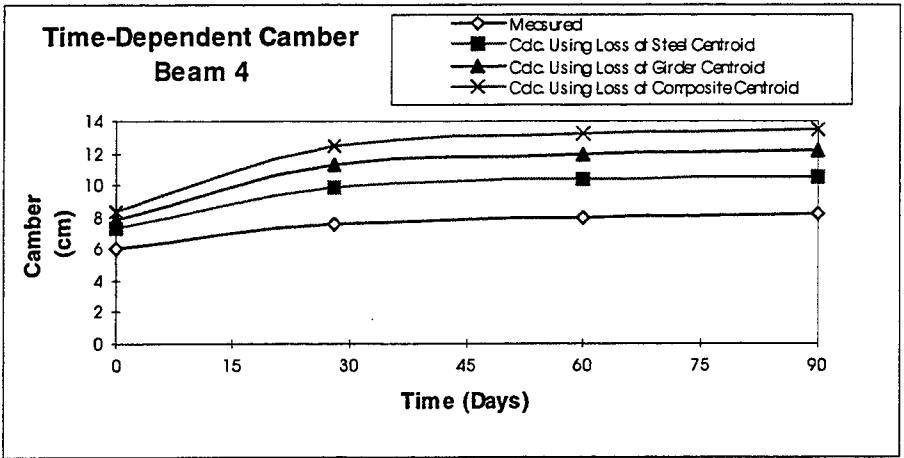
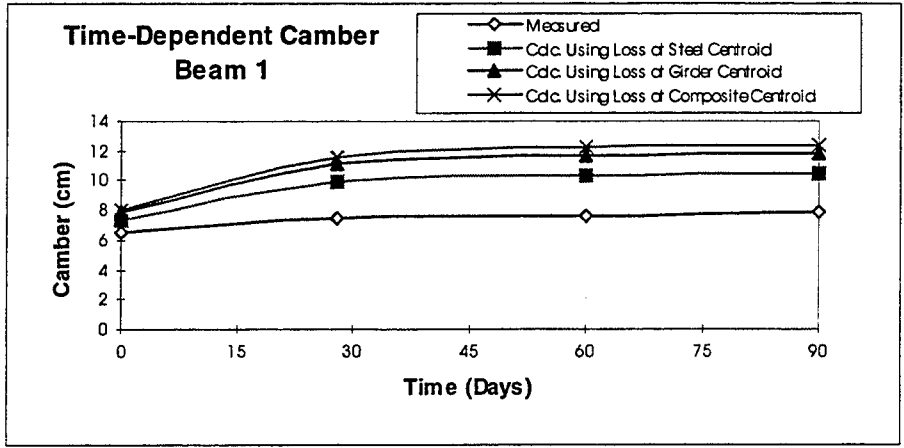


Figure 5-34 camber (a) Beam 1 (b) Beam 4 (c) Beam 3

CHAPTER 6

CONCLUSIONS

This report has presented the bridge instrumentation technique used in this research project, along with the bridge monitoring procedure, and methodologies employed for data collection and reduction. The report also discusses comparisons between the time-dependent pre-stress losses and concrete stresses, deduced from the strain measured in the field, and their empirically determined counterparts often used in various codes of practice, particularly ACI-PCI and AASHTO. The strain data utilized in this first phase of the project covered 150 days, starting from the date the bridge girders were cast at the pre-stressed concrete yard in Tampa, Florida. During this period the bridge deck slab was not in place yet, hence, the girders were loaded by the pre-stressing force and self-weight only. Therefore, composite action and effect of deck continuity which are also pertinent to this project, will be covered in the second phase report. The second phase of the study is currently underway.

The following observations and conclusions can be made at this early stage, of this investigation into the time-dependent behavior of pre-stressed concrete bridge girders.

- The immediate loss due to elastic shortening, the time-dependent losses up to 150 days, and the lump sum loss, all vary with the depth of the cross-section of the studied girders. In all cases, the smaller values were towards the top portion of the girder, and the larger values in the bottom portion. This is contrary to the uniform distribution of losses implicitly assumed by most codes, in using a single value of loss at the level of the pre-stressing steel centroid.

- The losses seem to be maximum at the gauge location closest to the extreme bottom fiber (3 inch cover from bottom fiber), than at the steel centroid as code design calculations assume.
- The nature of the variation of losses within a given cross-section appeared to be a segmental linear distribution, which is more pronounced at the mid-span of the girder, and nearly linear as one moves away from this location towards the end support.
- Introducing this depth variation of losses in the computation of stresses in the concrete leads to some non-linearity in the concrete stress distribution, both at transfer and at 150 days. However, these non-linear concrete stress distributions do not exceed the limiting service load stresses suggested by AASHTO or PCI in any case.
- The variation of the losses along the length of the girders, show that the elastic shortening loss at the quarter span exceeds those at mid-span below the composite centroid level, based on the data up to 150 days. However the effect of this observation on the lump sum losses seem to be dissipating with time. Because the time-dependent losses at the mid-span seems to be increasing with time.
- Care needs to be taken with the stress in the draped tendons just after the development length, since the tendon stress obtained in this region is very close to the limiting value.
- Field measured values of the elastic shortening loss exceeded that of the codes in the bottom portion of the cross-sections at the mid-span, quarter-span, and at 1.52m from the support. The elastic shortening percentages ranged from about 10.2% to 14.1%, compared to 8.4% to 8.8% suggested by the codes.
- The field measured lump sum losses at 150 days, expressed as a percentage of Code estimated losses, vary from as little as 30% in the topmost gauge at 1.52 m from the support, to as high as 87% in the bottommost gauge at the quarter-span.

- However, the field measured lump sum losses up to 150 days, ranges from about 23% to 25% of the jacking stress, compared to 29% to 30% given by ACI-PCI and AASHTO. These apparent high percentages may suggest that the code values will be exceeded at a later point in time. But evaluation of data collected after placement of the slab is necessary, and will provide better insight to this regard.
- Therefore, further investigation should be conducted with the data collected after placement of the slab.
- Field measured camber and deflection corresponded well with calculated camber and deflection using the field measured losses at the level of the steel centroid.
- Plots of variation of the lump sum losses with relative humidity and temperature form the basis for determining shrinkage losses, and separation of the various contributing components to the time-dependent losses. This separation of different sources of loss will be conducted in the second phase of the study.

APPENDIX A

PLOTS OF EXPERIMENTAL STRESS-STRAIN CURVES

The plots of experimental stress-strain curves were used to determine the modulus of elasticity for the concrete used on the Westbound Gandy Bridge. The tests were performed for 1, 2, 3, 5, and 7 days and the results are shown here.

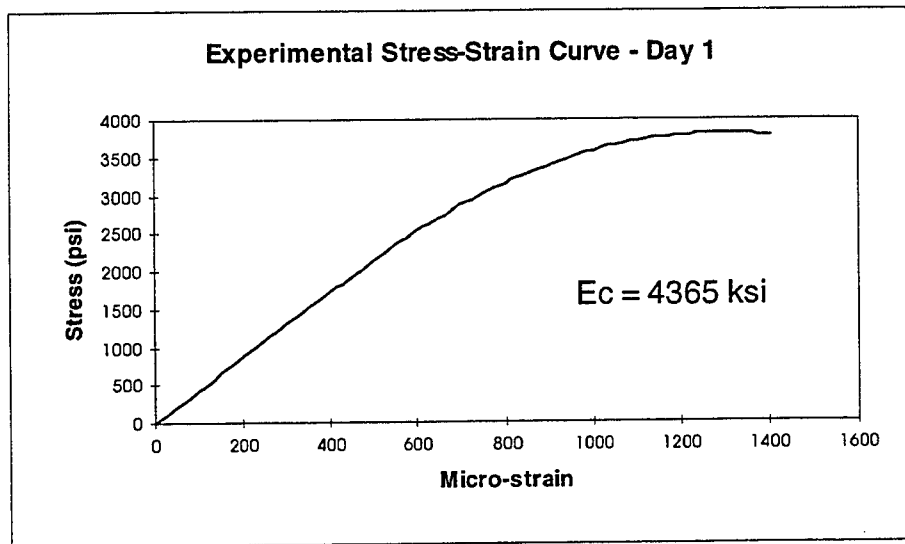


Figure A-1 Experimental stress-strain curve for Day 1

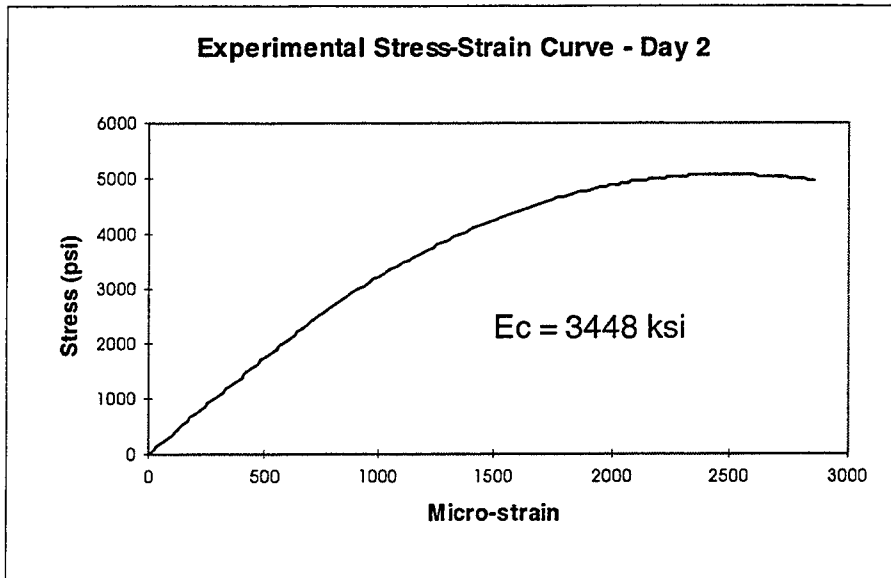


Figure A-2 Experimental stress-strain curve for Day 2

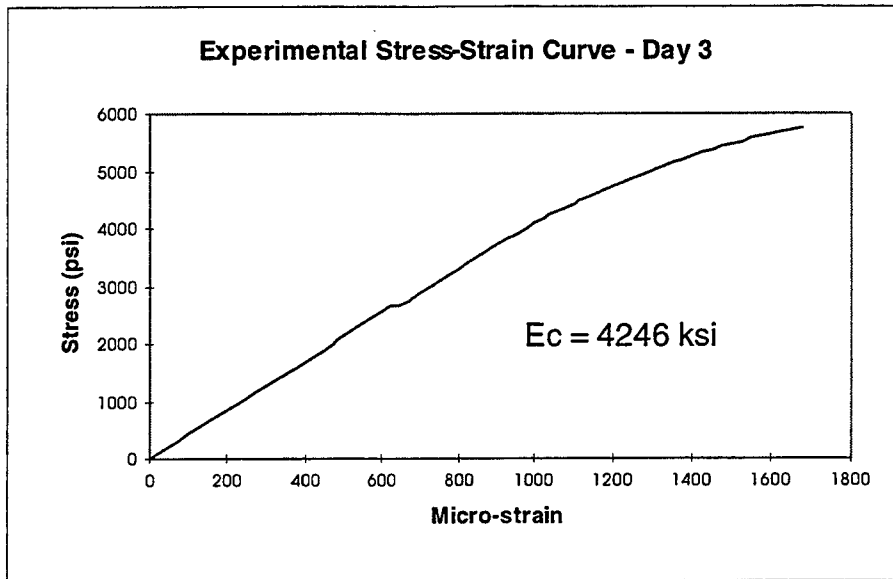


Figure A-3 Experimental stress-strain curve for Day 3

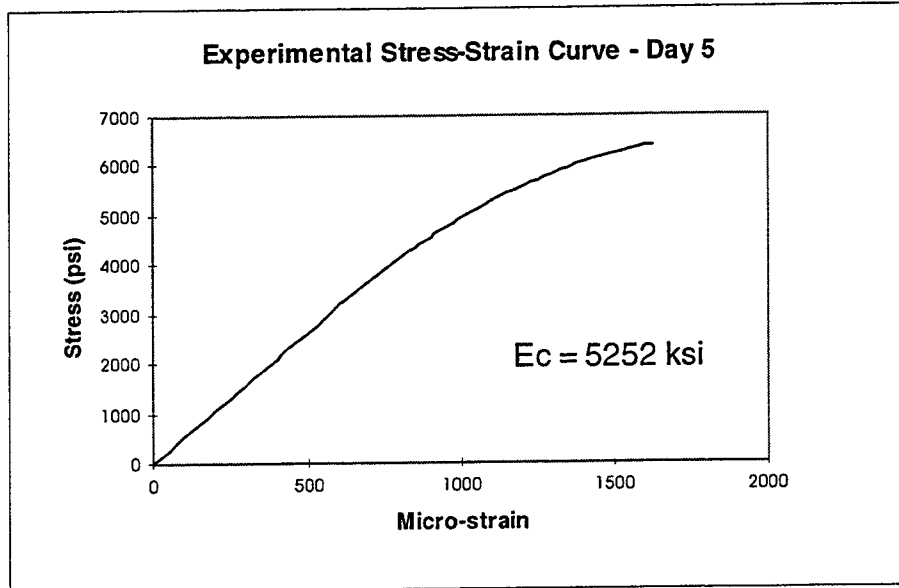


Figure A-4 Experimental stress-strain curve for Day 5

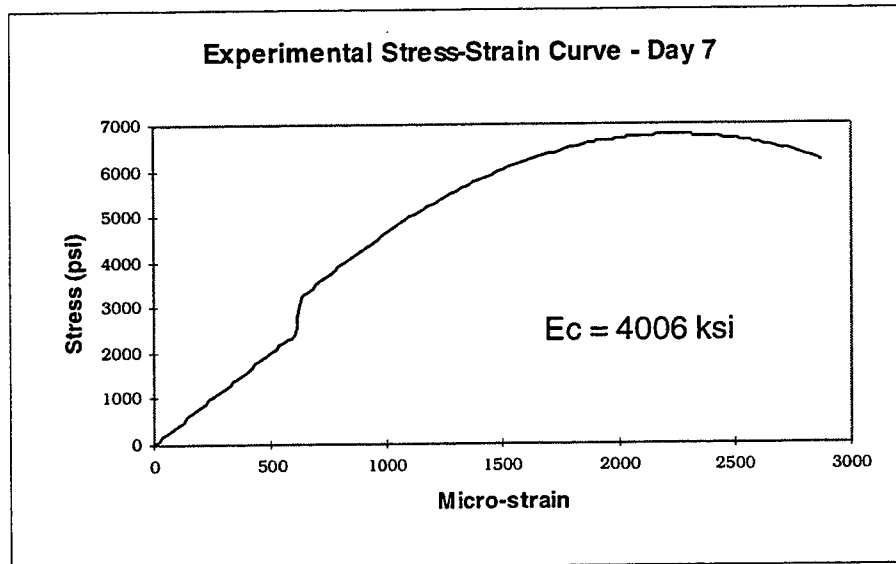


Figure A-5 Experimental stress-strain curve for Day 7

APPENDIX B

ACI COMMITTEE 209 METHOD FOR DETERMINING $E_c(t)$

In the book “Concrete Structures: Stresses and Deformations,” by Ghali and Farve [12], it suggests a few different methods for determining the time-dependent modulus of elasticity of concrete. The method used here is that which was suggested by the ACI Committee 209 [16]. This committee suggests the following equation:

$$\frac{E_c(t_0)}{E_c(28)} = \left(\frac{t_0}{\alpha + \beta t_0} \right)^{\frac{1}{2}} \quad (\text{B-1})$$

In Equation B-1, $E_c(t_0)$ is the modulus of elasticity of concrete at any time t_0 , α and β are constants based on the type of cement used, and $E_c(28)$ is the modulus of concrete at 28 days. The modulus of concrete, $E_c(28)$, can be determined by Equation 3-1, but for high strength concrete ($f_c' > 6000$ psi) it will be overestimated. Carrasquillo, Nilson, and Slate suggest to use the following equation:

$$E_c = 40,000\sqrt{f_c'} + 10^6 \text{ psi} \quad (\text{B-2})$$

Equation B-2 requires f_c' to be in psi and the corresponding result, E_c will also be in psi [16].

Table B-1 Modulus of elasticity of concrete calculated according to ACI Committee 209

Design and Calculated Values for E_c			
	Design	Beams 1 and 4	Beams 2 and 3
f'_c	44.818 MPa	57.316 MPa	54.879 MPa
Time (Days)	E_c (MPa)	E_c (MPa)	E_c (MPa)
3	29.138	19.516	19.186
7	30.892	24.187	23.779
14	31.637	27.059	26.602
28	32.030	28.837	28.350
40	32.151	29.586	29.087
60	32.246	30.119	29.611
80	32.293	30.397	29.884
100	32.322	30.567	30.051
120	32.341	30.682	30.164
400	32.409	31.096	30.571
2000	32.432	31.242	30.714
10000	32.437	31.271	30.743

All the calculated E_c values were multiplied by 0.9 in accordance with FDOT guidelines for concrete using limerock aggregate.

APPENDIX C

Relative Humidity vs. Lump Sum Loss

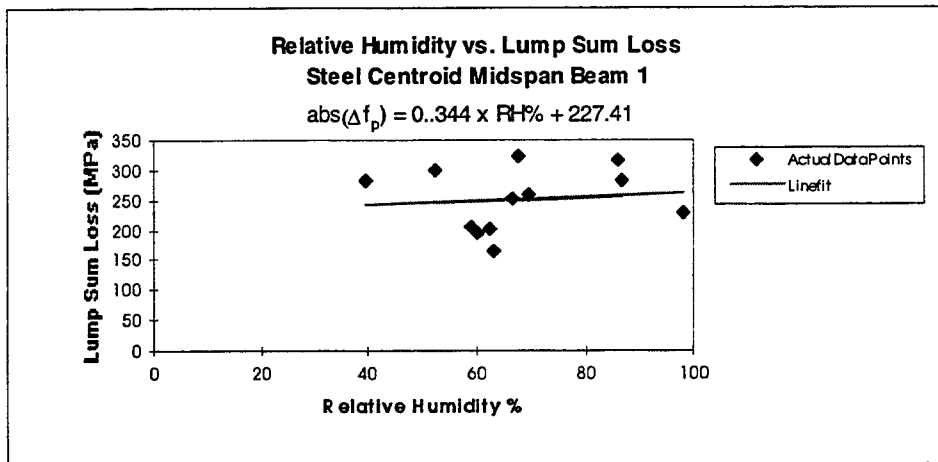
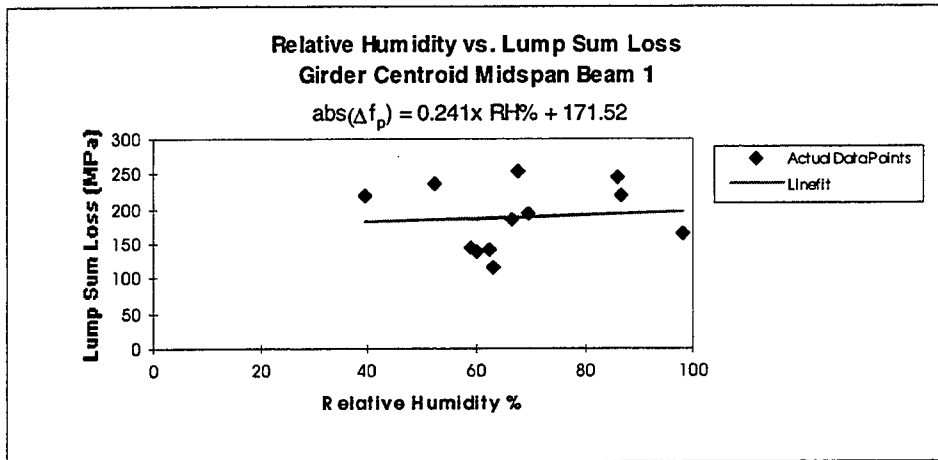
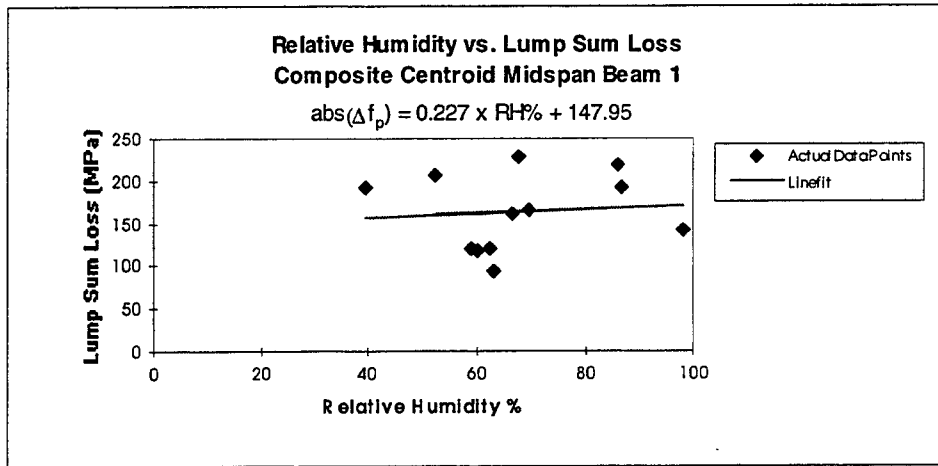


Figure C-1 Relative Humidity Midspan Beam 1

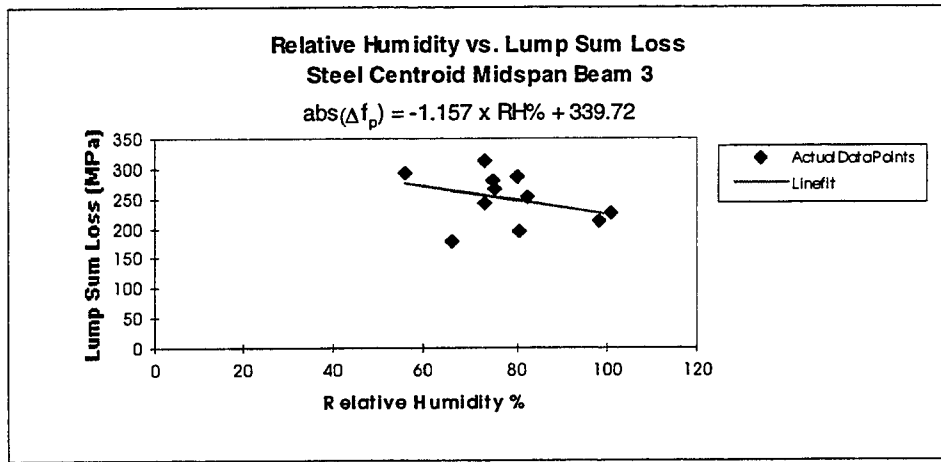
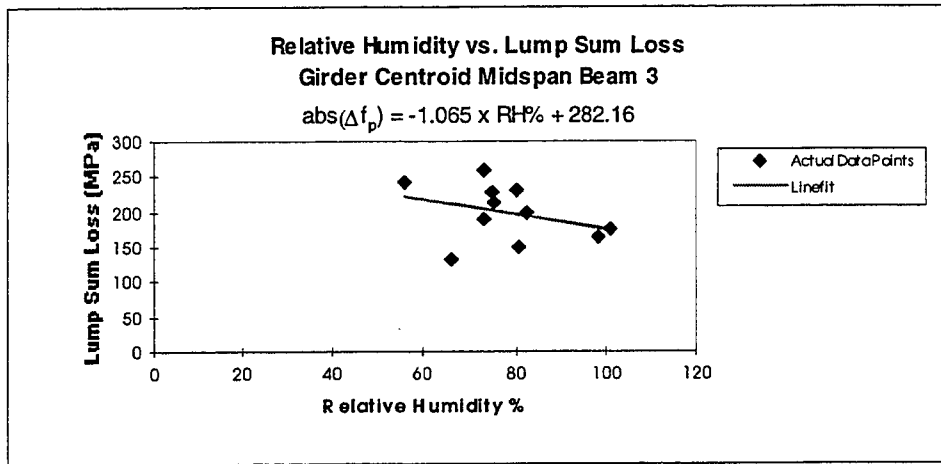
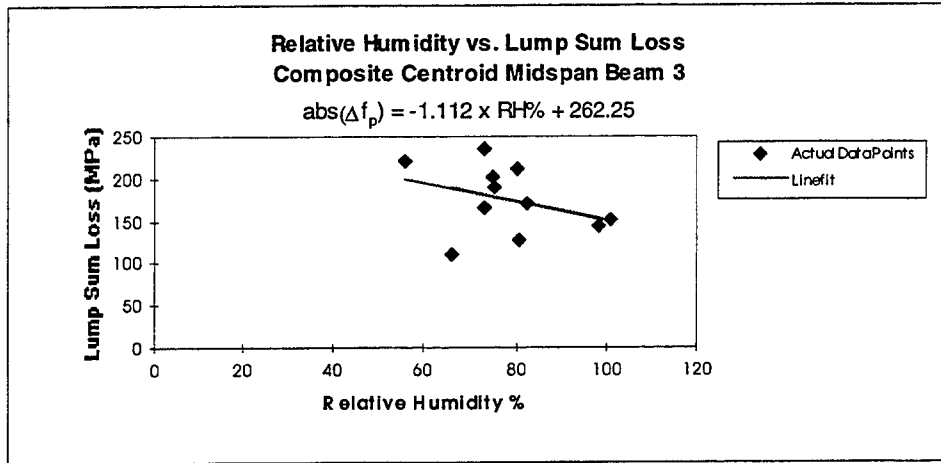


Figure C-2 Relative Humidity Midspan Beam 3

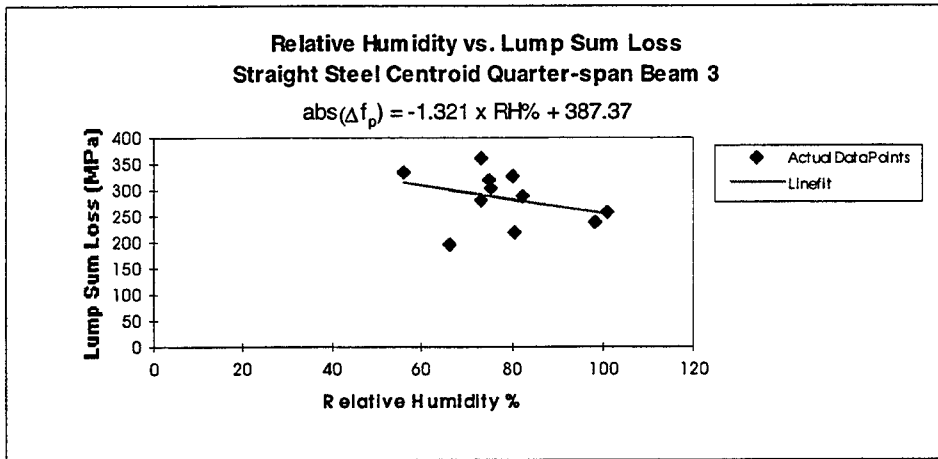
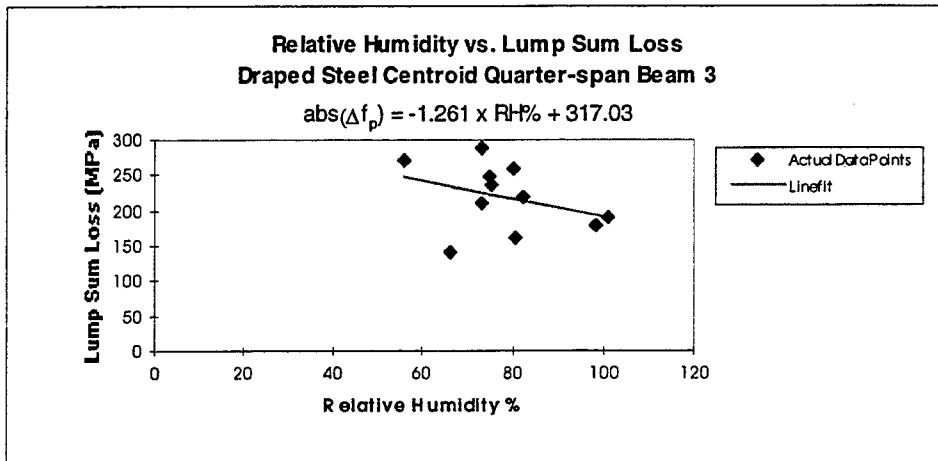
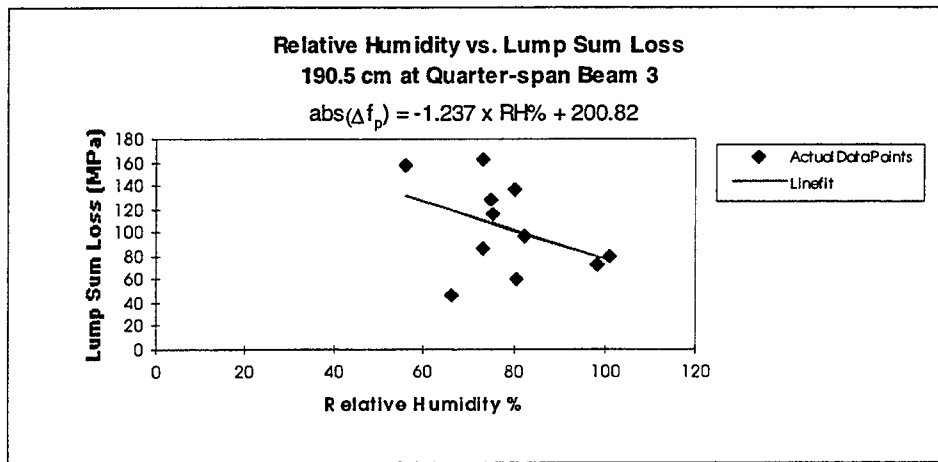


Figure C-3 Relative Humidity Quarter-span Beam 3

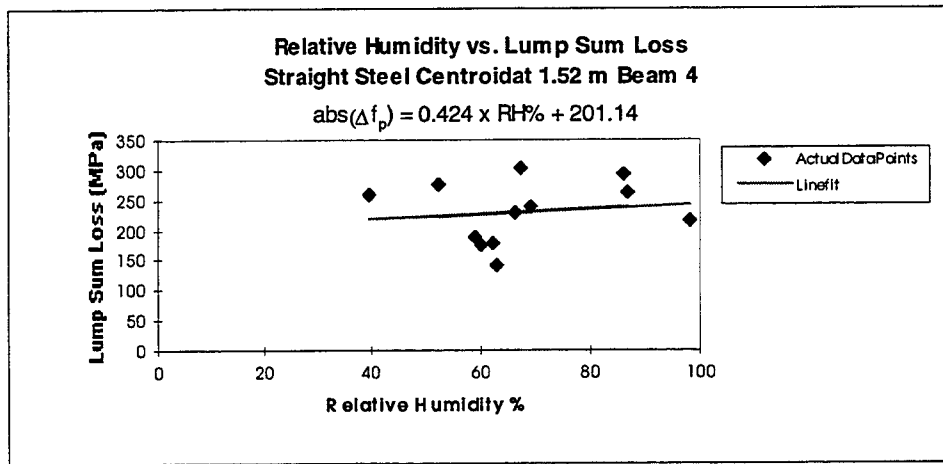
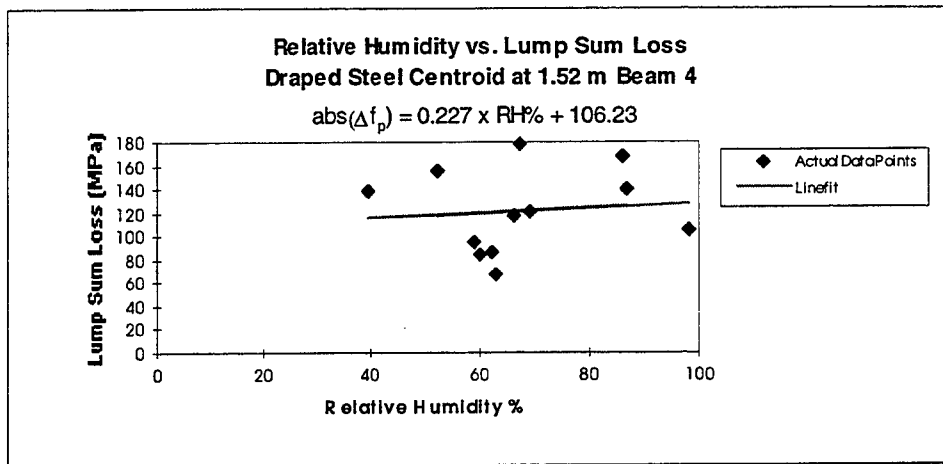
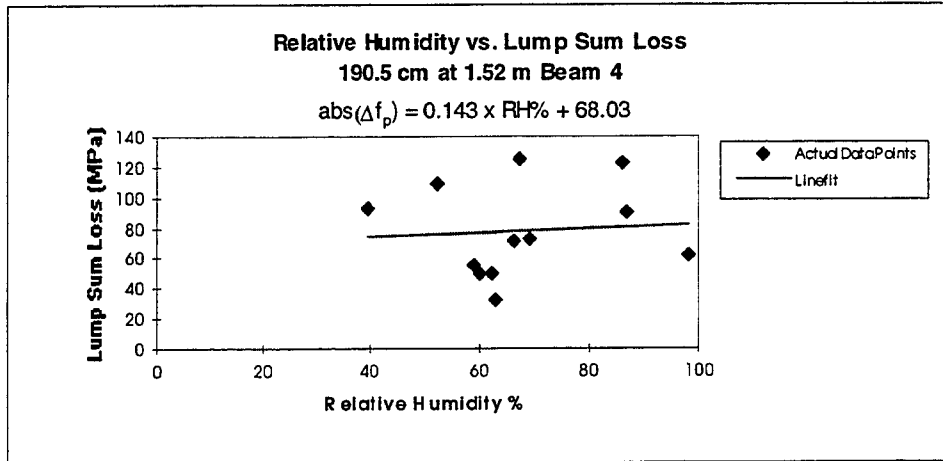


Figure C-4 Relative Humidity 1.52 m - Beam 4

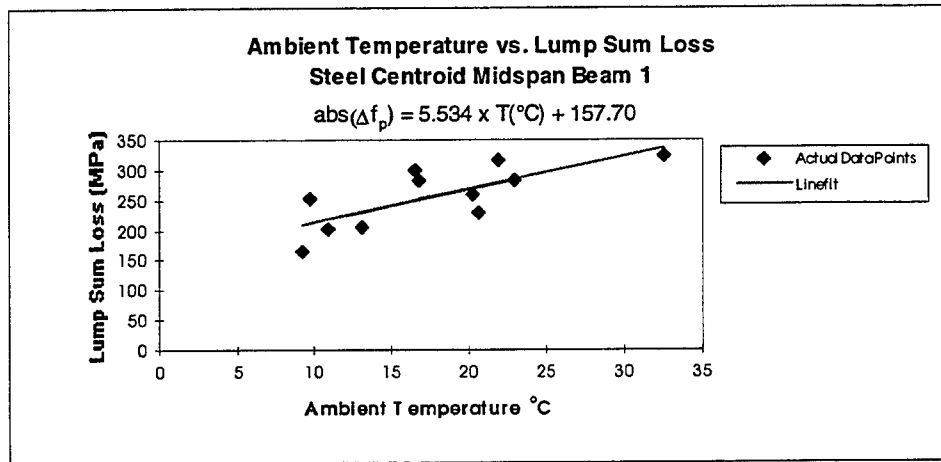
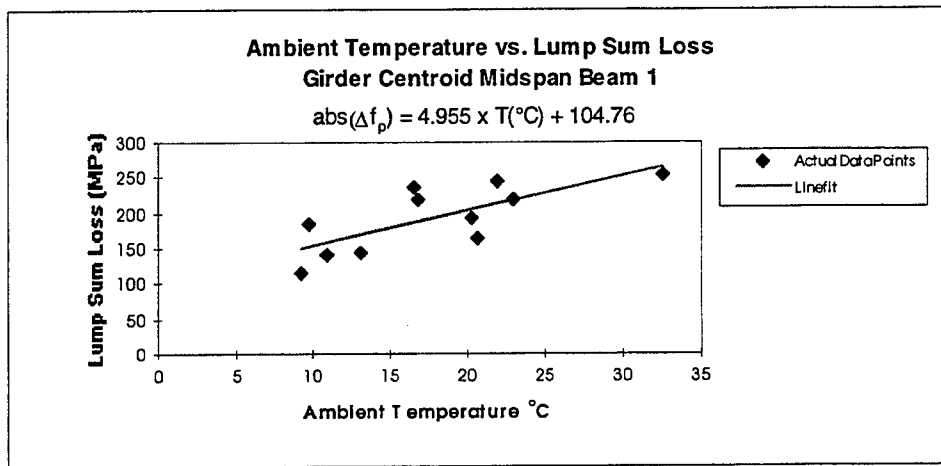
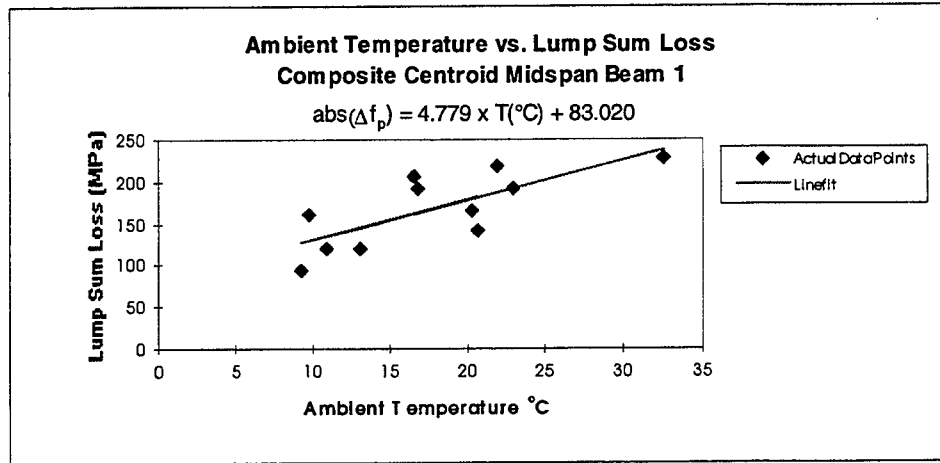


Figure C-5 Ambient temperature Midspan Beam 1

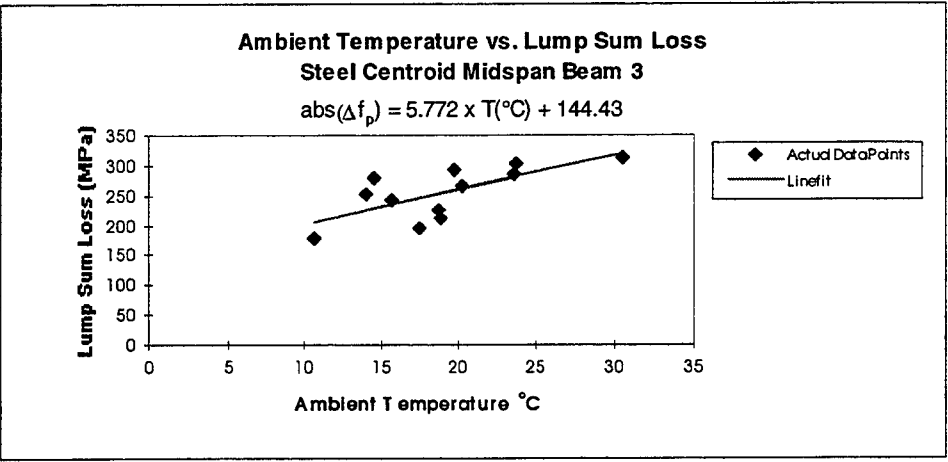
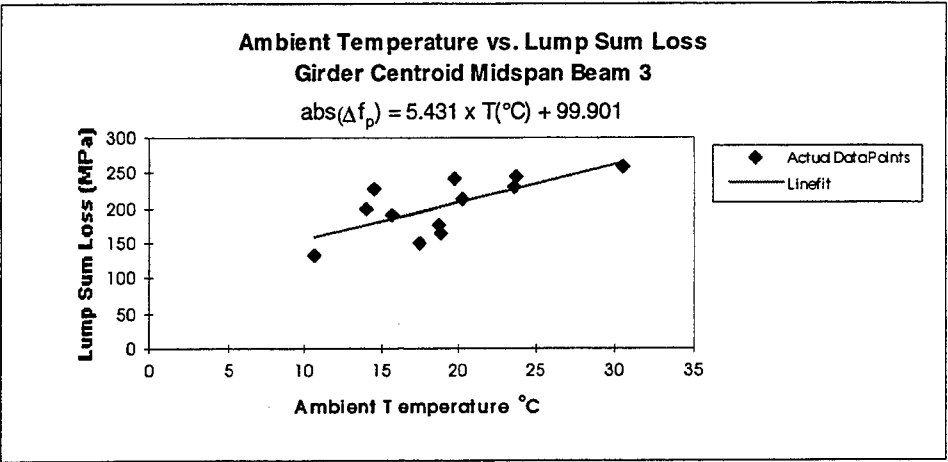
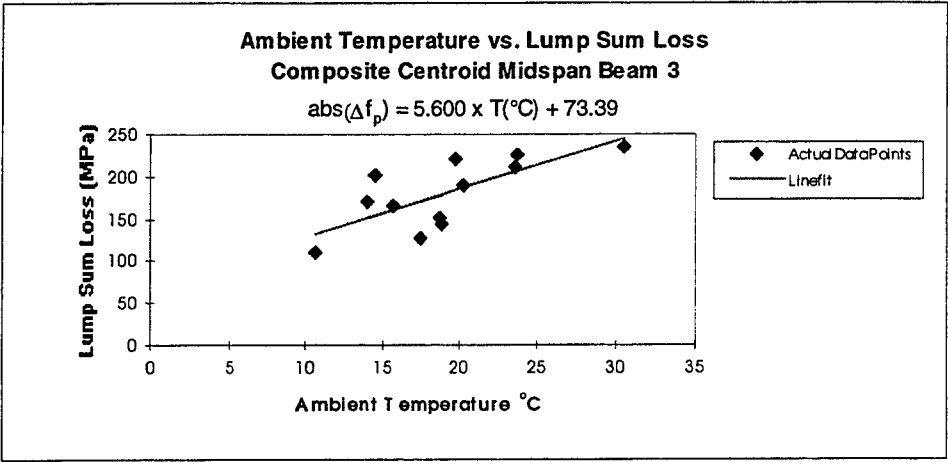


Figure C-6 Ambient temperature Midspan Beam 3

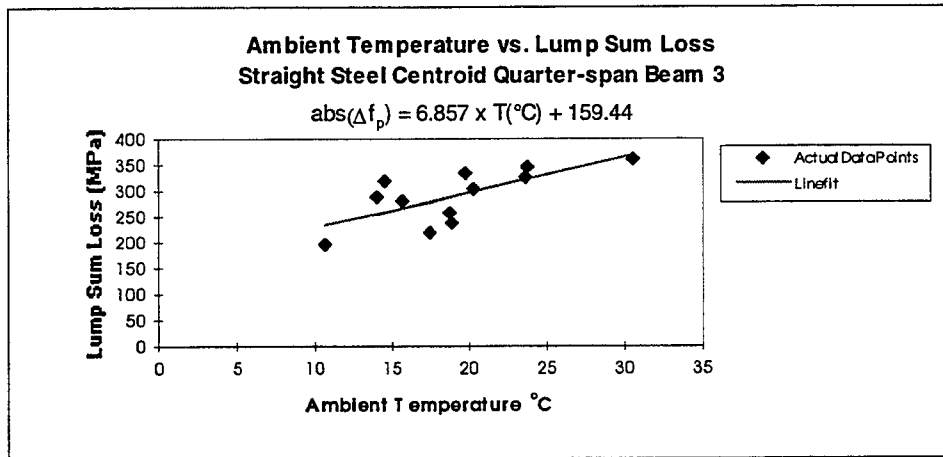
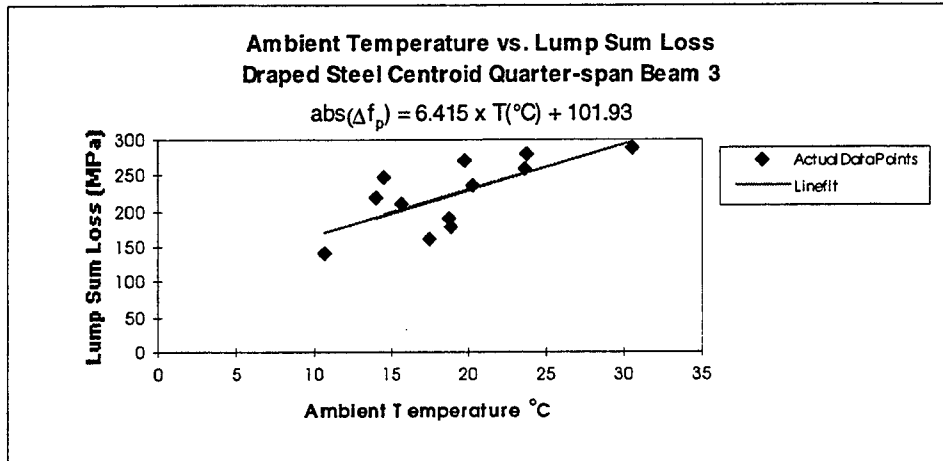
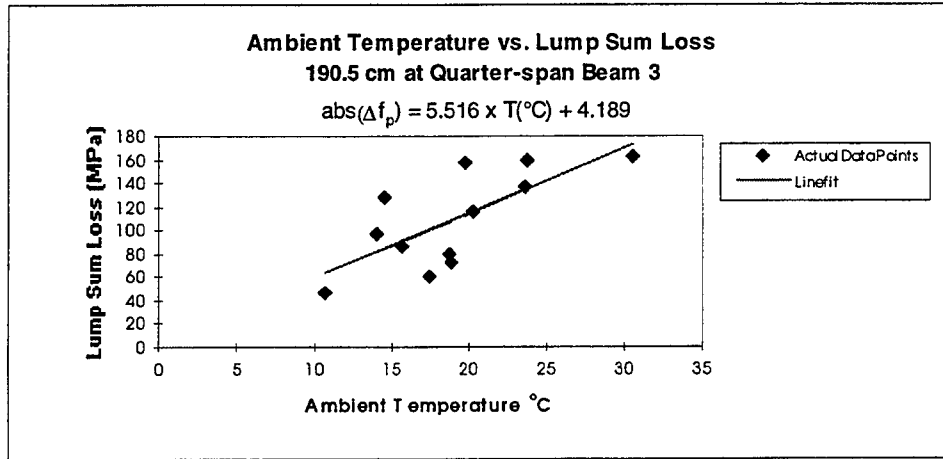


Figure C-7 Ambient temperature Quarter-span Beam 3

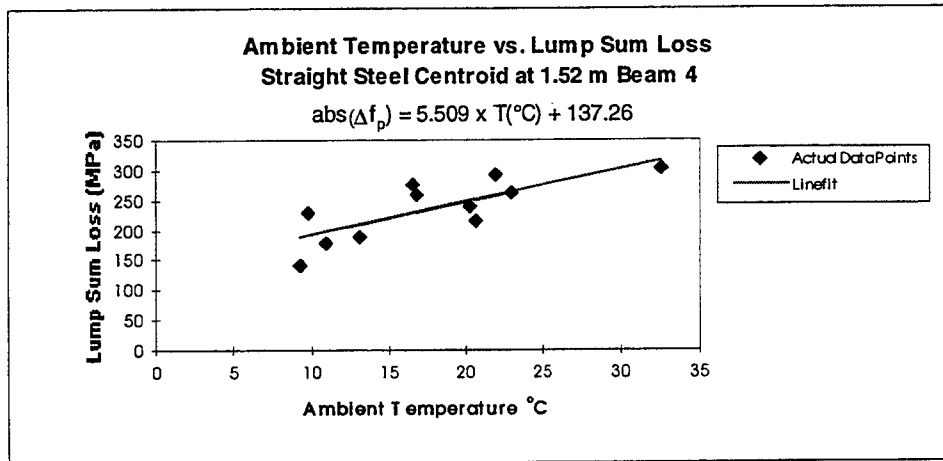
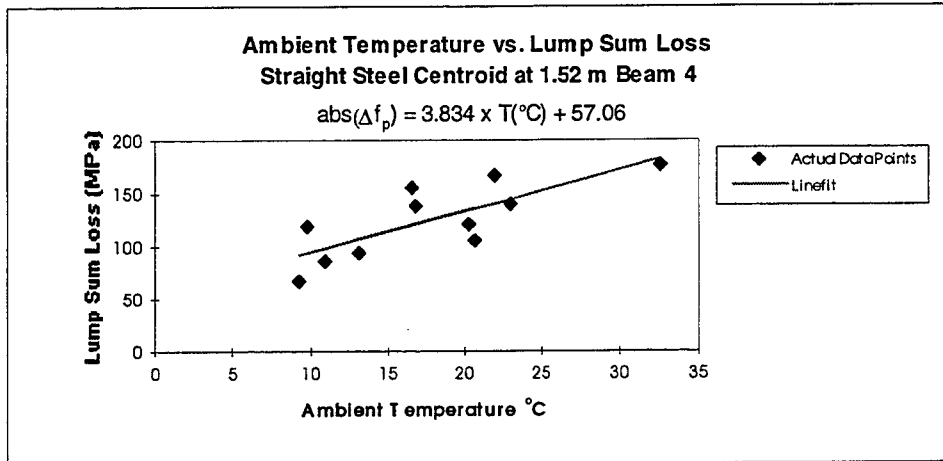
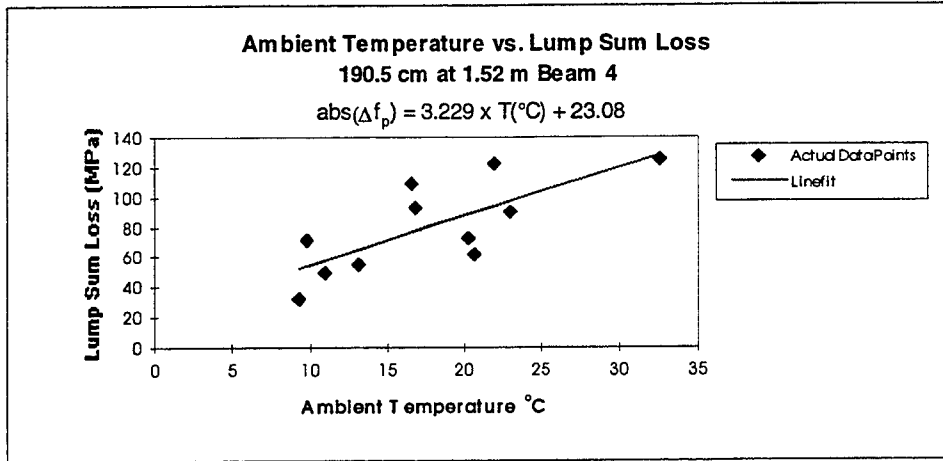


Figure C-8 Ambient temperature 1.52 m - Beam 4

REFERENCES

- [1] Finley McNary/Janssen Spaans. State Road No. 600 Westbound Gandy Brridge (Value Engineering Contract). Tallahassee, 1995.
- [2] Gepkoninc. Istruction Manual: Models VCE-4200/4202/4210 Vibrating Wire Strain Gages. Lebanon, New Hapshire: 1995.
- [3] ACI. Building Code Requirements for Reinforced Concrete (ACI 318-95). Detroit, Michigan: American Concrete Institute, 1992.
- [4] Ghali, A and Farve, R. Concretre structures: Stresses and Deformations 2nd Ed. London: E & FN Spon, 1994.
- [5] CEB-FIP 1990. Model Code for Concrert Stuctures (MC-90). London: Thomas Telford, 1993.
- [6] AASHTO. AASHTO LRFD Bridge Design Specifications 1st Edition 1994. Washington, D.C.: American Association of State Higway and Transportation Officials, 1994.
- [7] Zia, Preston, Scoot and Workman. "Estimating Prestress Losses" Concrete International June 1979: 32-38.

NTIS does not permit return of items for credit or refund. A replacement will be provided if an error is made in filling your order, if the item was received in damaged condition, or if the item is defective.

Reproduced by NTIS

National Technical Information Service
Springfield, VA 22161

*This report was printed specifically for your order
from nearly 3 million titles available in our collection.*

For economy and efficiency, NTIS does not maintain stock of its vast collection of technical reports. Rather, most documents are printed for each order. Documents that are not in electronic format are reproduced from master archival copies and are the best possible reproductions available. If you have any questions concerning this document or any order you have placed with NTIS, please call our Customer Service Department at (703) 487-4660.

About NTIS

NTIS collects scientific, technical, engineering, and business related information — then organizes, maintains, and disseminates that information in a variety of formats — from microfiche to online services. The NTIS collection of nearly 3 million titles includes reports describing research conducted or sponsored by federal agencies and their contractors; statistical and business information; U.S. military publications; audiovisual products; computer software and electronic databases developed by federal agencies; training tools; and technical reports prepared by research organizations worldwide. Approximately 100,000 *new* titles are added and indexed into the NTIS collection annually.

For more information about NTIS products and services, call NTIS at (703) 487-4650 and request the free *NTIS Catalog of Products and Services*, PR-827LPG, or visit the NTIS Web site
<http://www.ntis.gov>.

NTIS

***Your indispensable resource for government-sponsored
information—U.S. and worldwide***



U.S. DEPARTMENT OF COMMERCE
Technology Administration
National Technical Information Service
Springfield, VA 22161 (703) 487-4650
